

**Activation and Inhibition of Lys63-linked Polyubiquitination
via Ubc13 modulation**

by

Curtis Daniel Hodge

A thesis submitted in partial fulfillment of the requirements for
the degree of

Doctor of Philosophy

Department of Biochemistry

University of Alberta

© Curtis Daniel Hodge, 2015

Abstract

DNA is a detailed layout of instructions for cellular function. The integrity of human DNA is constantly challenged by a barrage of exogenous and endogenous sources. A regime of genome stability maintenance has evolved to repair the many different types of DNA damage. A form of communication involved in the majority of cellular functions is ubiquitination. This entails a process whereby a small protein called ubiquitin is tagged singularly or successively to other proteins to confer a specific signal that is recognized by a host of different ubiquitin binding domains. The functional unit used to perform ubiquitin chain building is an E2 conjugating enzyme and E3 ligase pair (E2:E3). In particular, really interesting new gene (RING)/U-box E3s are known to provide a target for ubiquitination and stimulate the E2-conjugating activity of E2 enzymes that catalyze ubiquitin conjugation. One very important functional unit is the E2 Ubc13 and RING E3 RNF8 pair that interact to build ubiquitin chains with a specific lysine 63 (Lys63) linkage. E3s are traditionally thought to provide a target for E2 enzymes. Lys63 chains recruit DNA repair enzymes to the sites of DNA double strand breaks (DSBs). Ubc13 has recently been shown to participate in the pathogenesis of a number of different cancers. Here, we investigate two small-molecule inhibitors of Ubc13, through structural, biochemical and cellular methods. We developed a Ubc13 mutant which resists inhibition by one of these compounds and, using this mutant, we show that the inhibition of cellular DNA damage and NF- κ B

signaling is largely due to specific Ubc13 inhibition. We propose that unique structural features near the Ubc13 active site could provide a basis for the rational development and design of specific Ubc13 inhibitors. Using X-ray crystallography, SAXS, and cell biology, we also separate E3-dependent E2-targeting from stimulation and demonstrate that the DNA damage response critically depends on the stimulatory activity for proper recruitment of DNA repair factors. Overall we reveal important insights into the function of the critical Ubc13:RNF8, E2:E3 ubiquitination pair.

Preface

The research in this thesis is my original work. The data in Chapter 2 was collected as part of a contribution to Stephen Campbell's (Glover lab) first author publication.

Chapter 2 of this thesis has been published as Campbell, S. J., Edwards, R. A., Leung, C. C., Neculai, D., Hodge, C. D., Dhe-Paganon, S. & Glover, J. N. Molecular insights into the function of RING finger (RNF)-containing proteins hRNF8 and hRNF168 in Ubc13/Mms2-dependent ubiquitylation. *J. Biol. Chem.* **287**, 23900-23910, doi:10.1074/jbc.M112.359653 (2012). I was responsible for the generation of the selenomethionine derivative crystal structure.

Chapter 3 of this thesis has been published as Hodge, C. D., Edwards, R. A., Markin, C. J., McDonald, D., Pulvino, M., Huen, M. S., Zhao, J., Spyropoulos, L., Hendzel, M. J. & Glover, J. N. Covalent Inhibition of Ubc13 Affects Ubiquitin Signaling and Reveals Active Site Elements Important for Targeting. *ACS Chem Biol* **10**, 1718-1728, doi:10.1021/acscchembio.5b00222 (2015).

Chapter 4 of this thesis is currently in preparation for submission as Hodge, C. D., Edwards, R. A., Hura, G., Tainer, J. A., Hendzel, M. J., & Glover, J. N. M. The DNA damage response requires E2-ubiquitination enzyme stimulation by RING E3.

Dedication

For those who strive for a better world...

Acknowledgments

I would like to thank my supervisor Dr. Mark Glover, who gave me the guidance and freedom necessary to become a real scientist. The mentorship and enjoyable scientific environment that Mark provided is a gift that I will remember fondly and cite as the place I built the foundation for my career. Despite my great respect for Mark, I can proudly say that our formal relationship has largely evolved into a friendship with a sprinkle of professionalism (just a sprinkle).

I was also very fortunate to have received mentorship from Dr. Michael Hendzel. Although not written on paper, Mike has very much been a second supervisor to me, particularly in the later years of my PhD where I had the privilege of learning cellular biological techniques in his lab. The opportunity to learn from Mike and his lab members has given me a rare breadth of experience early in my career, which I intend to further develop in my future work, and am very thankful for.

I thank my graduate studies supervisory committee members, Dr. Michael Weinfeld and Dr. Joanne Lemieux, for their guidance and support.

I would like to thank Dr. Leo Spyropoulos for the opportunity to collaborate on subjects of mutual interest. It was fun and fruitful. I am also thankful to Dr. Andrew MacMillan for honest uninhibited discussions about science, politics, and whatever else happened to be going on when he came to sequester Mark for coffee. I would also like to acknowledge all my fellow Glover lab members from over the years. They were an integral part of the fun working environment of the lab. I thank Darin MacDonald and Dr. Ismail Ismail for showing me the ropes of cell biology during my time working in the Hendzel lab.

A tremendous amount of what I've learned in the lab was from Dr. Ross Edwards, or more (in)formally Rick Ross the Boss. He demonstrated great patience in the hands-on teaching of practical X-ray crystallography, SAXS, and many wet-work techniques. Perhaps more importantly he became a great friend, one of my best. The discussions, laughs, and brewing were and continue to be priceless. Thanks man.

I have made so many great friends during my PhD, that to write a paragraph each would be to write another thesis. I want to thank my friends Craig Markin, Joe Primeau, Magnus Friis, Charles Leung, Rebecca

Gibeault, Kristen Konn, Rory Shott, Nico Coquelle, Grant Kemp, and Jen Wang. All of these people are awesome. Craig, I hope to collaborate with you in the future, as you are an excellent scientist and great friend.

To a dear friend lost, Stephen Campbell, I miss your infectious laugh, and meaningful discussions. Stephen made me feel welcome in the lab, and taught me techniques in the early days of my PhD. The world would certainly be a better place with you in it.

I thank my family and friends on both sides of the country. Simon, Justine, Tammy, and Christenberry, you all contributed to my development as a person, and I would not be the same without you. Dawson, Sean, and Jason, you have always been loyal friends, for which I am ever grateful.

I am ever thankful to my wife, Robyn Hodge. She has been an anchor for me during the rollercoaster of highs and lows that is graduate school and science in general. Robyn you encouraged and supported me during all those late nights and long hours at work, which made it so much easier than it would have been otherwise. As I said when I married you “you are the calm to my storm, and the sweet to my bitter.” You really are my better half, and I love you.

Mom, it has been just over 15 years since I last saw you. Back then I was a boy with a desire to do something meaningful in the world and now I’m a man with the skills to do so. Your strength and love during your life and struggle with cancer inspires me daily. The work in this thesis is merely my first stand against cancer, and I will continue the fight. Dad, it will be 10 years this winter since I lost you. You instilled in me a drive and work ethic second to none. I am thankful for the sacrifices you made, the support you gave during difficult times and the things that you did to enhance my life. I have found my passion, and I think you would be happy with my choice. I love and miss you both and hope you knew what you meant to me.

I thank the funding agencies that funded my PhD research: Natural Sciences and Engineering Research (NSERC) and Alberta Innovates Health Solutions (AIHS).

Table of Contents

Chapter 1 Introduction.....	1
1.1 Types of DNA damage and their link to cancer/disease	2
1.1A: Endogenous DNA damage.....	2
1.1B: Exogenous DNA damage	4
1.2 DNA damage repair in the cell.....	5
1.2A: Overview of all types of DNA repair	5
1.2C: DSB repair via Non-Homologous End Joining	9
1.3 Cellular Ubiquitination	10
1.3A: Overview of ubiquitination	10
1.3B: K63 linked ubiquitination, enzymes, and signaling	14
1.4 RNF8/Ubc13 dependent PTMs	23
1.5 Pathogenic hijacking of RNF8 and other repair factors	29
1.6 Methodology Overview	30
Chapter 2 Overview: Assigning the RNF8 coiled-coil amino acid register	34
Chapter 3 Overview: Covalent inhibition of Ubc13	34
Chapter 4 Overview: E2-stimulation by the E3 ligase RNF8.....	35
Chapter 5 Overview: General Discussion	36
Chapter 2 ¹ Assigning the RNF8 coiled-coil amino acid register	37
2.1 Introduction.....	38
2.2 Results.....	39
2.2A: A selenomethionine derivative of RNF8.....	39
2.3 Discussion.....	43
2.4: Materials and Methods	47
2.4A: Selenomethionine protein production	47
Chapter 3 ¹ Covalent inhibition of Ubc13 affects ubiquitin signaling and reveals active site elements important for targeting	50
3.1 Introduction.....	51
3.2 Results.....	54
3.2A: Ubc13 covalent inhibitors bind to a groove near the active site	54
3.2B: Development of an inhibitor-resistant Ubc13 mutant	63
3.2C: Ubc13 ^{QD} is resistant to NSC697923 but not BAY 11-7082.....	65

3.2D: Inhibition of the DDR and NF-κB signalling by NSC697923 is due to targeting of Ubc13.....	69
3.3 Discussion.....	84
3.4: Materials and Methods	95
3.4A: Protein production.....	95
3.4B: Crystallization and structure determination.....	95
3.4C: Ubiquitination inhibition assay	97
3.4D: <i>In vitro</i> inhibition absorbance assay.....	97
3.4E: NMR of ¹⁵ N-Ubc13 ^{C87S} and NSC697923	98
3.4F: Generation of stably integrated Ubc13 MEFs.....	99
3.4G: Assay for NF-κB signaling and DNA damage localization in MEFs	99
3.4H: Multiplex Mouse Cytokine Array	100
3.4I: CellProfiler and Statistical Analyses	101
3.4J: Accession codes.....	101
3.5 Acknowledgments	101
Chapter 4 ¹ The DNA damage response requires E2-ubiquitination enzyme stimulation by RING E3	103
4.1 Introduction	104
4.2 Results.....	106
4.2A: The crystal structure of RNF8/Ubc13~Ub reveals an activated ubiquitin conformation	106
4.2B: RNF8 L451 is required for full stimulation of Ubc13 catalytic activity in vitro	111
4.2C: SAXS analysis of the RNF8/Ubc13~Ub complex show ubiquitin conformational selection in solution	115
4.2D: The RNF8 L451D mutation severely impairs Lys63-linked polyubiquitin DNA damage signaling.....	122
4.3 Discussion.....	128
4.3A: RNF8 stimulates Ubc13 catalytic activity by stabilizing ubiquitin in a closed conformation.....	128
4.3B: The RNF8 residue L451 is critical to the E2-stimulation mechanism, while R441 is not	130
4.3C: The E2-stimulating role of RNF8 is vital to the DNA damage response	134

4.4 Methods.....	136
4.4A: Protein production.....	136
4.4B: Crystallization	137
4.4C: Structure solution and refinement	137
4.4D: SAXS data collection and analysis	138
4.4E: Surface Plasmon Resonance	139
4.4F: Ubiquitination assay.....	140
4.4G: Generation of stably integrated RNF8 MEFs	140
4.4H: DNA damage localization assay.....	141
4.4I: Accession codes.....	141
4.4J: Acknowledgements	141
Chapter 5 Discussion and Conclusions	143
5.1 Overview of findings.....	144
5.2 Concerning RNF8 coiled-coil	146
5.3 Concerning Ubc13 inhibition with small-molecule inhibitors	147
5.4 Concerning RNF8-dependent Ubc13 conjugation stimulation	151
5.5 Cancer-associated mutations in Ubc13 and RNF8	156
5.6 Impact of Results and Future Studies	158
References	162

List of Tables

Table 1. Data Collection and refinement statistics of SeRNF8/Ubc13/Mms2	49
Table 2. Data Collection and refinement statistics of mutant and inhibited Ubc13	96
Table 3. X-Ray diffraction data collection and refinement statistics of RNF8/Ubc13~Ub	142

List of Figures

Figure 1. RNF8 pathway that leads to DSB repair via HR.....	8
Figure 2. Different ubiquitin linkages cause different chain topologies.....	11
Figure 3. E1-E2-E3 ubiquitination cascade.....	13

Figure 4. Formation of K63-linked ubiquitin chains by Ubc13/Mms2.....	15
Figure 5. RNF8/Ubc13/Mms2 structure.....	17
Figure 6. OTUB1 inhibits Ubc13~Ub.....	20
Figure 7. RAP80 tandem UIM binds K63-linked diubiquitin.	22
Figure 8. E3 RING residue position important for nucleosome recognition.	24
Figure 9. Paircoil2 prediction of RNF8 coiled-coil domain.....	41
Figure 10. Amino acid sequence and coiled-coil register of RNF8 ₃₄₅₋₄₀₀	42
Figure 11. Crystal structure of the selenomethionine derivative RNF8 ₃₄₅₋₄₈₅ in complex with the Ubc13/Mms2 heterodimer.....	43
Figure 12. Coiled-coil overlay of low resolution RNF8 ₃₄₅₋₄₈₅ with high resolution RNF8 ₃₅₁₋₄₈₅	45
Figure 13. Crystal packing of the shortened RNF8 ₃₅₁₋₄₈₅ causes the coiled-coil to fray.....	46
Figure 14. NSC697923 and BAY 11-7082 covalently modify the Ubc13 active site.	56
Figure 15. NSC697923 leaves a 5-nitrofuranyl adduct on Ubc13 Cys87.	58
Figure 16. NSC697923 reacts with β ME and BAY 11-7082 leaves a prop-2- enenitrile adduct on Ubc13 Cys87.....	60
Figure 17. No NSC697923 pre-reaction binding to Ubc13 was detected and E2 structural alignments highlight active site loop variations.	62
Figure 18. Design and structure of a NSC697923 resistant Ubc13 mutant.....	64
Figure 19. Ubc13 ^{QD} is resistant to NSC697923 but not BAY 11-7082.	67
Figure 20. Ubc13 ^{QD} synthesizes Lys63-linked but not Lys48-linked polyubiquitin chains.....	68
Figure 21. Ubc13 expression in Ubc13 ^{WT} and Ubc13 ^{QD} MEF cell lines is similar.....	70
Figure 22. Inhibition of Ubc13 is required for significant disruption of cellular NF- κ B signalling by NSC697923.....	72
Figure 23. Ubc13 ^{-/-} MEF cells are deficient in p65 translocation and NSC697923 does not alter p65 expression in ^{-/-} , WT, or QD MEF cell lines.....	73
Figure 24. Normalized inhibition of Ubc13-dependent, NF- κ B-driven cytokine release by NSC697923.	75
Figure 25. NF- κ B-driven cytokine release of ^{-/-} and WT Ubc13 MEFs upon stimulation with LPS.	77
Figure 26. Inhibition of Ubc13-dependent, NF- κ B-driven cytokine release by NSC697923.....	78
Figure 27. γ H2AX foci change in Ubc13 ^{-/-} MEFs with and without NSC697923 and IR, and γ H2AX/53BP1 foci localization in WT and QD Ubc13 MEFs in the absence of IR.....	80
Figure 28. Inhibition of Ubc13 is required for disruption of cellular DNA damage signalling by NSC697923.....	84
Figure 29. Ubc13 structures demonstrate loop 114-124 changes and pocket disruption upon acceptor ubiquitin binding.....	87

Figure 30. Conformational changes in Ubc13 loop 114-124 upon ubiquitin binding.....	88
Figure 31. Multiple sequence alignment of all 34 known catalytically active E2 enzymes.	90
Figure 32. Superposition of Ubc13 structures and PDB codes of available E2 enzyme structures.	91
Figure 33. RNF8/Ubc13~Ub structure and comparison to RNF4/UbcH5a~Ub. .	107
Figure 34. RNF8 coiled-coils have flexibility and make long distance crystallization contacts in the RNF8/Ubc13~Ub crystal lattice.	108
Figure 35. Electron density of the RNF8/Ubc13~Ub complex at 8.3 Å resolution.	110
Figure 36. RNF8 mutations affect Ubc13 catalytic activity.	112
Figure 37. RNF8-ubiquitin interface mutations do not significantly affect binding to Ubc13.	114
Figure 38. Raw SPR curves for RNF8 constructs.	115
Figure 39. SAXS analysis and defining a minimal RNF8/Ubc13~Ub ensemble.	117
Figure 40. Guinier and flexibility plots of the WT RNF8/Ubc13~Ub complex derived from SAXS.	120
Figure 41. Guinier and flexibility plots of the L451D RNF8/Ubc13~Ub complex derived from SAXS.	121
Figure 42. RNF8 levels are similar in the WT and L451D MEF populations.	123
Figure 43. RNF8 colocalization with γ H2AX foci after ionizing radiation.	123
Figure 44. RNF8 L451D mutation sharply reduces Lys63-linked polyubiquitin chain formation in MEF cells.	125
Figure 45. The effects of the RNF8 L451D mutation on DNA DSB repair via a RNF8/53BP1 IRIF time-course.	128
Figure 46. Models of RING E3 dimers and heterodimers relative to E2~Ub.	133
Figure 47. Amino acid sequence and predicted coiled-coil register of RNF8 ₃₀₁₋₃₃₃	147
Figure 48. Crotonamide Michael addition mechanism.	151
Figure 49. Potentially important residues for RNF8 selectivity of E2 enzymes. .	153
Figure 50. RNF8 and RNF168 selectivity of E2 enzymes.	155

List of Abbreviations

6-4 PPs	6-4 photoproducts
A-NHEJ	alternative non-homologous end joining
APC/C	anaphase-promoting complex cyclosome
ATP	adenosine triphosphate
BCL10	B-cell lymphoma/leukemia 10
BER	base excision repair
CDK1	cyclin-dependent kinase 1
CPDs	cyclobutane pyrimidine dimers
DDR	DNA damage response
DLBCL	diffuse large B-cell lymphoma
DNA	deoxyribonucleic acid
DNA-PKcs	DNA-dependent protein kinase, catalytic subunit
DR-GFP	direct-repeat green fluorescent reporter
DSB	double-strand break
DUB	deubiquitinase
E1	E1 activating enzyme

E2	E2 conjugating enzyme
E3	E3 ubiquitin ligase
EBV	Epstein-Barr virus
EGFR	epidermal growth factor receptor
FA	Fanconi anemia
G-CSF	granulocyte-colony stimulating factor
GFP	green fluorescent protein
GM-CSF	granulocyte-macrophage-colony stimulating factor
HA	hemagglutinin
HCS	high content screening
HECT	homology to E6AP C terminus
HR	homologous recombination
IL-5	interleukin-5
IR	ionizing radiation
IRIF	ionizing radiation induced foci
KO	knockout
LPS	lipopolysaccharide

MCP-1	monocyte chemoattractant protein 1
MEF	mouse embryonic fibroblast
MES	minimal ensemble search
MIU	motif interacting with ubiquitin
MMR	mismatch repair
MRN	Mre11-Rad50-Nbs1
NER	nucleotide excision repair
NHEJ	non-homologous end-joining
NMR	nuclear magnetic resonance
NO	nitric oxide
PARP	poly (ADP-ribose) polymerase
PNKP	polynucleotide kinase/phosphatase
PRC1	polycomb repressive complex 1
PTM	post-translational modification
RBR	RING-between-RING
RING	really interesting new gene
ROS	reactive oxygen species

RU	response unit
SAM	S-adenosylmethionine
SAXS	small-angle X-ray scattering
SPR	surface plasmon resonance
SSB	single-strand break
TLS	translesion DNA synthesis
UBD	ubiquitin binding domain
UEV	ubiquitin enzyme variant
UIM	ubiquitin-interacting motif
UV	ultraviolet
VCP	AAA-ATPase valosin-containing protein

Chapter 1

Introduction

1.1 Types of DNA damage and their link to cancer/disease

Past scientific inquiry into the inner workings of the cell has revealed an extremely intricate network of complex machinery fine-tuned through billions of years of evolution to survive and thrive on planet Earth. With life comes struggle. On a molecular level this struggle is represented by a barrage of endogenous and exogenous factors that attack the very fabric of life itself, the deoxyribonucleic acid (DNA), on a daily basis. In fact, it is estimated that 10^5 DNA damage events (lesions) occur per cell, per day^{1,2}. The endogenous sources of DNA damage arise from normal cellular metabolism, which create reactive metabolites and oxygen species (ROS) and more simply from the reliance on water as a cellular solvent, which causes hydrolysis^{1,3}. In addition to these, there are also alkylating agents, cholesterol/estrogen metabolites, and lipid peroxidation products. Exogenous DNA damaging agents include radiation such as ultraviolet (UV), a natural component of sunlight, and genotoxic chemicals¹. Cancer formation is thought to be a result of the interplay between the more rare exogenous and frequent endogenous DNA damage accumulation, therefore a look at a few more specific examples are warranted.

1.1A: Endogenous DNA damage

There are a number of well-characterized reactive species that damage DNA through oxidation, that arise through chemical change of molecules naturally employed by the cell. One such molecule is nitric oxide (NO), which is involved in neurotransmission, immune response,

and vasodilation^{3,4}. It can react with the ROS superoxide ($O_2^{\cdot-}$), generated during mitochondrial respiration, to form the reactive peroxynitrite (ONO_2) which can cause DNA base oxidation and strand breaks^{3,4}. Superoxide itself can be detrimental to cells, which deal with it by first using superoxide dismutase to convert it to hydrogen peroxide (H_2O_2), and then to water by catalase and glutathione peroxidase³. This can, however, be thwarted by the presence of transition metals, such as iron, which can reduce H_2O_2 to exceptionally reactive hydroxyl radicals (HO^{\cdot}) with limited diffusion potential. A primary outcome of these reactive species are modified DNA bases, which can cause base transversions, transitions, or abasic sites³. These are repaired via the base excision repair (BER) pathway.

Some other sources of endogenous DNA damage are alkylation and hydrolysis. A major contributor to alkylation is S-adenosylmethionine (SAM), a methyl donor for natural enzyme-mediated methylation (a form of post-translational modification (PTM)), which can also react non-enzymatically with DNA to cause mutagenic lesions^{3,5,6}. Examples of the consequences of this are DNA synthesis and replication inhibition in the case of 3-methylcytosine and 3-methylthymine, respectively³. These lesions are also primarily repaired via the BER pathway. Hydrolysis of the DNA glycosidic bond between the deoxyribose and base can lead to abasic sites, which cause a propensity of adenine incorporation across from them by DNA polymerases^{3,7}. Base deamination can happen

spontaneously via hydrolysis^{1,3}. Although these examples do not exhaust the large number of different types of endogenous DNA damage, they demonstrate that the cellular environment is naturally fraught with hazardous chemicals that threaten the integrity of the genetic material on a daily basis.

1.1B: Exogenous DNA damage

One merely needs to go outside on a sunny day, or even a cloud covered day to encounter a dangerous source of DNA damage; sun-emitted UV radiation. This particular source of DNA damage is heavily associated with the onset of both melanoma and non-melanoma skin cancers⁸. Considered the major carcinogenic form of UV radiation, UVB radiation has a wavelength of 280 to 315 nm and causes 6-4 photoproducts (6-4 PPs), DNA cross-links, cyclobutane pyrimidine dimers (CPDs), and DNA strand breaks^{8,9}. CPDs and 6-4 PPs are repaired via the nucleotide excision repair (NER) pathway, which is extremely important for UV-induced DNA damage.

People can be exposed to ionizing radiation (IR) in clinical/scientific settings, and through radioactive material produced by nuclear energy plants¹⁰⁻¹². IR is also generated naturally from decay of uranium in the soil and rock to radioactive radon gas. This is a large contributor to background radiation levels, but can also accumulate to harmful levels in enclosed spaces such as mines and homes¹². Included under the umbrella of IR, are alpha, beta, and neutron particles, as well as gamma rays (high-

energy electromagnetic photons)¹⁰. IR causes many different types of DNA lesions including base damage, bulky lesions, protein-DNA crosslinks, single-strand (SSBs) and double-strand breaks (DSBs)¹³. Both endogenous and exogenous sources of DNA damage can lead to replication stress, such as stalled replication forks¹⁴. These can lead to both SSBs and DSBs, among other detrimental changes. There are many more known exogenous DNA damaging agents, such as those found in cigarette smoke and nitrite-treated meat^{1,3}, however, there are undoubtedly still many unknowns contributing to DNA mutation in humans.

1.2 DNA damage repair in the cell

1.2A: Overview of all types of DNA repair

Mammalian cells have evolved a variety of mechanisms to deal with the many different types of DNA damage. The NER and BER DNA damage response (DDR) pathways were previously mentioned, which primarily deal with UV-induced photoproducts and reactive species-induced base adducts/SSBs, respectively¹⁵. In addition to these DDR pathways there is also mismatch repair (MMR), Fanconi anemia (FA) pathway, translesion DNA synthesis (TLS), non-homologous end-joining (NHEJ – classical and alternate), and homologous recombination (HR)¹⁵⁻¹⁷. The MMR acts on DNA mismatches and DNA replication-dependent insertion/deletion loops. DNA inter-strand crosslinks are handled and repaired through the FA pathway. TLS is a bypass mechanism that allows for continuation of DNA replication despite base damage by interchanging

polymerases, with subsequent repair¹⁶. HR and NHEJ are two DDR pathways that can repair DNA DSBs, but are employed in different stages of the cell cycle. In order to focus on research more pertinent to the topics of this thesis, only HR and NHEJ will be further discussed in-depth.

1.2B: DSB repair via Homologous Recombination

The response to a DSB is cell cycle dependent¹⁷. During S (DNA replication) or G2 phase the cell makes use of a newly replicated sister chromatid as an accurate template for repair of the damaged DNA. HR is initiated when the Mre11-Rad50-Nbs1 (MRN) complex binds the broken DNA ends to process them and recruits ataxia-telangiectasia mutated (ATM) to phosphorylate the histone H2AX, termed γ -H2AX¹⁸⁻²² (Figure 1). ATM also phosphorylates a host of other DDR factors including CHK2 and p53, involved in cell cycle arrest, senescence, or apoptosis². This provides a binding platform for the sizeable adaptor protein MDC1, which binds γ H2AX through its BRCT domain²³⁻²⁵. It then undergoes two important phosphorylations²⁴. The first is by casein kinase 2 (CK2), a kinase that constitutively phosphorylates Ser-Asp-Thr motifs on MDC1 that mediate binding interactions with Nbs1 (MRN nuclease complex component)²³. The second is by the ATM kinase, which allows for RNF8 binding through its FHA domain^{23,26,27}. RNF8 is an E3 ubiquitin ligase that binds the Ubc13/Mms2 E2 heterodimer with its RING domain to form Lysine-63 (K63) linked ubiquitin chains²⁷⁻³¹. It is likely that RNF8 then ubiquitinates an unknown substrate, which recruits RNF168 through its motifs

interacting with ubiquitin (MIUs) to amplify the K63 chains. Once recruited RNF168 can then function with the E2 enzyme UbcH5c to monoubiquitinate histones H2A/H2AX on K13-15^{20,32,33}. The K15 ubiquitinated H2A (H2AK15ub) then serves as a target for 53BP1 binding, which may actually promote NHEJ in opposition to BRCA1³⁴. The extended K63 chains from the cooperative RNF8/RNF168 activity further recruit RAP80 through its ubiquitin-interacting motifs (UIMs), which results in the binding of ABRA1 and BRCA1, which promote HR^{2,35-37}.

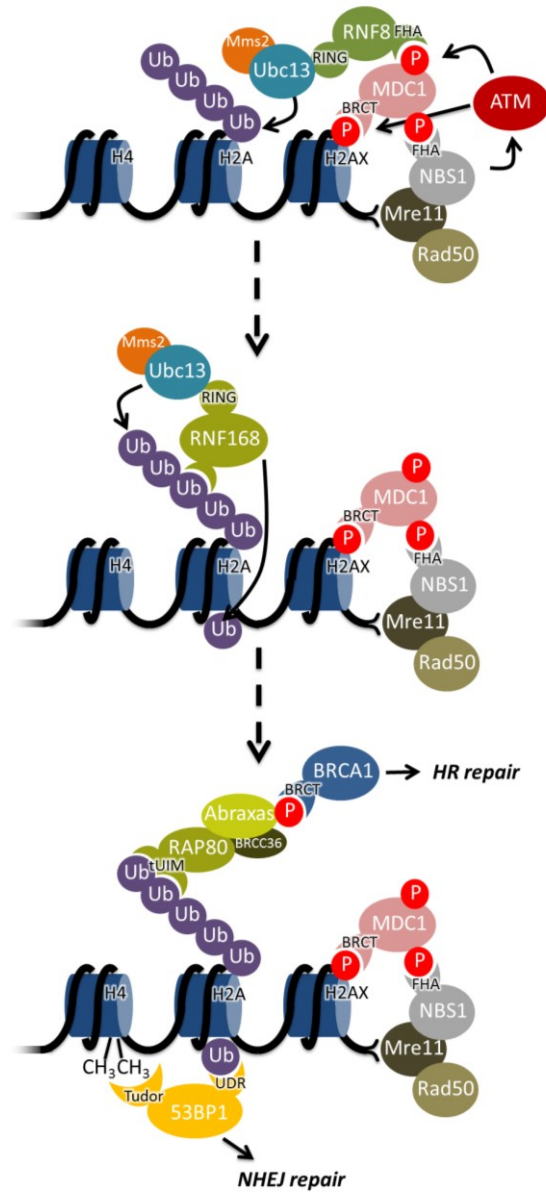


Figure 1. RNF8 pathway that leads to DSB repair via HR.

Upon DNA damage a signaling cascade largely controlled by ATM is initiated. This involves RNF8/RNF168-mediated ubiquitination of local histones, along with other post translational modifications. The cell cycle determines whether the initial pathway leads to HR repair (S/G2 only) or NHEJ, which involve BRCA1 or 53BP1, respectively.

Multiple nucleases further resect the broken DNA ends to form 3' single-stranded overhangs, which get coated by the proteins RPA, RAD54, and RAD51^{38,39}. With the help of RAD52, this nucleoprotein filament invades the homologous sister chromatid forming a D-loop, the 3' overhang is extended by a polymerase, and the resulting Holliday junction is eventually resolved¹⁷.

1.2C: DSB repair via Non-Homologous End Joining

NHEJ is not cell cycle dependent, which means that it is the predominant repair pathway and that there is a competition between it and HR during S/G2 phase¹⁷. The details of this competition have not yet been worked out, but it likely has to do with whether MRN or Ku binds the broken DNA ends first²¹. The first major step in NHEJ is the binding of the broken DNA ends by the Ku heterodimer, composed of Ku70 and Ku80^{17,21,40}. Structurally the Ku70/80 heterodimer forms a ring-like DNA binding domain that can fit two DNA-double strand turns with a preference for overhangs (5'-3' or 3'-5'), and blunt ends, as opposed to single-stranded or circular DNA^{17,41-43}. After Ku70/80 DNA binding, a DNA-dependent serine/threonine protein kinase catalytic subunit (DNA-PKcs) is recruited to the damage sites and is activated through interaction with DNA-bound Ku^{17,21,40}. This complex brings the broken DNA ends into close proximity and stabilizes them for further processing. As DNA breaks are neither planned, nor desired, the resulting ends are likely often unable to be directly ligated. A number of repair factors are thought to function in

cleaning up these messy DNA ends, such as polynucleotide kinase/phosphatase (PNKP), Mre11, Exo1, WRN, aprataxin, and Artemis⁴⁴⁻⁵⁰. The remaining gaps are then filled in by the μ and λ polymerases⁴⁰. The ligation complex that ligates the ends together is composed of DNA ligase IV, XRCC4, and XLF^{17,40}. The timing of recruitment of factors in NHEJ is still under investigation, as there is evidence to suggest it happens dynamically, and different factors may be required for different broken-DNA substrates. It is worth noting that there is also a “backup” or alternative pathway called alternative non-homologous end joining (A-NHEJ), which may be used more heavily in the event of a mutated or missing classical NHEJ factor²¹. A-NHEJ uses the MRN complex, XRCC1, and PARP1 to create microhomology (5-25bp) areas on the broken DNA ends through nucleolytic degradation, which then form short complementary regions¹⁷. Polymerase β can then fill in the gaps, and ligation can occur via ligase I or III. After repair RNF8 may be involved in the removal of Ku from DNA through K48 ubiquitination-mediated degradation by the proteasome^{40,51}.

1.3 Cellular Ubiquitination

1.3A: Overview of ubiquitination

Ubiquitination is a prime example of how evolution has exploited the use of small proteins as signaling molecules. The larger size of a protein compared with signaling modifications such as phosphorylation, methylation or acetylation provides more complexity and consequentially a

wider range of utility than the former small modifications. Of course there are benefits to small and large PTMs, hence the existence of both. Ubiquitin is a ~8 kDa protein that can be conjugated to other proteins by its C-terminal carboxylate through the formation of an isopeptide bond resulting in a monoubiquitinated substrate^{52,53}. It can also be used to form homogenous, mixed, linear or branched polyubiquitin chains through successive isopeptide bond formation using one of its seven lysine residues (K6, K11, K27, K29, K33, K48, K63) or its N-terminal methionine (M1)^{52,53}. Figure 2 demonstrates the various diubiquitin topologies of six of the available linkage types.

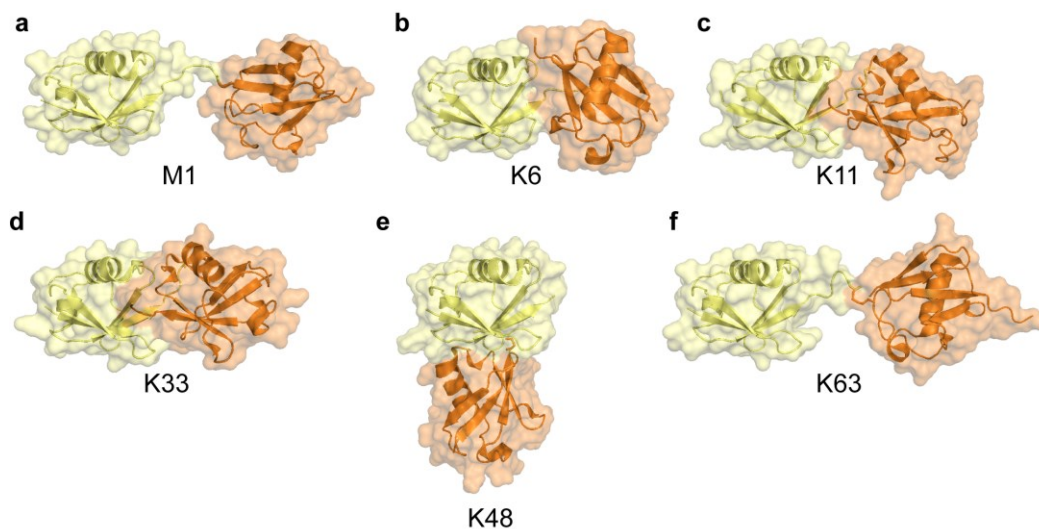


Figure 2. Different ubiquitin linkages cause different chain topologies.

All distal ubiquitins are aligned in the same orientation for better comparison of diubiquitin chain topology. (a) M1 diubiquitin chains form flexible open linear linkage. (b) K6 chains form compact diubiquitin. (c) K11 diubiquitin form both compact and open conformations. (d) K33 form compact diubiquitin. (e) K48 diubiquitin is compact. (f) K63 linkage form flexible linear open conformations. Higher order chains can change the topology and flexibility of polyubiquitin chains⁵². Distal ubiquitins are

yellow, proximal ubiquitins are orange. Protein Data Bank accession codes (PDBs): M1 is 2W9N, K6 is 2XK5, K11 is 3NOB, K33 is 4XYZ, K48 is 2PE9, and K63 is 2JF5.

There is a generally accepted E1-E2-E3 enzymatic cascade that is used to create most chains, regardless of linkage type, with linkage specificity based on the particular E2 conjugating enzyme (E2) used (Figure 3)⁵⁴⁻⁵⁷. The cascade commences with an E1 activating enzyme (E1) binding adenosine triphosphate (ATP) and a magnesium cation. The ATP molecule is used to create a ubiquitin adenylate with a free ubiquitin C-terminus. The E1 enzyme contains an active site cysteine, which attacks the ubiquitin adenylate with its sulfhydryl group, forming a covalent linkage to the ubiquitin molecule (E1~Ub). The E1 can then undergo another ubiquitin adenylate formation reaction. At this point the E1~Ub binds to an E2 that also has an active site cysteine, which attacks the covalently linked ubiquitin molecule, and forms its own covalent linkage with the C-terminus of ubiquitin (E2~Ub), termed a transthioylation reaction. The last step in the cascade is achieved using an E3 ubiquitin ligase (E3). The E3 is responsible for providing target specificity by bringing the E2~Ub into close proximity with the target so that the ubiquitin can finally be transferred to a target lysine residue. Polyubiquitin chains are formed by repeating the E1-E2 step with stimulation by the E3, where the donor ubiquitin C-terminus is linked to an acceptor ubiquitin lysine instead of the

lysine residue of the substrate (target) protein⁵⁴⁻⁵⁷. We discuss in Chapter 4 how an E3 role is also to stimulate the E2 conjugating activity.

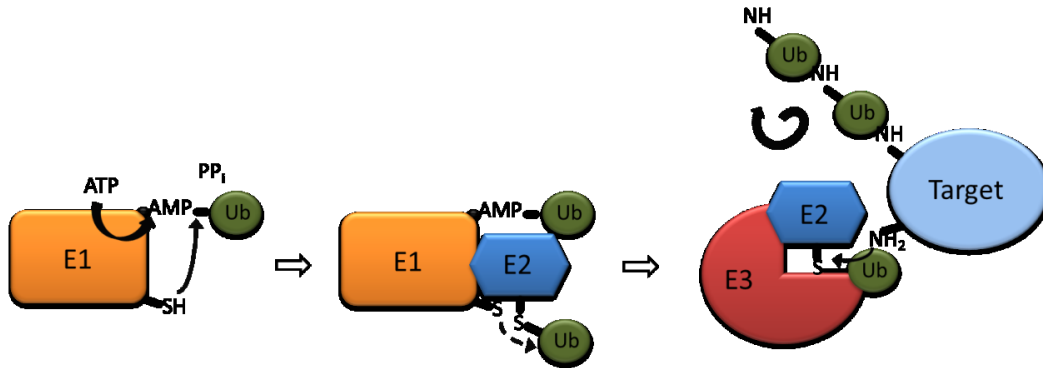


Figure 3. E1-E2-E3 ubiquitination cascade.

Ubiquitin chains are formed through repetition of the E1-E2-E3 ubiquitination cascade using ubiquitin lysines as target residues for isopeptide bond formation.

The two most studied types of ubiquitin chains are linked through ubiquitin lysine 48 (K48), the canonical signal for proteasomal degradation, and K63, involved in DDR signaling, although all types have been identified in proteomics studies of eukaryotes^{52,58,59}. K29 and K6 chains may be involved in proteasomal degradation and DNA repair, respectively^{53,60,61}. The K11 chains also target substrates for proteasomal degradation and are known to be formed by the anaphase-promoting complex cyclosome (APC/C), which functions in cell cycle regulation^{53,62}. Linear M1 chains are required for activation of the NF- κ B pathway through binding by NEMO⁶³⁻⁶⁵. Currently there is little data as to the cellular roles

of K27 and K33 ubiquitin chains, although enzymatic systems have recently been discovered to make K33 chains *in vitro*, with suggested possible roles in apoptosis^{66,67}. There is still much to learn about how the cell uses ubiquitin and its diverse chains. It should be noted that in addition to ubiquitin, there are a number of ubiquitin-like modifiers, such as SUMO and NEDD that share similarities to ubiquitin, but possess distinct differences, which much still remains to be characterized⁵³. A more in-depth look at the well-characterized K63 chains will provide further insight into just how effectively nature has made use of ubiquitination to regulate and transmit information in the cell.

1.3B: K63 linked ubiquitination, enzymes, and signaling

The actual chemical formation of a K63 ubiquitin chain is achieved by the Ubc13/Mms2 E2-conjugating heterodimer. A number of studies worked out the details of this mechanism, however a structure of the analogous yeast yUbc13~Ub/Mms2 was determined in 2006 that demonstrates this mechanism nicely in one snapshot (Figure 4)^{28,68}. The previously mentioned E1-E2 transthiolation reaction results in a donor ubiquitin covalently linked to the active site cysteine (C87) of Ubc13. Importantly a second acceptor ubiquitin molecule binds to Mms2 non-covalently, which positions the ubiquitin K63 so that it points into the active site at the Ubc13^{C87}-donor ubiquitin thioester linkage^{28,69}.

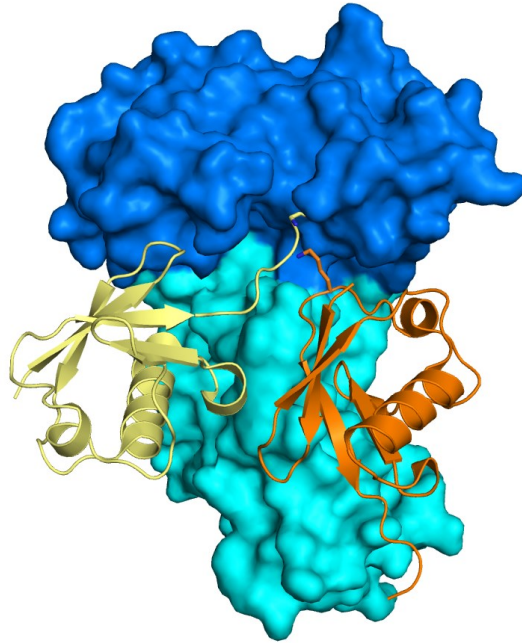


Figure 4. Formation of K63-linked ubiquitin chains by Ubc13/Mms2.

Nucleophilic attack by the acceptor ubiquitin K63 on the E2-ubiquitin thioester forms a K63-linked diubiquitin chain. Ubc13 is blue, Mms2 is cyan, donor ubiquitin is yellow, acceptor ubiquitin is orange. PDB: 2GMI.

The Mms2-ubiquitin non-covalent interaction is largely mediated by the canonical hydrophobic ubiquitin patch (L8, I44, V70) and the Mms2 residues M54, I56, and I67^{28,70}. Suppression of the pKa and deprotonation of the ubiquitin K63 promotes nucleophilic attack on the thioester resulting in the formation of an isopeptide bond⁷¹. This reaction likely forms an oxyanion thioester intermediate, and the developing negative charge on the carbonyl oxygen is thought to be stabilized by the conserved Ubc13 N79⁷². The K63 ubiquitination is further enhanced by the presence of a RING E3 ligase.

In general, one of many possible E3 ligases can bind the E2~Ub complex to provide the target. There are three different types of E3 ligases: really interesting new gene (RING), homology to E6AP C terminus (HECT), and RING-between-RING (RBR)^{29,73-76}. RING domains can be monomeric or dimeric, and bind two zinc ions in a cross-brace structure⁷⁶. In addition to providing a target, RING domains can stimulate the conjugating activity of the E2 enzyme²⁹. Both HECT and RBR E3 ligases act as an intermediate to the substrate through the use of an active site cysteine⁷⁶. HECT E3s possess an N lobe, which first interacts with a E2~Ub conjugate to bring it into contact with the active site cysteine of the C lobe for transfer. The E2~Ub bound C lobe then brings the conjugate into contact with a substrate acceptor lysine⁷⁶. The RBR E3 ligases have functional similarity to both the RING and HECT E3s. RBR E3s contain two RING domains: one which acts like a canonical RING and another that contains an active site cysteine like a HECT E3. RBRs can possess other domains that regulate its E3 activity, such an auto-inhibitory domain like the one demonstrated in the RBR E3, Parkin⁷⁶.

Our lab previously discovered how the RING E3 ligase RNF8 binds the E2-conjugating heterodimer Ubc13/Mms2 by solving an X-ray crystal structure of this complex (Figure 5a)²⁹. The RNF8 RING domain binds to Ubc13, and forms a heterodimer largely mediated through an extended N-terminal coiled-coil. The sidechains of proteins in X-ray crystal structures become quite difficult to discern at resolutions lower than ~3.5 Å

resolution. Despite the inability to see the residue side chains at 4.8 Å resolution, predicted interacting residues and mutational analysis provided insight into the binding interface between RNF8 and Ubc13. Residues in RNF8 zinc fingers (I404, I405, P438, and I439) contact a conserved S96-P97-A98 motif in Ubc13 (Figure 5b). These interactions were similar to those seen in U-box-type and RING-type E3 ubiquitin ligases CHIP and TRAF6, respectively.

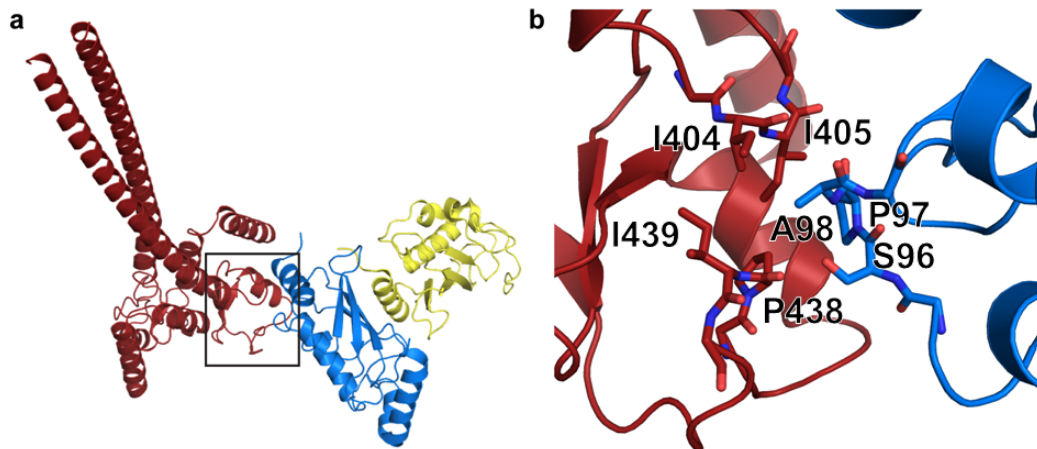


Figure 5. RNF8/Ubc13/Mms2 structure.

(a) Overview of RNF8/Ubc13/Mms2 structure. (b) Close-up of the RNF8/Ubc13 binding interface. Residues important for E2-E3 binding are shown as sticks. RNF8 is red, Ubc13 is blue, and Mms2 is yellow. PDB:4ORH.

Some of the mutations made to the RNF8 RING (I404D, I405A, I439D), and a few made to Ubc13 (S96D, A98D) individually abolished the RNF8/Ubc13 interaction as monitored by size exclusion

chromatography²⁹. Interestingly they all eliminated the RNF8 ability to stimulate Ubc13 conjugating activity, except for RNF8 mutants I404D and I405A, which both maintained some degree of stimulatory ability. This suggests that stable complex formation is not necessary for partial E3-dependent stimulation of E2 conjugating activity, and that this can be achieved transiently (as suggested for RNF168/Ubc13 ubiquitination). The other main points of this study are that the RNF8 dimer can bind two Ubc13 proteins, RNF8 greatly enhances the E2-conjugating activity of Ubc13, and RNF168 does not form a stable complex with Ubc13²⁹. Structurally, Ubc13 shares a great degree of similarity with other E2 enzymes, with a few distinct differences that are later described in Chapter 3.

OTUB1 is a deubiquitinase (DUB), which is an isopeptidase that can cleave a ubiquitin-substrate isopeptide bond that is specific for K48-linked ubiquitin chains^{77,78}. It was found to negatively regulate chromatin ubiquitination at DSB sites, by binding to Ubc13 and subsequently inhibiting its E2-conjugating activity⁷⁸. OTUB1 knockdown caused persistence in both conjugated-ubiquitin (FK2) foci and 53BP1 foci⁷⁸. Conjugated ubiquitin species can be stained with the FK2 antibody that recognizes poly- and mono-ubiquitinated substrates, regardless of linkage type⁷⁹. The lowered OTUB1 levels also restored HR-mediated DSB repair in ATM-inhibited cells, monitored through a direct-repeat green fluorescent reporter (DR-GFP) assay that measures repair of an endonuclease site-

specific DSB via HR^{80,81}. OTUB1 can also bind E2s of the UBE2E and UBE2D families^{77,78,82}. A number of structures of OTUB1 with UbcH5b~Ub or Ubc13~Ub and free ubiquitin molecules were solved by separate groups in 2012^{77,83}. Both structures showed the same ternary complex configuration with an E2~Ub and free ubiquitin bound at the same positions relative to OTUB1. The studies also revealed similar information about how OTUB1 inhibits a subset of E2s independent of its isopeptidase activity. Figure 6a shows the binding of a hybrid human (residues 1-45)/worm (OTU domain) OTUB1 to Ubc13~Ub. The hybrid was made because the important N-terminus of worm OTUB1 has poor conservation compared to human⁸³. This N-terminal OTUB1 extension was shown to be necessary for E2 inhibition and interferes with the Mms2/Uev1A binding site on Ubc13 when it is conjugated to ubiquitin (Ubc13~Ub), Figure 6b⁸³.

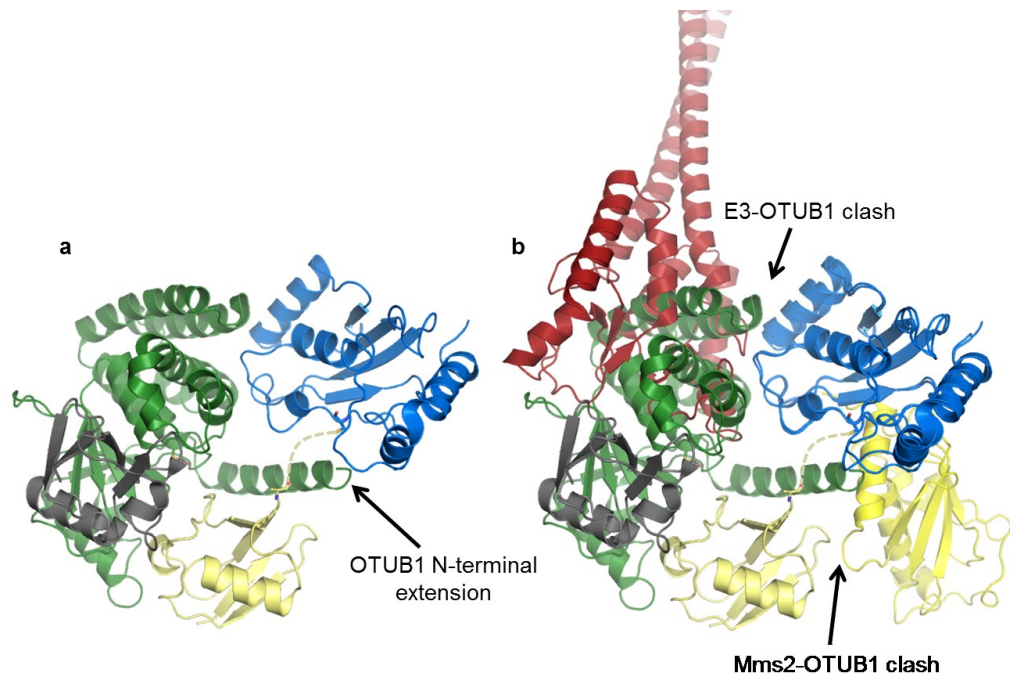


Figure 6. OTUB1 inhibits Ubc13~Ub.

(a) Structure of OTUB1 bound to Ubc13~Ub with a free ubiquitin bound to OTUB1. (b) OTUB1 Ubc13-binding overlaps with the RNF8 binding site and its N-terminal extension is predicted to interfere with Mms2 binding. OTUB1 is green, Ubc13 is blue, donor ubiquitin is yellow, free ubiquitin is gray. PDB: 4DHZ.

The OTUB1 N-terminal extension also binds to the E2-linked donor ubiquitin in a similar manner to a UIM domain, shields the linkage, and prevents its interaction with the E2, which is important for its conjugation activity⁷⁷. Interestingly, the free ubiquitin that bound to a distal site of OTUB1 in the structures, was shown to greatly enhance OTUB1 binding affinity selectively towards conjugated Ubc13~Ub over free Ubc13^{77,83}. The positions of the E2-linked donor, and free ubiquitin in the OTUB1 structures resembles a K48-linked diubiquitin poised for isopeptidase

deubiquitination where the hypothetical K48 linkage would be very close to the OTUB1 catalytic cysteine residue. Another obvious inhibitory feature of OTUB1 binding to Ubc13~Ub (or E2~Ub) is that it greatly occludes/overlaps with the RING E3 binding site. This is shown in Figure 6b.

After RNF8/Ubc13/Mms2 creates K63-linked polyubiquitin chains in the DDR, they are used to recruit downstream repair factors. The way that these factors interact with K63 ubiquitin chains is through ubiquitin binding domains (UBDs). The previously mentioned homologous recombination repair factor RAP80 binds K63-linked ubiquitin chains directly using its UIM UBDs during DSB repair via HR repair^{37,84}. UIM domains are composed of one α -helix that, like many UBDs, bind ubiquitin on its canonical I44 hydrophobic patch (Figure 7), while MIUs are functionally similar, but are positioned in the opposite orientation in the protein⁸⁵.

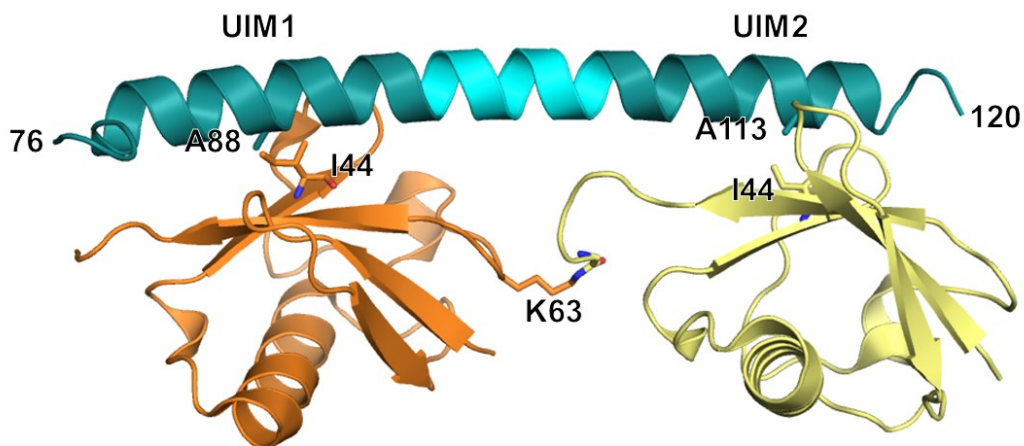


Figure 7. RAP80 tandem UIM binds K63-linked diubiquitin.

The UIM domains contain central alanines and bind the canonical ubiquitin I44 hydrophobic patch. Distal ubiquitin is yellow, proximal ubiquitin is orange. RAP80 UIMs are colored deep teal and the intervening residues are cyan. PDB:3A1Q.

The UIM is based around a central alanine residue, and UIMs are often found in tandem. Interestingly, it was shown that the length of the region between tandem UIMs determines the linkage specificity for polyubiquitin chains, and that this region does not contact the ubiquitins directly (cyan in Figure 7)³⁷. The study found that the inter-UIM region of RAP80 has a favorable length to accommodate the distance between the K63-diubiquitin molecules so that the I44 ubiquitin patch of both ubiquitins can interact with the ubiquitin binding surfaces of both UIMs. In fact, another group built upon this principle, and studies of other UIMs, and developed a very high affinity ($K_d \leq 200$ pM), K63-ubiquitin chain specific three-UIM peptide⁸⁶. It seems that nature has optimized the tandem UIM so that it

has high enough affinity for stable protein-protein interactions, but not so high as to limit dissociation. After understanding how K63 ubiquitin chains are created, and recognized by UBDs, it is necessary to look at how they are biologically blocked and disassembled.

1.4 RNF8/Ubc13 dependent PTMs

There are a whole host of histone modifications that regulate the DNA damage response. It has been shown that various E3 enzymes are involved in histone ubiquitination, for example RING1B/BMI1, a polycomb repressive complex 1 (PRC1) E3 ligase, is involved in ubiquitinating H2A/H2AX on K119, which is required for proper repair of DNA DSBs⁸⁷⁻⁹³. It was also demonstrated that polyubiquitination of H2AX required TIP60-mediated acetylation on H2AX K5, which seems to involve the participation of Ubc13⁹⁴. As previously mentioned RNF168 ubiquitinates H2A/H2AX on K13/K15, and this was shown to be necessary for 53BP1 recruitment to DSBs³². Mattrioli et al. were also able to pinpoint a residue position at the bottom of the RING domains in these histone modifying E3 ligases (RING1B, RNF8, and RNF168) that either facilitates or hinders recognition of nucleosomal H2A/H2AX as a substrate for ubiquitination (Figure 8).

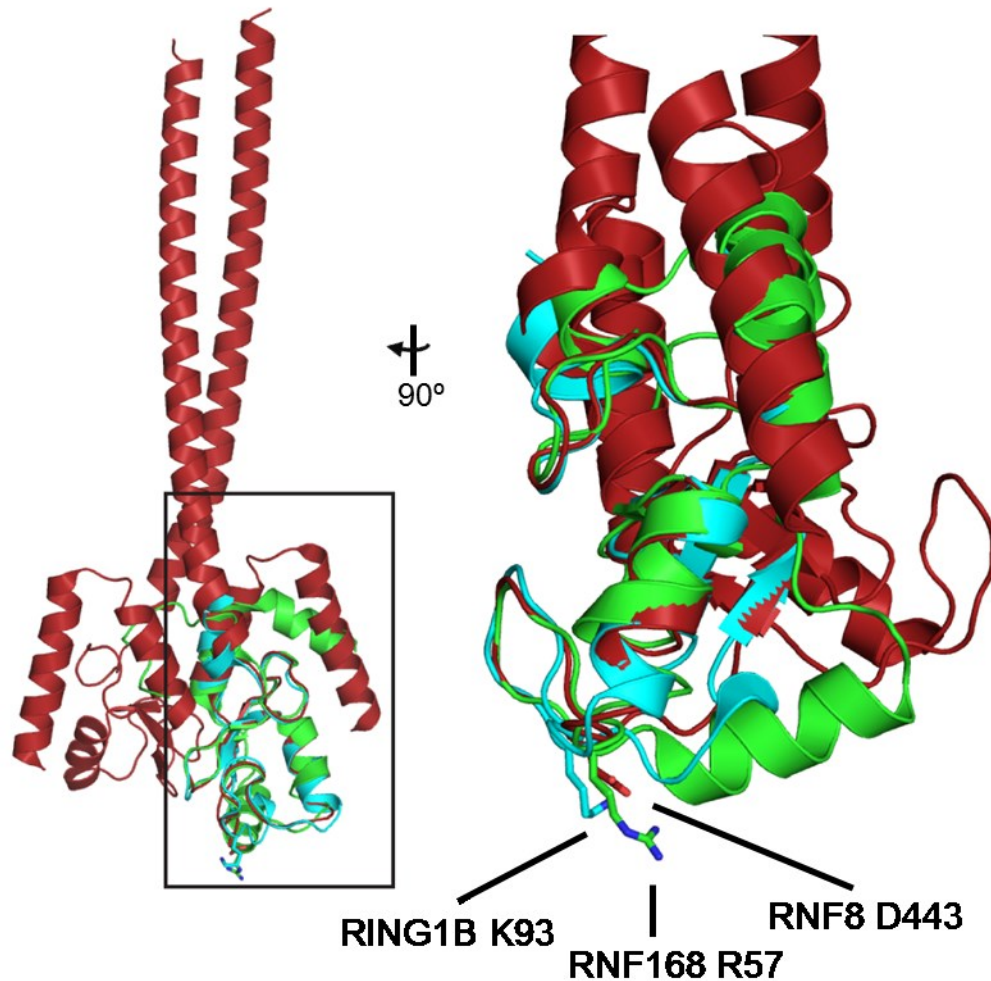


Figure 8. E3 RING residue position important for nucleosome recognition.

A positively charged residue at the bottom of a RING domain confers nucleosome binding, while a negatively charged residue inhibits it. PDBs: RNF8 (red) is 4ORH, RNF168 (green) is 3L11, RING1B (cyan) is 2CKL.

The corresponding residues are RNF168 R57, RING1B K93, and RNF8 D443. Interestingly, a positively charged residue at this site is key to the recognition of nucleosomal H2A/H2AX, as mutation of RNF8 negatively charged aspartic acid residue to a positively charged arginine residue

(D443R) allowed it to recognize H2A in the context of nucleosomes³². Conversely, the RNF168 (R57D) and RING1B (K93D) charge-reversal mutations inhibited their ability to recognize nucleosomal H2A. These mutations were shown to maintain their ubiquitination ability as a control and the necessity of this residue was also validated in human cells for the RNF168 mutation.

A number of less-characterized DDR factors are influenced by, or regulate RNF8, which affect downstream repair protein recruitment to DNA damage. JMJD2A is a lysine demethylase that removes the methyl groups from di- and tri-methylated H3K36 and H3K9, and also contains a tandem tudor domain that allows it to bind H4K20me2/ H4K20me3⁹⁵. L3MBTL1 is a Polycomb factor that interacts with H4K20me1 and H4K20me2⁹⁶. It has previously been shown that a yeast homolog of 53BP1 requires H4K20 methylation for proper DNA damage dependent recruitment^{97,98}. RNF8 ubiquitinates JMJD2A and L3MBTL1 upon DNA damage induction^{95,96} and in the case of JMJD2A, this leads to proteasomal degradation, preventing its demethylase activity. The RNF8-dependent ubiquitination of L3MBTL1 results in its removal from sites of DNA damage^{95,99}. The way in which it is removed may be through the RNF8-ubiquitination dependent recruitment of AAA-ATPase valosin-containing protein (VCP)⁹⁵. Release of L3MBTL1 from chromatin is accomplished through the ATPase activity of VCP. In all these ways, RNF8 is able to promote and prepare DSB sites for 53BP1 binding. Conversely, to moderate this and prevent over-ubiquitination at

sites of DSBs, the DUB OTUB2 uses its deubiquitinating activity to remove ubiquitin from L3MBTL1, which slows the DDR at an early stage after DNA damage⁹⁹.

Another demethylase, JMJD1C was recently characterized in terms of the DDR¹⁰⁰. JMJD1C interacts with RNF8 and RNF168, and is ubiquitinated by the latter in response to IR. The interaction between RNF8 and JMJD1C is independent of RNF8 E2-stimulating activity, as it is maintained with a RING-mutant RNF8¹⁰⁰. It was demonstrated that JMJD1C promotes the interaction of RNF8 with MDC1 by demethylating MDC1 at K45, which was necessary for the proper recruitment of RAP80/BRCA1, but not 53BP1 to DSBs. The region of JMJD1C that is required for the RNF8 interaction was mapped out, however the RNF8 region is still unknown and will be interesting to find out in the future.

An interesting and necessary phenomenon occurs in mitotic cells that have undergone DNA DSBs. They suppress repair to prevent dangerous telomere fusions that result in aneuploidy¹⁰¹⁻¹⁰³. The inhibition of the DDR, which prevents BRCA1, 53BP1, and RNF8 IR induced foci in mitosis, is effected through disruption of RNF8 recognition of phosphorylated MDC1 at T752^{101,103}. This is caused by the cell cycle-dependent phosphorylation of RNF8 T198 by cyclin-dependent kinase 1 (CDK1). A T198A RNF8 mutant resulted in a CDK1-insensitive RNF8. This allowed an interaction of the T198A mutant RNF8 with a MDC1 T752 phosphopeptide demonstrated by a pull down assay, regardless of CDK1

presence. Conversely, a phospho-mimic mutation, T198E created a RNF8 mutant unable to interact with the MDC1 phosphopeptide¹⁰¹. Orthwein et al. used these RNF8 mutants to validate the phosphorylation-dependent regulation of RNF8 in human cells. As expected the T198A CDK1 phospho-insensitive RNF8 mutant facilitated RNF8 recruitment to DSBs in both mitosis and interphase, compared to the interphase-only wild type RNF8¹⁰¹. Interestingly, it restored the more downstream BRCA1 recruitment to DNA DSBs in mitosis, but not 53BP1. The T198E RNF8 mutant was poorly recruited to sites of DSBs in both interphase and mitosis. Further, phosphorylation-mediated regulation of 53BP1 (at T1609/S1618) in mitosis was shown to account for the previously mentioned lack of recruitment rescue by RNF8 T198A¹⁰¹. The authors were able to use the dual RNF8 and 53BP1 alanine mutations that allow for mitotic DNA DSB repair to demonstrate that a lack of DDR suppression in mitosis leads to telomere fusions that cause detrimental aneuploidy.

A protein called B-cell lymphoma/leukemia 10 (BCL10) participates in the activation of the NF- κ B pathway¹⁰⁴. It was recently shown to be phosphorylated by ATM in response to DNA damage, and colocalize with DNA damage dependent γ H2AX foci. BCL10 also associates with RNF8, and this seems to be partially dependent on the RNF8 FHA domain. The authors offer the suggestion that RNF8 FHA may bind to BCL10 (T91) TQXF motif (known to be targets for phosphorylation)¹⁰⁴. RNF8 ubiquitinates BCL10 predominantly with K63 ubiquitin chains, which

requires the previously mentioned BCL10 phosphorylation. The group found that upon siRNA-mediated knockdown of BCL10 expression, the binding of RNF8 and Ubc13 was diminished. They conclude that “BCL10 presents Ubc13 to RNF8,” however the fact that Ubc13 and RNF8 efficiently bind *in vitro* (see Chapter 4), suggests that it is more likely that BCL10 disrupts association of either Ubc13 or RNF8 with another factor, which allows their subsequent binding.

A few studies have reported an interesting protein-protein interaction between Ubc13 and p53 involved in the DDR and transcription/translation regulation. These studies do not seem to have been followed by further research after their initial publications, however are still noteworthy. It was shown that Ubc13 regulates the subcellular distribution of p53 through its ubiquitination activity¹⁰⁵. There is an interaction between the C-terminus of p53 and Ubc13, which also requires either Mms2 or Uev1A (i.e. the functional E2 heterodimer). The proteasomal degradation of p53 is suppressed by K63 ubiquitination via Ubc13. This Ubc13-dependent ubiquitination also prevents p53 tetramerization (promotes monomeric), attenuates its transcriptional activity, and localizes it to the cytoplasm¹⁰⁵. Interestingly, but not surprisingly these Ubc13-dependent changes to the state of p53 are diminished upon IR, which likely reflects the need for their individual participation in the DDR. This is also likely due, in part, to p53-mediated downregulation of Ubc13 expression upon DNA damage¹⁰⁵. The same

group also found a p53/Ubc13 association on actively translating polysomes¹⁰⁶.

1.5 Pathogenic hijacking of RNF8 and other repair factors

Unfortunately we as humans, with all our highly evolved cellular systems, fight a continual battle with pathogens that try to use our warm, aqueous cellular environments for their own proliferation and survival. The advent of modern medicine in the 20th century saw the revolutionary discovery of antibiotics and vaccines, which were huge successes in arming humanity against deadly disease. However, there are still many known, and likely countless unknown (or new strains) of viruses in the world that are pathogenic to humans for which there are currently no vaccines. One such virus is a herpes virus called Epstein-Barr (EBV) has infected over 95% of the world's adults and infects resting B lymphocytes; this can cause continuous cellular proliferation^{107,108}. EBV is associated with a number of cancers such as gastric carcinoma, nasopharyngeal carcinoma, Hodgkin and non-Hodgkin lymphomas, Burkitt lymphoma, multiple sclerosis, and it is the primary cause of infectious mononucleosis^{107,108}. The EBV expresses a protein in the host involved in transcription and viral replication called BZLF1 that facilitates the transition from the latent to the lytic (virion-producing) stage of its life cycle, which is associated with the development of the aforementioned diseases^{108,109}. BZLF1 was shown to impair DNA DSB repair through prevention of the accumulation of RNF8 and 53BP1 at damaged sites. Largely through

immunoprecipitation and subcellular fractionation experiments, it was demonstrated that BZLF1 prevents RNF8 from binding MDC1, and its subsequent accumulation on chromatin¹⁰⁸. Interestingly this is not the only example of viral RNF8 manipulation. During infection, the herpes simplex virus-1 uses its own E3 ubiquitin ligase, ICP0, as bait that is first phosphorylated by cellular CK1, which causes RNF8 binding through its FHA domain¹¹⁰. This promotes RNF8 degradation, and contributes to enhanced viral replication, transcription and virion production.

It is clear that there is a wealth of data that highlights the very important roles that Ubc13 and RNF8 play in the DNA damage response, and cellular ubiquitin signalling. The data presented in this thesis represent multiple investigations into both the structure and functions of these important proteins, as well as the mode and consequences of small-molecule inhibition of their cooperative ubiquitination. It employs a wide variety of both biophysical and cellular techniques in order to provide thorough support for the hypotheses presented. A brief overview of the methodologies employed and overview of each chapter follows.

1.6 Methodology Overview

X-ray crystallography is a technique that allows for determination of a static macromolecular structure. The first step toward a structure is a pure, monodispersed protein or protein fragment. Flexible segments of a protein often present issues with crystallization and are therefore typically omitted from the design of a stable protein construct. Secondary structure

prediction software such as JPred¹¹¹ can be used to predict the boundaries of stable secondary elements such as alpha-helices or beta-sheets. The pure, monodispersed protein is then concentrated to a moderate to high concentration (~4-20 mg/mL) and added to different buffered conditions with a wide range of pH that contain various precipitants, such as salts, organic solvents and polymers of ethylene glycol (PEGs)¹¹². The precipitant and/or pH cause protein supersaturation, so that small protein aggregates, or nuclei form, which act as the basis for crystal growth. Once a protein is crystallized it is often cryo-protected, and flash frozen in liquid nitrogen to help prevent radiation damage and stabilize the crystal lattice. The frozen crystals are exposed to an X-ray beam, and the diffraction pattern of the X-rays diffracted by the electrons in the macromolecule is collected. The electron density distribution in the repeating unit of the crystal (unit cell), is calculated with a Fourier transform of the intensities and phases of the diffraction pattern¹¹². The electron density is then used to build a model of the macromolecule. Iterative changes to the model, or refinement, is then performed, which compares the observed structure factors (derived from the intensities) to those calculated by the model.

Small-angle X-ray scattering (SAXS) is a low resolution (~50-10 Å) solution technique that allows for assessment of the dynamics of macromolecular structures¹¹³. SAXS is a method that contrasts the average electron density of the bulk solvent with that of the

macromolecules of interest to derive a scattering signal. This scattering signal is the average of all of the random orientations of the macromolecule in solution¹¹³. Similar to X-ray crystallography, the starting sample of the macromolecule of interest should be monodisperse and homogeneous. This solution is exposed to X-rays and the resulting scattering curve can be analyzed in multiple ways. One important factor in determining whether the scattering curve should be used for further analysis is the degree of interparticle interference and aggregation. The occurrence of significant amounts of either of these is typically concentration-dependent and these effects preclude the data from further analysis¹¹³. Comparison of SAXS scattering curves from different samples can demonstrate large conformational changes of macromolecular domains, relative to one another. The interdomain motions of macromolecules can also be modeled using molecular dynamics software, for example BILBOMD¹¹⁴, and a minimal ensemble (MES) can be determined. In solution the macromolecule has many conformations, and a MES is a weighted average of the individual scattering curves of the most probable components of the multiconformational population¹¹³.

Surface plasmon resonance (SPR) is a technique that allows measurement of affinities and kinetics of binding interactions between macromolecules¹¹⁵. When incident light strikes a gold surface at a particular angle, some of the photons are absorbed by and excite the electrons in the gold, which is called plasmon resonance. The angle that

allows for surface plasmon resonance is dependent on the refractive index of the medium near the gold surface; therefore immobilization of a macromolecule to the gold surface changes the angle necessary for SPR to occur, which can be monitored by a detection of the reflected light¹¹⁵. In an SPR experiment, a solution containing an analyte macromolecule flows over the gold surface that has the immobilized probe macromolecule and the binding of the two macromolecules results in a refractive index increase. The change in the angle required for SPR is measured as response units (RUs) and is sensitive to analyte binding¹¹⁵. The binding kinetics and affinities of the analyte macromolecule to the immobilized macromolecule can therefore be measured using SPR.

High content screening microscopy (HCS) is a high-throughput technique that allows for automated image acquisition of immunofluorescently labeled cells. First the cells are seeded into a high performance 96 well glass bottom dish that is made so that the glass is highly uniform in its dimensions. The system uses a laser-based autofocus, which is calibrated by the user at the outset of the experiment. Upon detection of the bottom of the glass, and bottom of the well of one well, the system can detect the DAPI-stained nuclei of the cells. After calibration of the autofocus, the user can setup a program to acquire images along a grid with defined spacing between images for each well. A z-stack acquisition can be chosen, which varies the depth of the focal plane by small user-defined increments that are combined to create an

image that contains a greater depth of information. The program will then apply the same detection and acquisition for each well specified in the 96 well plate. Multiple wavelengths can be chosen for different fluorescently labeled probes.

Chapter 2 Overview: Assigning the RNF8 coiled-coil amino acid register

Our lab previously solved the X-ray crystal structure of the RNF8 RING domain dimer with a novel extended coiled-coil bound to the E2 heterodimer Ubc13/Mms2, and showed the importance of this complex for K63 ubiquitin chain formation *in vitro*. At the time this was the first RNF8 structure determined, but the resolution was limited to 4.8 Å. Due to the low resolution we could not confidently assign the positions of the amino acid residues in the extended coiled-coil. To solve this problem we generated a selenomethionine derivative of RNF8, and crystallized it in the same space group with the bound E2, Ubc13/Mms2. From these data an anomalous difference map was rendered, which clearly showed the position of selenomethionine 393 and this allowed us to correctly assign the amino acid register of the RNF8 coiled-coil.

Chapter 3 Overview: Covalent inhibition of Ubc13

We uncover the mechanism for Ubc13 inhibition by two small-molecule compounds, which reveals a small pocket at the active site that is unique to Ubc13 among the family of E2 enzymes, the integrity of which is required for inhibition by NSC697923. Based on our structural data, we

design a mutant that resists NSC697923 *in vitro* but maintains the ability to build ubiquitin chains. Ubc13-knockout mouse embryonic fibroblasts (MEFs) retrovirally reconstituted with this mutant are significantly resistant to inhibition of NF- κ B and DNA damage signaling by NSC697923 compared to a wild type control, demonstrating that the selective inhibition of Ubc13 by NSC697923 is primarily responsible for the inhibition of cellular signaling. Our work uncovers aspects of the active site structure of Ubc13 that are unique within the family of ubiquitin conjugating enzymes, which can be targeted for the development of selective small molecule inhibitors of this critical regulator of key cancer-associated signaling pathways.

Chapter 4 Overview: E2-stimulation by the E3 ligase RNF8

We investigate the RING E3 ligase RNF8 and its role in activating/increasing the catalytic conjugating activities of the E2 enzyme Ubc13. Based on our previous work described in Chapter 2, we hypothesized that RNF8 stimulates the ubiquitination abilities of Ubc13/Mms2 by holding ubiquitin in a folded-back conformation, which optimizes the orientation of the thioester linkage for nucleophilic attack by an incoming lysine, resulting in increased catalysis. To address our hypothesis we made a stable complex of the RNF8 RING dimer, bound to Ubc13 with a covalently linked ubiquitin attached (Ubc13~Ub) and determined the X-ray crystal structure to 8.3 Å resolution. The optimized ubiquitin position mediated by RNF8 also occurs in solution as

demonstrated through small-angle X-ray scattering (SAXS) data, which agrees well with the crystal structure. In order to investigate the importance of the E3-mediated E2-stimulation via ubiquitin conformational selection, we created a point mutation that severely disrupts the ability of RNF8 to activate the Ubc13 conjugating activity *in vitro*. We show that the binding of RNF8 to Ubc13 is not significantly affected using surface plasmon resonance (SPR). Further we stably integrate both this mutant and wildtype RNF8 into RNF8 knockout MEFs and perform IR induced foci formation experiments. We show that the DDR is dependent on the RNF8 ability to stimulate Ubc13 E2 conjugating activity through the donor ubiquitin conformational selection.

Chapter 5 Overview: General Discussion

This final chapter will discuss interesting possibilities for further investigations of the work presented in this thesis. The discussion will also highlight how these results fit into the larger picture of cellular signalling and human disease.

Chapter 2

¹Assigning the RNF8 coiled-coil amino acid register

¹This chapter forms part of the publication: Campbell, S. J., Edwards, R. A., Leung, C. C., Neculai, D., Hodge, C. D., Dhe-Paganon, S. & Glover, J. N. Molecular insights into the function of RING finger (RNF)-containing proteins hRNF8 and hRNF168 in Ubc13/Mms2-dependent ubiquitylation. *J. Biol. Chem.* **287**, 23900-23910, doi:10.1074/jbc.M112.359653 (2012).

2.1 Introduction

Our initial studies on the interaction between RNF8 and Ubc13 stemmed from the desire to see how RING E3s interacted with E2 conjugating enzymes. This led us to look at the RING E3s RNF8 and RNF168, which were both reported to bind and function with the E2 Ubc13. We found that a RNF8 construct from amino acid residues 345-485 bound the Ubc13/Mms2 heterodimer and increased its catalytic activity²⁹. In contrast, we did not observe stable interactions between Ubc13/Mms2 and either of two RNF168 RING constructs as assessed via size exclusion chromatography, and neither RNF168 protein was able to stimulate Ubc13 catalytic activity.

We found predicted coiled-coil domains adjacent to the RING domains in both RNF8 and RNF168 that mediated homodimer formation. We were able to solve a low resolution crystal structure of RNF8₃₄₅₋₄₈₅/Ubc13/Mms2 to 4.8 Å resolution. At the time, this was the first crystal structure that contained the RING domain of RNF8. Higher resolution data was unattainable, which presented a problem. The RNF8 construct used contained an extended coiled-coil N-terminal to the RING domain²⁹. At 4.8 Å resolution, the side chains and main chain of the protein appear as curving cylinders or tubes of electron density. Due to the more intricate features of the RING domain, and the pairs of zinc ions seen in an anomalous difference map, the approximate positions of these amino acids could be determined.

The coiled-coil presented a greater challenge with respect to amino acid placement, as there were no identifiable ions, and fewer discernible features (i.e. no turns). Due to these limitations the positions of the residues in the coiled-coil domain remained obscure, and confidence in how to build a model to fit the density remained low. The solution was to make a selenomethionine derivative of the RNF8 construct with the goal of exchanging the natural sulphur atoms for selenium atoms in the methionine residues (see Materials and Methods for more details) and to crystallize it with Ubc13/Mms2. There are three methionine residues in the RNF8₃₄₅₋₄₈₅ construct. The first is at position 351, the second at 382, and the third at the end of the coiled-coil domain where the helices transition into the RING domains at position 393²⁹. Generating selenomethionine derivative crystals is routinely used for phasing novel structures, however here we demonstrate it can also be used in combination with partial molecular replacement to determine amino acid placement in low resolution structures.

2.2 Results

2.2A: A selenomethionine derivative of RNF8

To make the initial RNF8 coiled-coil, alpha-helices were first built in Coot and rigid body refined with Phenix, which means the constructed alpha-helices were fixed as one rigid body during the refinement¹¹⁶. These alpha-helices were then loaded into a program called Coiled-coil Crick Parameterization¹¹⁷, which allowed adjustment of the coiled-coil

parameters to create an ideal coiled-coil. This was then rigid body refined and checked against the density and statistics. This process was repeated iteratively until an idealized coiled-coil was found that best fit the electron density, corresponding to the lowest R-factor after refinement. Coiled-coils contain a repetitive seven residue pattern called a heptad, in which residue types (e.g. hydrophobic) occur at regular positions. This repetitive nature allowed the development of prediction algorithms that calculate the probability of a coiled-coil through identification of the heptad repeat in a protein sequence. An example of one is Paircoil2, which uses a known two-stranded coiled-coiled-coil sequence database to calculate the probability of a given amino acid to pair with any other amino acid at each position (a-g) in the heptad repeat of a coiled-coil^{118,119}. These probabilities are then applied to the user-input sequence, and a predicted coiled-coil region and register is output (Figure 9). The coiled-coil register of RNF8 shows that there are three methionine residues present at positions “a” (351), “d” (382), and “a” (393) (Figure 10a). This meant that a selenomethionine derivative RNF8 was possible, and a good signal from one methionine could reveal the coiled-coil register.

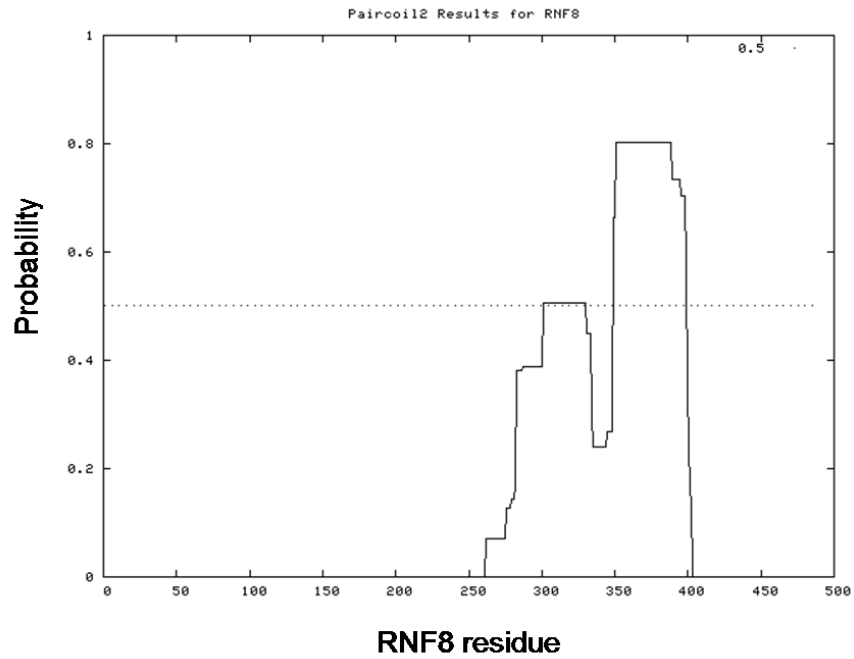


Figure 9. Paircoil2 prediction of RNF8 coiled-coil domain.

The crystallized coiled-coil from residues 345 to 400 is predicted with a high probability. The default probability threshold is 0.5 (dotted line).

position of methionine 393, we applied the heptad prediction (Figure 10a) to the RNF8 sequence and were able to determine the remaining amino acid positions and assign them to our model.

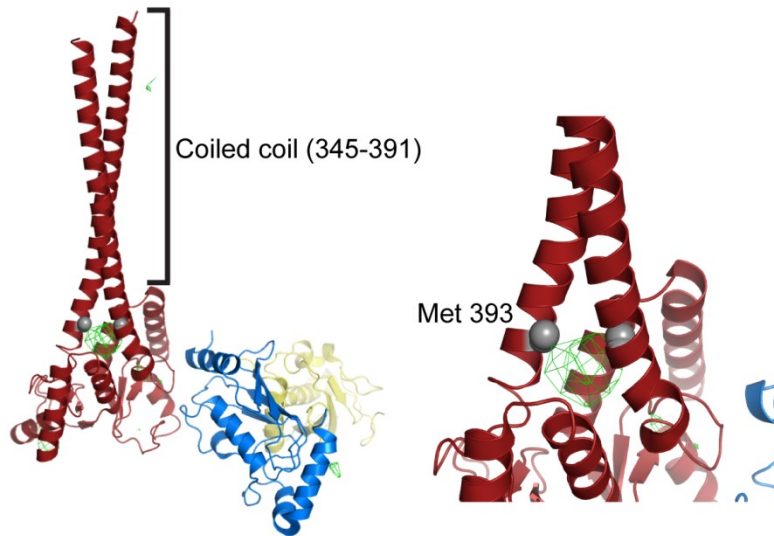


Figure 11. Crystal structure of the selenomethionine derivative RNF8₃₄₅₋₄₈₅ in complex with the Ubc13/Mms2 heterodimer.

The position of the methionine 393 alpha carbons are shown as gray spheres in both RNF8 protomers (red). The anomalous difference density is colored green and contoured to 3σ . Ubc13 is colored blue and Mms2 is colored yellow.

2.3 Discussion

The selenomethionine derivative RNF8₃₄₅₋₄₈₅/Ubc13/Mms2 structure allowed correct determination of the amino acid register of RNF8. This was later validated by a high resolution (1.9 Å) structure of a slightly shorter RNF8 construct (351-485) determined by Mattioli et al.³², although

its N-terminal section deviates from our coiled-coil (Figure 12). The shorter RNF8 construct starts on a coiled-coil heptad repeat position “a” (Met 351), while our longer construct starts on position “b” (Gln 345) (Figure 10). Classically, the a and d positions are considered the interacting residues in a two-stranded coiled-coil, which are often hydrophobic¹²⁰. The shorter RNF8₃₅₂₋₄₈₅ construct should therefore be able to make a stable interaction at Met 351, suggesting that this is likely not the reason for the N-terminal fray. The crystal packing, however, demonstrates that a C-terminal alpha-helix in the RING domain of one RNF8 homodimer packs between the frayed coiled-coil alpha-helices of another (Figure 13). This interaction is likely a crystallization artifact favored due to stable crystal packing and explains the frayed coiled-coils.

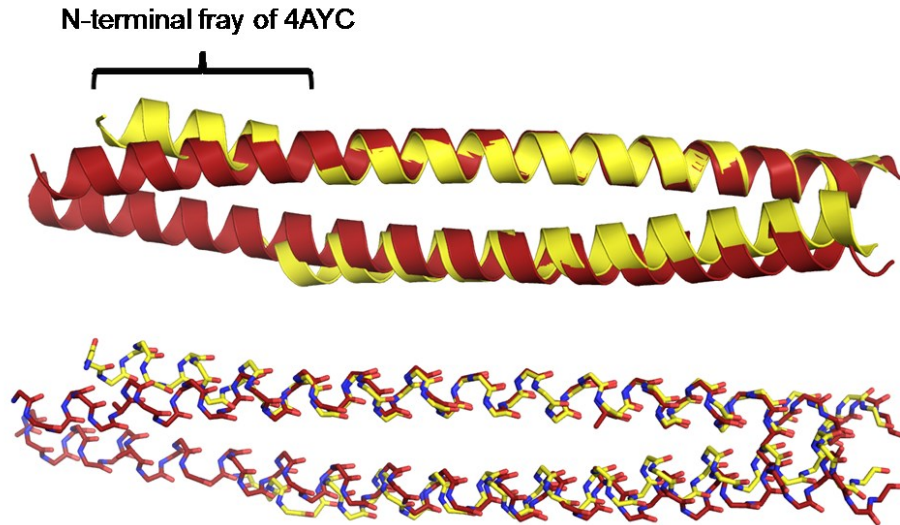


Figure 12. Coiled-coil overlay of low resolution RNF8₃₄₅₋₄₈₅ with high resolution RNF8₃₅₁₋₄₈₅.

Superposition of the coiled-coil of the shorter RNF8₃₅₁₋₄₈₅ onto our longer RNF8₃₄₅₋₄₈₅ reveals the unraveling of the coiled-coil in the shorter structure. RNF8₃₄₅₋₄₈₅ is colored red. RNF8₃₅₁₋₄₈₅ (PDB:4AYC) is colored yellow.

The use of a selenomethionine derivative was possible because each of the three methionines in the RNF8₃₄₅₋₄₈₅ construct is at least 10 residues separated in the primary sequence. This means that an anomalous signal for any of them should unambiguously reveal its position in the coiled-coil electron density and allow determination of the amino acid register. Indeed, Met 393 at the base of the coiled-coil gave a large anomalous peak, while there was no density for the other more N-terminal two. Due to the transition from coiled-coil to RING at the Met 393 position, there is more space between the alpha helices in the coiled-coil. This extra space may allow the sidechains of Met 393 to be in close contact (which contain

the selenium atoms), whereas the sidechains of the other two methionines are predicted to point away from each other (parallel) based on coiled-coils of other structures such as the GCN4 leucine zipper that have two helical turns every seven residues or heptad repeat ($7/2$ periodicity)¹²⁰. Thus it is possible that the presence of an anomalous peak corresponding to the Met 393 residues appeared because they merge in the low resolution map causing an increased signal to noise. Indeed, this is supported by the high resolution structure of RNF8, which shows that the sidechains of Met 382 are further away from each other than those of Met 393.

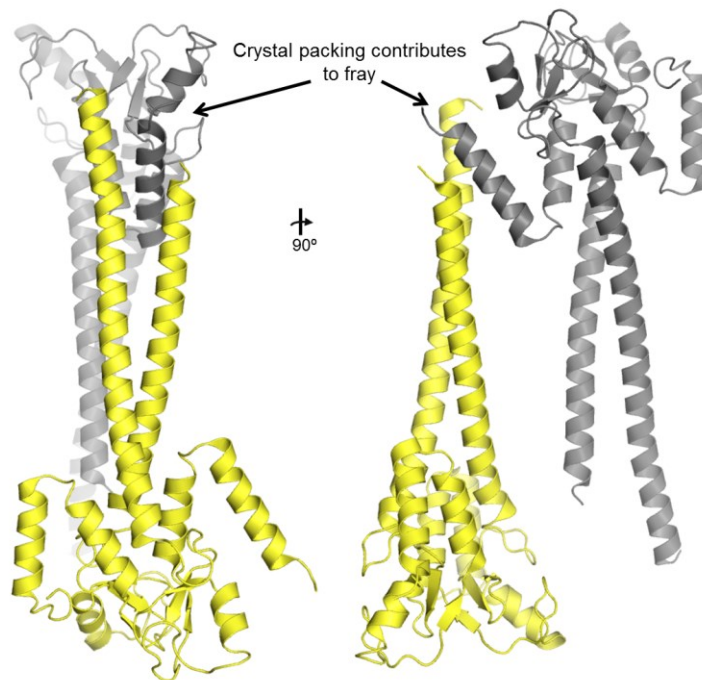


Figure 13. Crystal packing of the shortened RNF8₃₅₁₋₄₈₅ causes the coiled-coil to fray.

The C-terminus of a symmetry related RNF8₃₅₁₋₄₈₅ homodimer (gray) packs between the coiled-coils of another (yellow). PDB:4AYC.

This method of combining partial molecular replacement solutions with selenomethionine derivative data could be employed in the future for determination of amino acid sequence register in low resolution structures that contain sufficient methionine residues. The increasing complexity of protein-protein interactions will continue to fuel efforts to crystallize larger, more intricate protein complexes. This will likely increase the need for strategies to solve low resolution crystal structures as well.

2.4: Materials and Methods

2.4A: Selenomethionine protein production

A starter culture was commenced by inoculation of LB medium with BL21 (DE3) E.coli cells harboring the RNF8₃₄₅₋₄₈₅ DNA in a pGEX6P1 (GST) vector, and growth at 37°C overnight. Four 6 litre flasks containing one litre of LB each were inoculated with the starter culture and grown until an optical density at 600 nm wavelength (OD₆₀₀) of approximately one. These cells were then pelleted and resuspended in M9 minimal medium. The M9 minimal medium contained 90 mM Na₂HPO₄, 22 mM KH₂PO₄, 8.6 mM NaCl, 18.6 mM NH₄Cl, 200 mM MgSO₄, 200 mM CaCl₂, 4% glucose, and 100 mg/mL of ampicillin. The cells were pelleted and washed twice with minimal medium to remove residual LB. The suspended cells were then used to inoculate one litre of minimal medium in a 6 litre flask, and this culture was grown to OD₆₀₀ of approximately one. At this point the amino

acids selenomethionine (50 mg/L), lysine-HCl (100 mg/L), threonine (100 mg/L), phenylalanine (100 mg/L), leucine (50 mg/L), isoleucine (50 mg/L), and valine (50 mg/L) were added to inhibit endogenous methionine synthesis and incorporate selenomethionine upon protein expression induction. The cultures were placed on a shaker for 30 minutes, prior to induction. The cells were induced to express the GST-RNF8 construct by the addition of 0.5 mM of isopropyl- β -d-thiogalactopyranoside (IPTG). The cell cultures were grown at 22°C overnight (17-18 hours) and harvested. The protein purification, complex formation, and crystallization has been previously described²⁹.

2.4B Structure determination

The non-derivative RNF8₃₄₅₋₄₈₅/Ubc13/Mms2 structure (PDB: 4ORH) was used as a search model for molecular replacement. Four cycles of rigid body refinement were completed in PHENIX¹¹⁶ and an anomalous map was calculated. Data statistics in Table 1.

Table 1. Data Collection and refinement statistics of SeRNF8/Ubc13/Mms2

	Se-Met RNF8/Ubc13/Mms2
Data Collection	
Space Group	P42212
Cell Dimensions	
a,b,c (Å)	204.0, 234.0, 234.2
α,β,γ (°)	90, 90, 90
Resolution (Å)	200.-9.0
² R _{sym}	13.5 (35.8)*
I/σI	7.2 (2.66)*
Completeness (%)	73.1 (70.3)*
Redundancy	4.3 (4.4)*

*Values in parentheses' are for highest resolution shell

Chapter 3

¹Covalent inhibition of Ubc13 affects ubiquitin signaling and reveals active site elements important for targeting

¹A version of this chapter has been published: Hodge, C. D., Edwards, R. A., Markin, C. J., McDonald, D., Pulvino, M., Huen, M. S., Zhao, J., Spyropoulos, L., Hendzel, M. J. & Glover, J. N. Covalent Inhibition of Ubc13 Affects Ubiquitin Signaling and Reveals Active Site Elements Important for Targeting. *ACS Chem Biol* **10**, 1718-1728, doi:10.1021/acscchembio.5b00222 (2015).

3.1 Introduction

Protein ubiquitination is a major post-translational system that regulates diverse aspects of eukaryotic intracellular signaling. The targeting of ubiquitin to specific proteins involves the initial ATP-dependent activation of ubiquitin by E1 enzymes that result in the thioester linkage of the C-terminal carboxylate of ubiquitin to the active site cysteine of the E1⁵⁴⁻⁵⁷. The activated ubiquitin is next transferred to the active site cysteine of any one of a number of ubiquitin conjugating enzymes (E2s), of which there are ~34 in the human genome^{121,122}. Most E2s function in cooperation with E3 proteins that bind and activate the E2 and recognize specific protein targets for ubiquitination^{29,74,75,123}.

The diverse effects of protein ubiquitination are driven in part by different forms of ubiquitin chains that can be linked to target proteins^{37,52,84}. Chains in which the ϵ -amino group of Lys63 of one ubiquitin is joined to the C-terminal carboxylate of the next ubiquitin via an isopeptide bond (Lys63-linked chains) have been shown to play especially critical roles in NF- κ B signaling¹²⁴⁻¹²⁶ and the DNA damage response (DDR)^{20,36}. The formation of these chains is specifically catalyzed by a specialized ubiquitin conjugating enzyme (E2) complex composed of the canonical E2, Ubc13 (also known as Ube2N), together with one of either of two E2-like ubiquitin enzyme variant (Uev) proteins, Uev1a or Mms2 (also known as Ube2V1 and Ube2V2, respectively)^{28,29}. The Uev proteins bind the incoming acceptor ubiquitin, positioning its Lys63 for attack on the

thioester of the donor ubiquitin covalently linked to the active site cysteine of Ubc13. The attack of the incoming lysine likely results in an oxyanion thioester intermediate that is thought to be stabilized by a conserved asparagine (Asn79 in Ubc13)⁷². This asparagine has also recently been implicated in maintaining the structural integrity of the Ubc13 active site loop (Ala114-Asp124)¹²⁷. Further, substrate lysine pK_a suppression and deprotonation contribute to Ubc13 catalysis^{71,128}.

The finding that the NF-κB pathway is constitutively activated in many forms of diffuse large B-cell lymphomas (DLBCLs) has driven efforts to develop small molecule inhibitors of this pathway. Recently, two independent reports^{125,126} have uncovered structurally related NF-κB inhibitors that biochemically target Ubc13. The first demonstrated that NSC697923 (2-[(4-methylphenyl)sulfonyl]-5-nitrofurane) inhibits Ubc13 and NF-κB activation, as well as the growth and survival of germinal center B-cell-like and activated B-cell-like DLBCLs¹²⁶. In addition, this compound was also shown to inhibit ubiquitin-dependent DNA damage signaling but not DNA damage-induced γH2AX foci formation, consistent with the specific targeting of Ubc13 in the nucleus. Another compound, BAY 11-7082 ((2*E*)-3-[(4-methylphenyl)sulfonyl]prop-2-enenitrile), previously thought to be a protein kinase inhibitor¹²⁹, has also been shown to inhibit Ubc13 through covalent modification of the active site cysteine¹²⁵. BAY 11-7082 was shown to inhibit not only Ubc13 but also other E2 enzymes as well as the proteasome. In contrast, NSC697923 was found to be specific

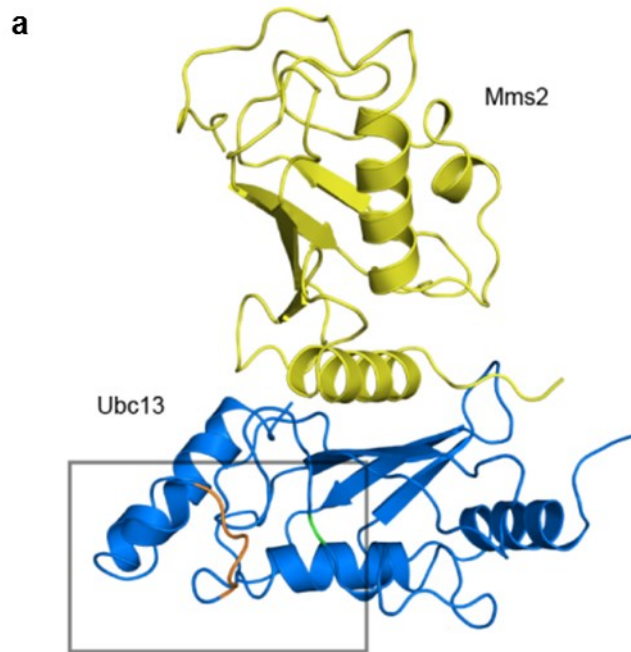
for Ubc13 in *in vitro* ubiquitination assays¹²⁶, suggesting that this compound might provide a more attractive lead toward the development of a targeted Ubc13 agent.

Here, we present the structures of Ubc13 inhibited by both NSC697923 and BAY 11-7082. The structures reveal that both inhibitors act via the covalent modification of the active site cysteine through a Michael addition¹²⁵. Interestingly, the cysteine adduct docks into an adjacent cleft that is not present in many other ubiquitin conjugating enzymes. To examine the role of this cleft in inhibition, we created a Ubc13 mutant in which the cleft is obscured by a change in the active site loop to a conformation that resembles that observed in the NSC697923-resistant homologue, Ubch5c. We show that the mutant is competent to build Lys63-linked polyubiquitin chains and is resistant to NSC697923 inhibition, but not to BAY 11-7082. Using this mutant, we conclusively demonstrate that inhibition of DNA damage and NF- κ B signaling by NSC697923 in mammalian cells is primarily due to Ubc13 inhibition. Our approach provides a means for future development of NSC697923 derivatives that exploit the unique Ubc13 binding cleft while alleviating overall cellular toxicity. Further, novel Ubc13 inhibitors can more effectively be discovered through the use of the mutant as a counter screen to identify compounds that exploit the unique Ubc13 binding cleft.

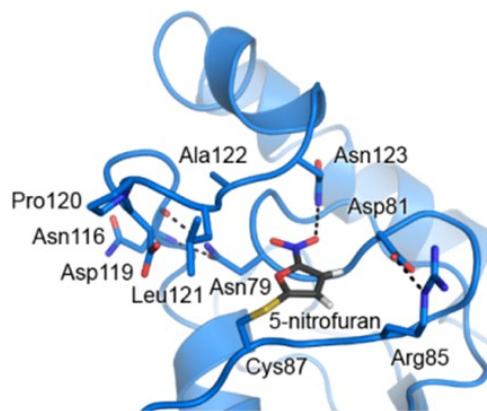
3.2 Results

3.2A: Ubc13 covalent inhibitors bind to a groove near the active site

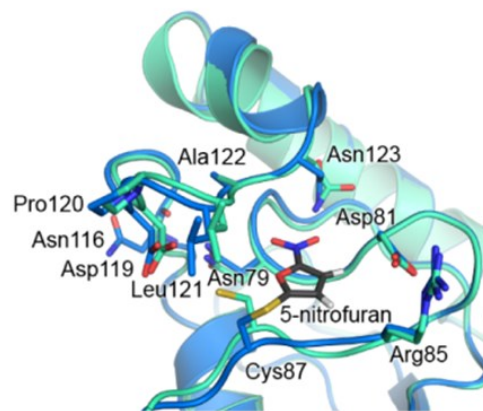
To understand how NSC697923 and BAY 11-7082 interact with and inhibit Ubc13, we determined the crystal structures of these compounds bound to Ubc13/Mms2 to 1.35 Å and 1.5 Å resolutions, respectively (Figure 14a-e). NSC697923 reacts with the sulfhydryl group of Cys87 through a Michael addition (Figure 14f), resulting in the addition of a 5-nitrofuranyl moiety to the Cys87 sulfur atom (Figure 14b and Figure 15a,b). NSC697923 also reacts with the free sulfhydryl of β -mercaptoethanol in a pH-dependent reaction that can be monitored via absorbance at 380 nm (Figure 16a,b). The 5-nitrofuranyl group is packed into a cleft leading to Cys87, the walls of which are composed of the residue 114-124 loop on one side, and the residue 81-85 turn on the other side (Figure 16c). The packing of this group within the cleft is largely hydrophobic with a single hydrogen bond between the nitro group and the side chain of Asn123. The conformation of Ubc13 is largely unchanged by reaction with the inhibitor, except for a 1.8 Å shift of Cys87 to accommodate the 5-nitrofuranyl.



b



c



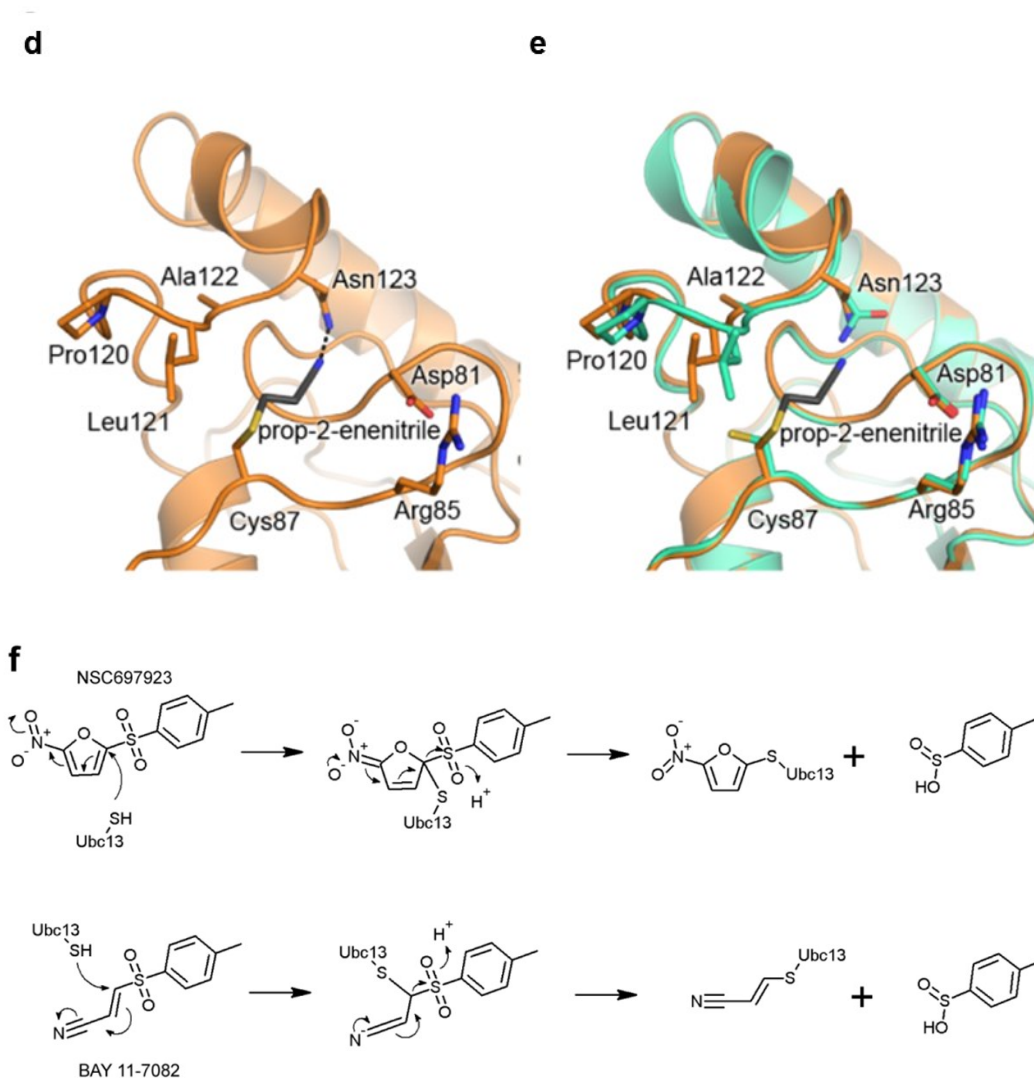
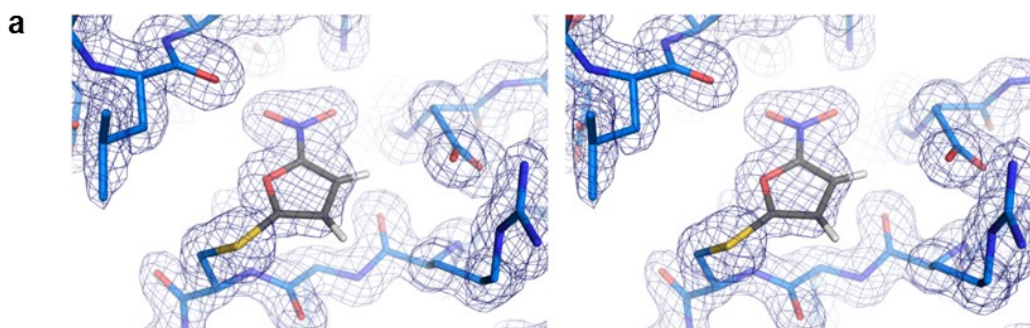


Figure 14. NSC697923 and BAY 11-7082 covalently modify the Ubc13 active site.

(a) Overview of Ubc13 (blue)/Mms2 (yellow) bound by the 5-nitrofuran moiety of NSC697923. The active site is boxed with the 114-124 loop in orange and the Cys87 region in green (Protein Data Bank accession 4ONM). (b) Active site view of Ubc13 bound by the 5-nitrofuran moiety of NSC697923. (c) Overlay of wild type Ubc13, PDB 1J7D (green-cyan), and 5-nitrofuran-bound Ubc13. (d) Active site view of Ubc13 bound by the prop-2-enitrile moiety of BAY 11-7082 (PDB 4ONN). (e) Overlay of wild type Ubc13 and prop-2-enitrile bound Ubc13. In panels (b) – (e), the view is rotated 90° from the orientation in (a). (f) Mechanisms of covalent attachment by NSC697923 and BAY 11-7082.

Similarly, BAY 11-7082 reacts with the sulfhydryl group of Cys87 through a Michael addition¹²⁵ (Figure 14f), which leaves a prop-2-enenitrile moiety on the Cys87 sulfur atom (Figure 14d and Figure 16d). The electron density shows that the prop-2-enenitrile adduct is directed toward Asn123 forming a hydrogen bond, positioned within the same groove as the 5-nitrofuranyl moiety of the NSC697923 complex. The electron density suggests that there may also be a proportion of Ubc13 in these crystals which are unmodified or where the adduct is disordered (Figure 16d). As in the NSC697923 complex, there is little movement of residues in the BAY 11-7082 structure compared to the uninhibited structure; however, unlike the NSC697923 complex, there is no shift in the main chain near Cys87 induced by reaction with the BAY 11-7082 inhibitor (Figure 14e).



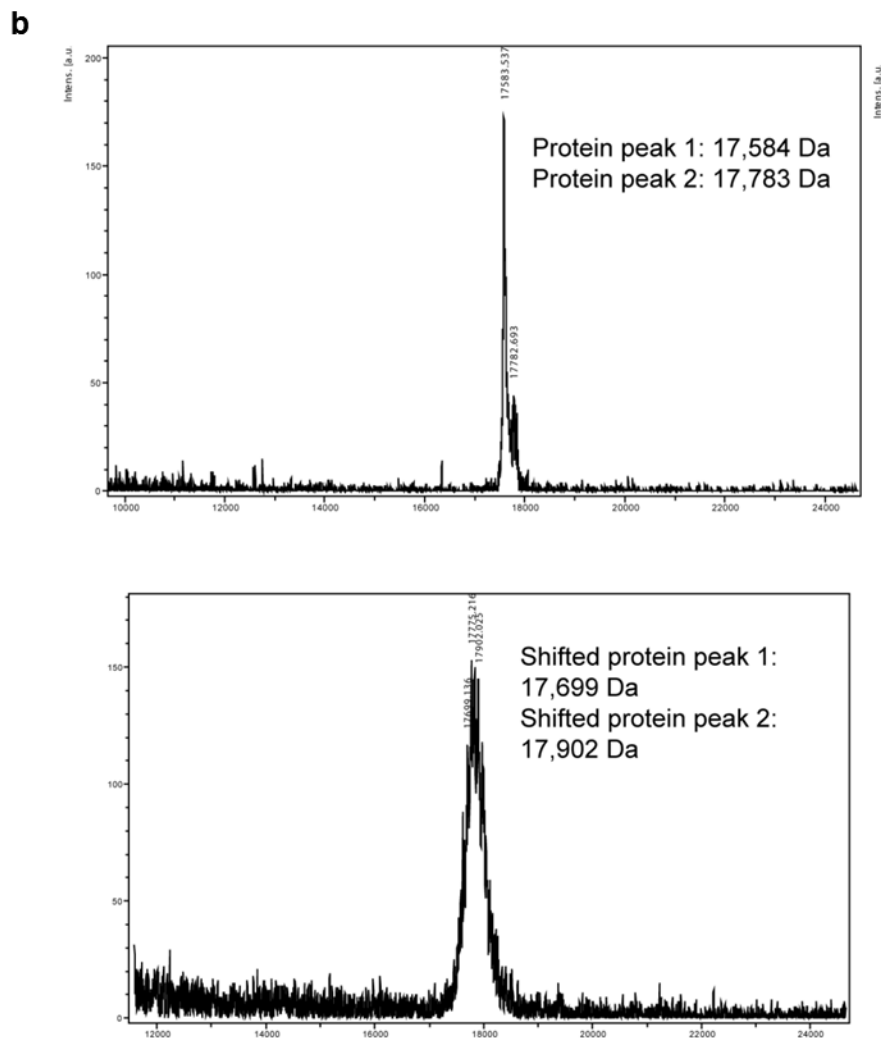
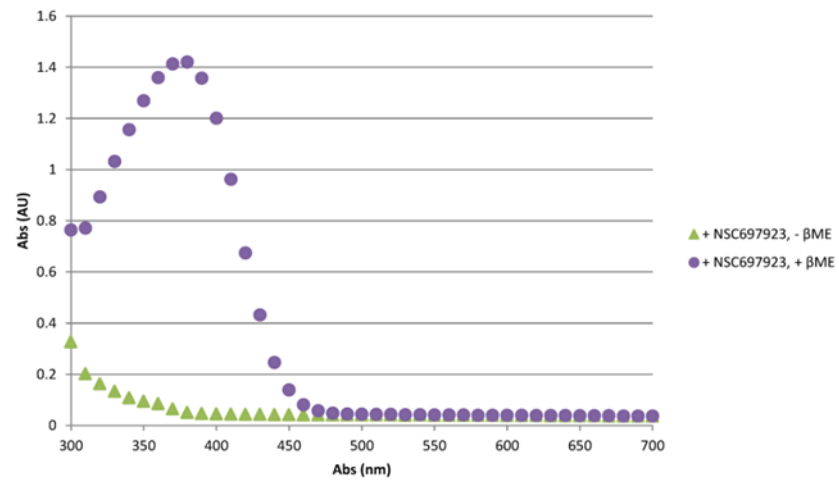


Figure 15. NSC697923 leaves a 5-nitrofuranyl adduct on Ubc13 Cys87.

(a) Electron density (1.35 Å resolution, 2Fo-Fc map contoured to 1.0 σ) of the 5-nitrofuranyl moiety attached to the cysteine 87 gamma sulfur atom of Ubc13. Image is in stereo. (b) MALDI-TOF analysis of Ubc13 without (left panel) or with NSC697923 (right panel). 4% DMSO was present in both samples. The difference in the molecular weight of the reacted and unreacted Ubc13 ($17,699 - 17,584 = 116 \text{ g mol}^{-1}$, $17,902 - 17,783 = 119 \text{ g mol}^{-1}$) is within $\pm 8 \text{ g mol}^{-1}$ of the expected mass change due to addition of a 5-nitrofuranyl adduct (112 g mol^{-1}) on Cys87, as measured by a Bruker Ultraflex MALDI TOF/TOF.

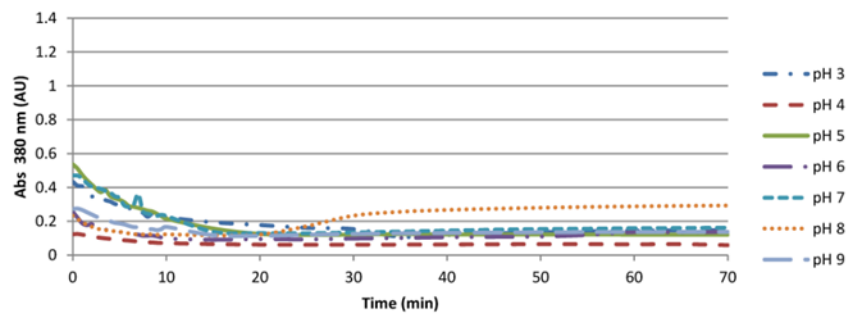
a

Wavelength scan of NSC697923 and β ME reaction

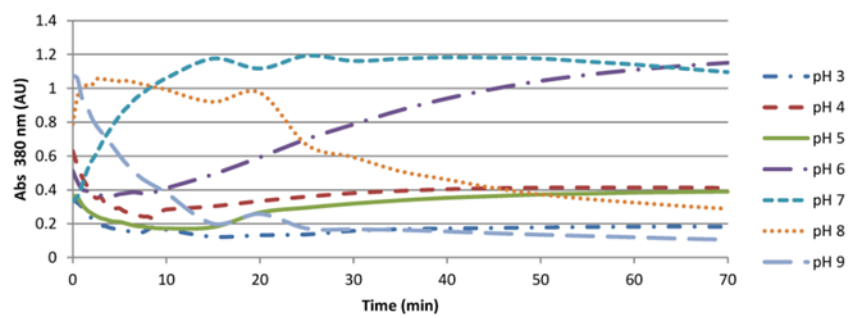


b

NSC697923 at varying pH



β ME and NSC697923 at varying pH



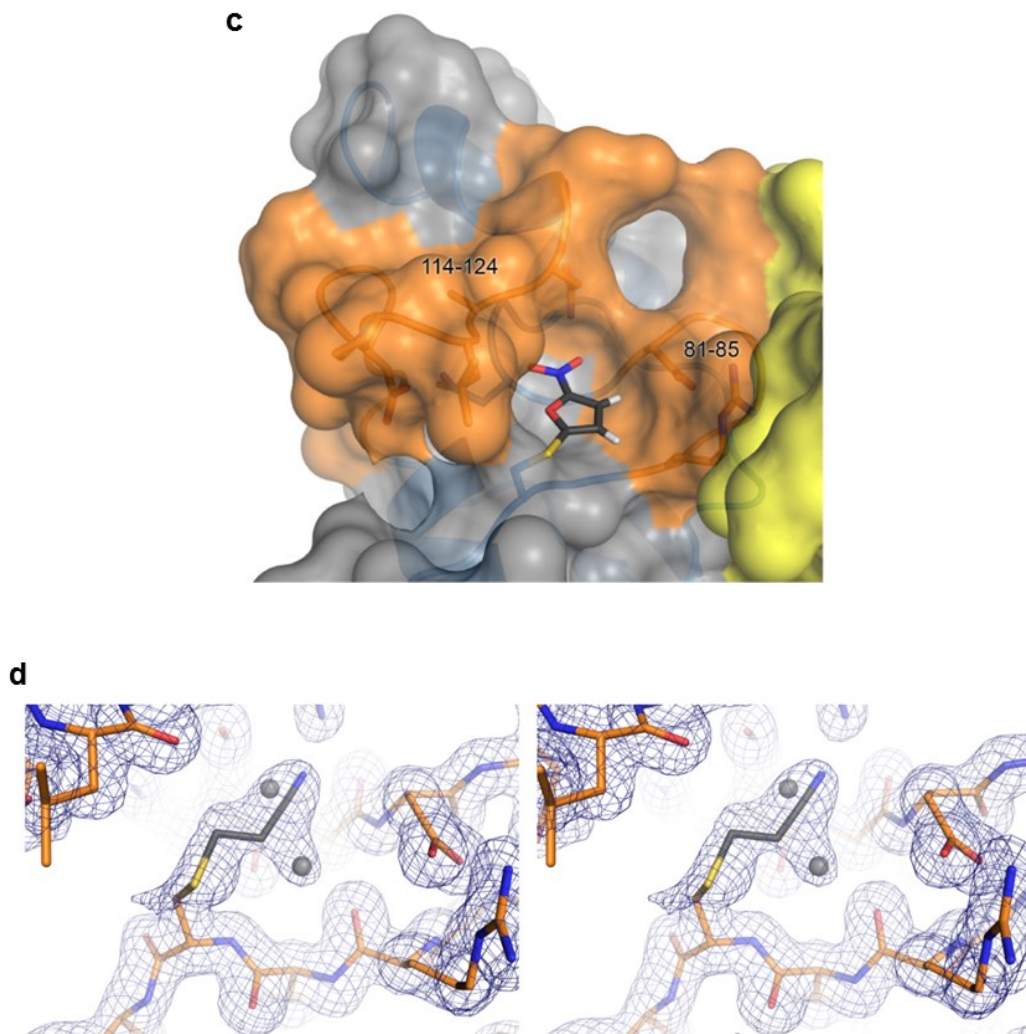


Figure 16. NSC697923 reacts with β ME and BAY 11-7082 leaves a prop-2-enitrile adduct on Ubc13 Cys87.

(a) A full wavelength scan of the reaction between NSC697923 and β -mercaptoethanol shows a product formed that absorbs at 380 nm compared to the control. (b) The reaction rate between β ME and NSC697923 increases with increasing pH (bottom panel). Control solutions are shown in the top panel. (c) Ubc13 contains a groove formed by the loop 114-124 on the left and the 81-85 turn on the right (orange), in which the 5-nitrofuranyl moiety is nestled. Ubc13 is shown as surface representation with cartoon underneath. Mms2 surface is yellow. (d) Electron density of BAY 11-7082 prop-2-enitrile adduct in the vicinity of Ubc13 Cys87 at 1.5 Å resolution, contoured to 1.0 σ . The electron density is interpreted as a mix of conformations. In one, the prop-2-enitrile moiety is attached to the Cys87 γ sulfur atom, in the second, the adduct is not visible in the cleft and instead two waters are present (gray spheres)

that are also observed in other unmodified structures. The image is in stereo.

The two inhibitors are similar in that they both contain a tosyl group that is released as a result of the reaction (Figure 14f). We wondered if the tosyl group might also play a role in the initial binding of the inhibitors prior to reaction. We tested the ability of NSC697923 to bind to a nonreactive Ubc13 mutant containing a Cys-Ser substitution at the active site by NMR. Comparison of the ^{15}N HSQC spectra of the C87S mutant incubated with 250 mM NSC697923 compared to a Ubc13^{C87S} + DMSO control revealed no significant shifts in any backbone amides, suggesting there is little if any specific prereaction binding of the compound near the active site (Figure 17a).

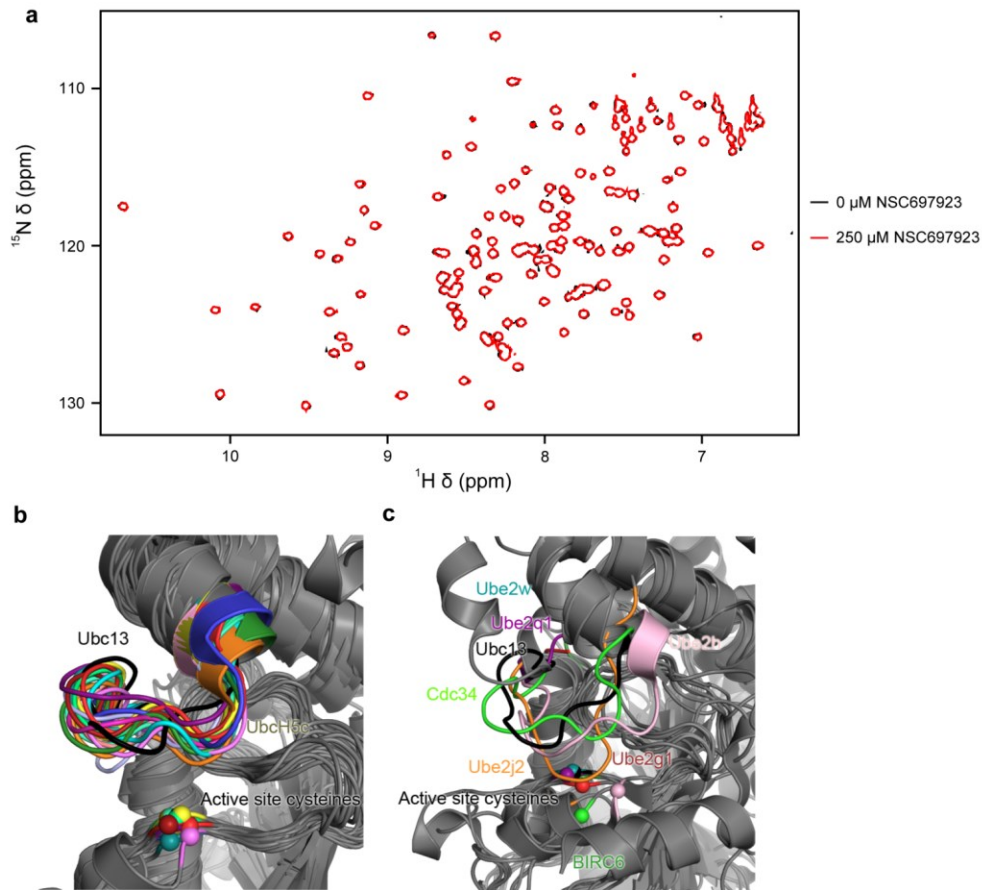


Figure 17. No NSC697923 pre-reaction binding to Ubc13 was detected and E2 structural alignments highlight active site loop variations.

(a) There are no chemical shifts (^{15}N NMR spectra) upon treatment of the unreactive $\text{Ubc13}^{\text{C87S}}$ mutant with NSC697923 dissolved in DMSO (red) compared to $\text{Ubc13}^{\text{C87S}}$ alone + DMSO control (black), indicating no specific non-covalent binding of the compound with Ubc13. (b) Structural superposition of 17 human E2s (colours) with UbH5c-like loops onto Ubc13 (black). (c) Structural superposition of 7 structurally divergent human E2s onto Ubc13 (black). Alpha carbon atoms of active site cysteines are coloured the same as their corresponding loops; remaining parts of structures are gray.

3.2B: Development of an inhibitor-resistant Ubc13 mutant

Previous work suggested UbcH5c is resistant to NSC697923 *in vitro*, under concentrations that effectively inhibit Ubc13¹²⁶. Comparison of the structures of Ubc13 and UbcH5c suggests a mechanism for this differential sensitivity to the inhibitor (Figure 18a,b). The groove that the nitrofuranyl substituent occupies in Ubc13 is occupied by a conserved leucine (Leu119) in UbcH5c. While an analogous leucine is present in Ubc13 (Leu121), this leucine is solvent exposed due to a different conformation of the 114-124 loop. An alignment of Ubc13 with the 17 available structurally similar catalytically active E2 structures in humans indicates that in the other E2s this loop often adopts the UbcH5c-like conformation with a residue frequently occluding the groove, providing a possible explanation for the specificity of NSC697923 for Ubc13 (Figure 17b). The other seven available E2 enzyme structures show considerable divergence from this basic fold (Figure 17c).

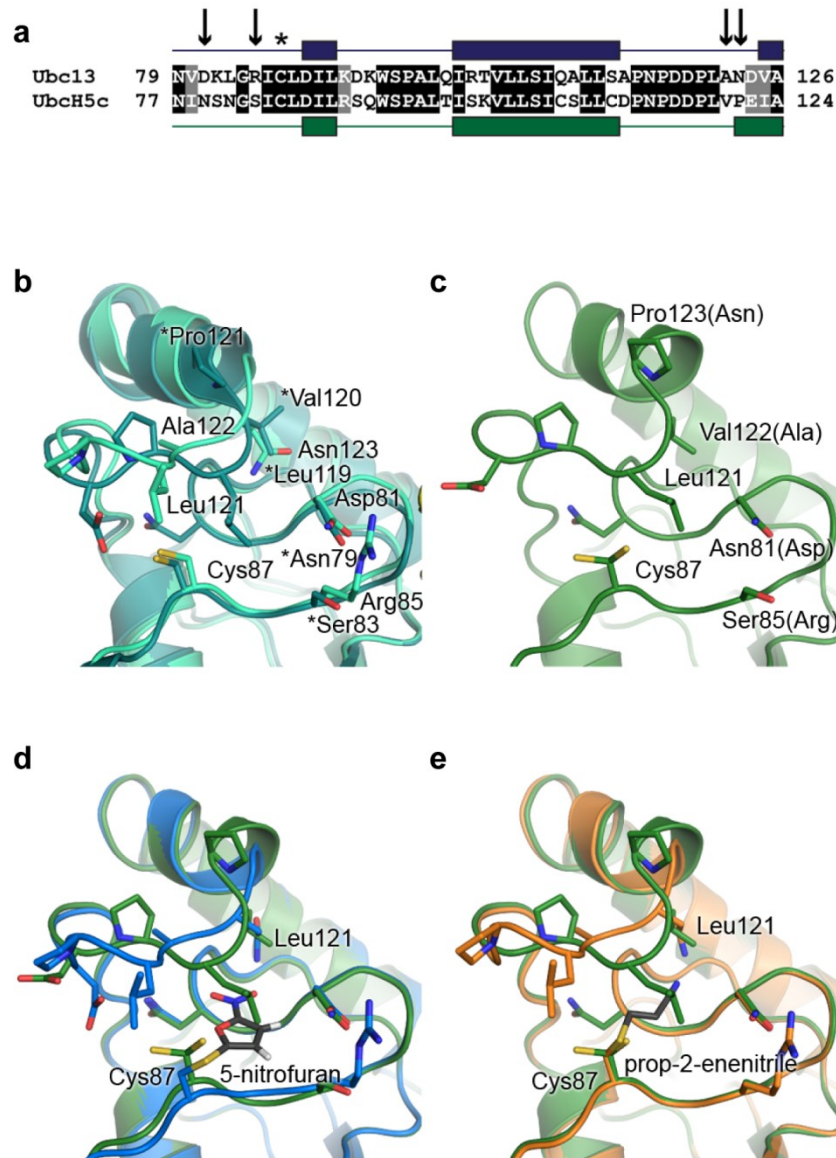


Figure 18. Design and structure of a NSC697923 resistant Ubc13 mutant.

(a) Amino acid sequence alignment of important active site residues in Ubc13 and Ubch5c, with secondary structural characteristics shown above. A line signifies a loop region and a box denotes an alpha helix. Arrows indicate mutations made to Ubc13 to mimic Ubch5c. The asterisk is above the active site cysteine. (b) Overlay of Ubch5c, PDB 1X23 (deep-teal), and Ubc13 (light green) shows their different active site loop conformations. Asterisks denote Ubch5c residues. (c) Active site view of the mutant Ubc13^{QD} (green) with the Ubch5c-type loop conformation (Protein Data Bank accession 4ONL). Brackets denote wild type residues. (d) Overlay of Ubc13 5-nitrofurane adduct (blue) and the resistant Ubc13^{QD}

(green). (e) Overlay of Ubc13 prop-2-enenitrile adduct (orange) and Ubc13^{QD}.

Analysis of the Ubc13 and Ubch5c structures and amino acid sequence alignments (Figure 18a,b), suggests that four amino acid substitutions might flip the orientation of the loop and alter the character of the groove adjacent to the Ubc13 active site, which could render the mutant resistant to NSC697923. Two of the mutations in the 114-124 loop, A122V and N123P, were predicted to alter the loop conformation, orienting Leu121 into the groove, while also shifting the position of Asn123, the sole hydrogen bonding partner for the nitrofurane. The other two mutations, D81N and R85S, were designed to alter the wall of the groove opposite the 114-124 loop to resemble Ubch5c. The crystal structure of the quadruple Ubc13 mutant (Ubc13^{QD}) bound to Mms2 reveals that the 114-124 loop does adopt a Ubch5c-like conformation such that Leu121 occupies the groove to potentially occlude the inhibitor (Figure 18c-e).

3.2C: Ubc13^{QD} is resistant to NSC697923 but not BAY 11-7082

We next compared the sensitivities of the Ubc13^{QD} mutant and wild type Ubc13 to inhibition using *in vitro* ubiquitination assays that contained stoichiometric amounts of the E3 RNF8, which stimulates Mms2/Ubc13-dependent formation of Lys63-linked polyubiquitin chains²⁹ (Figure 19a,b). Reactions performed in the absence of inhibitor reveal that the Ubc13^{QD} mutant is competent to build Lys63-linked poly-ubiquitin chains (Figure

20), and chain building efficiency under these reaction conditions is very similar to wild type. As seen in Figure 19a, Lys63-linked polyubiquitination catalyzed by wild type Ubc13 is inhibited by NSC697923 concentrations as low as 1 μ M, consistent with previous findings¹²⁶. In contrast, polyubiquitination catalyzed by Ubc13^{QD} is not markedly inhibited at similar concentrations of NSC697923. While these results reveal a significant resistance of the Ubc13^{QD} mutant to NSC697923, both Ubc13^{WT} and Ubc13^{QD} are similarly inhibited by BAY 11-7082 (Figure 19b). The fact that Ubc13^{QD} is highly sensitive to BAY 11-7082 but not NSC697923 suggests that the smaller BAY 11-7082 is able to evade the more restricted environment of the Ubc13^{QD} active site. This is consistent with previous results that indicate that BAY 11-7082 is able to inhibit ubiquitination catalyzed by a range of E2s, many of which adopt a 114-124 loop conformation that is very similar to that of the Ubc13^{QD} mutant¹²⁵.

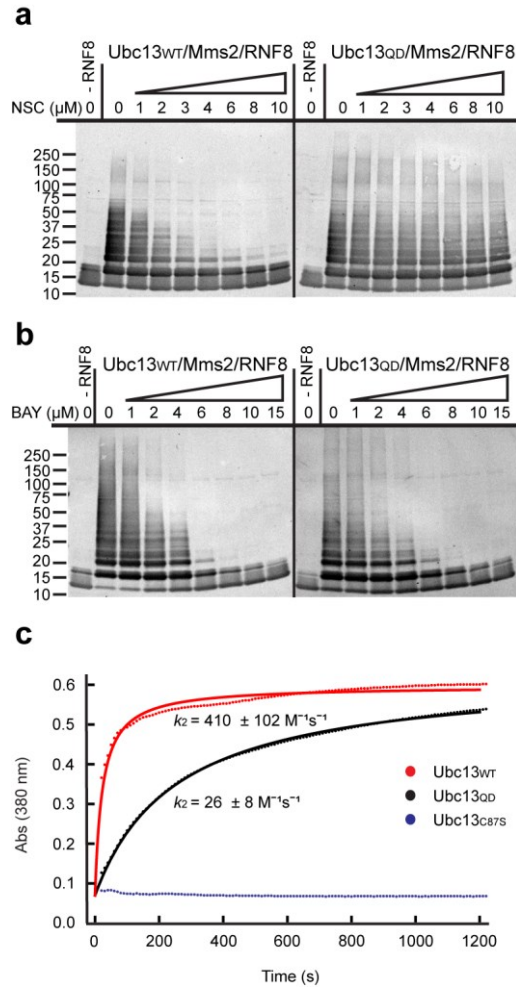


Figure 19. Ubc13^{QD} is resistant to NSC697923 but not BAY 11-7082.

(a) and (b) *In vitro* ubiquitination assays in which purified Ubc13/Mms2 (Ubc13^{WT} or Ubc13^{QD}) was incubated with ubiquitin, ATP, E1 enzyme, RNF8 and the indicated concentrations of inhibitor. Results were visualized by Western blotting with an anti-ubiquitin antibody. (a) Results for NSC697923. (b) Results for BAY 11-7082. (c) Representative graph of an *in vitro* inhibition assay monitored by absorbance at 380 nm. Reactions containing either Ubc13^{WT}, Ubc13^{QD}, or Ubc13^{C87S} were mixed with the NSC697923 inhibitor, and the resulting absorbance monitored. The experiment was done in triplicate and the average second-order rate constants (k_2) and standard errors are reported. Dotted lines indicate experimental data, curves indicate the fit to a second-order rate model.

These results suggest that the Ubc13^{QD} mutant reacts more slowly than the wild type protein with NSC697923. To directly test this, we used the finding that reaction of NSC697923 with sulfhydryl compounds can be followed by the formation of a reaction product that absorbs UV light at 380 nm (Figure 16a,b). We used this assay to quantitate the rate of reaction of NSC697923 with Ubc13^{QD} compared to the wild type protein (Figure 19c). Fitting of the data to a second order kinetic model gives a second order rate constant (k_2) for the reaction with wild type Ubc13 of $410 \pm 102 \text{ M}^{-1}\text{s}^{-1}$, whereas reaction with Ubc13^{QD} is ~16-fold slower (k_2 of $26 \pm 8 \text{ M}^{-1}\text{s}^{-1}$). No reaction was observed in control experiments with the catalytically inactive Ubc13^{C87S}.

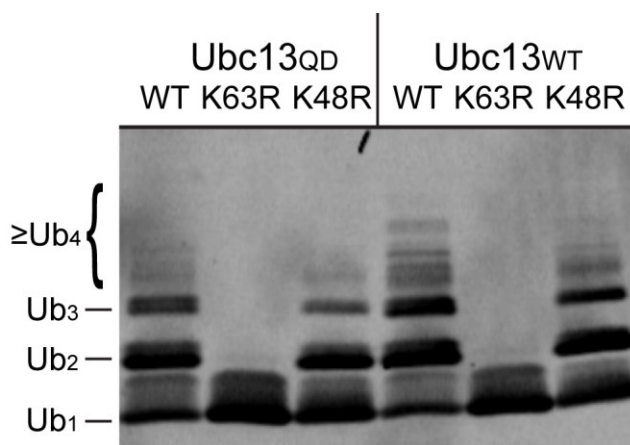


Figure 20. Ubc13^{QD} synthesizes Lys63-linked but not Lys48-linked polyubiquitin chains.

In vitro ubiquitination assays in which purified Ubc13/Mms2 (Ubc13^{WT} or Ubc13^{QD}) was incubated with either wild type (WT), Lys63-mutated (K63R), or Lys48-mutated (K48R) ubiquitin, ATP, E1 enzyme, and RNF8. Results were visualized by Western blotting with an anti-ubiquitin antibody.

3.2D: Inhibition of the DDR and NF- κ B signalling by NSC697923 is due to targeting of Ubc13

Our development of a functional Ubc13 variant that is resistant to NSC697923 presented the opportunity to test if the ability of NSC697923 to inhibit the cellular DNA damage response and NF- κ B signaling is due to inhibition of Ubc13 or an off-target effect. In these experiments, we utilized a Ubc13 knockout mouse embryonic fibroblast line (MEF) in which we reintroduced either wild type Ubc13 or Ubc13^{QD}, Figure 21. NF- κ B activation was induced by treatment with lipopolysaccharide (LPS) and monitored by following the cellular localization of the NF- κ B p65 subunit, which translocates from the cytoplasm to the nucleus upon I- κ B degradation in a manner that depends on the action of Uev1a/Ubc13¹³⁰.

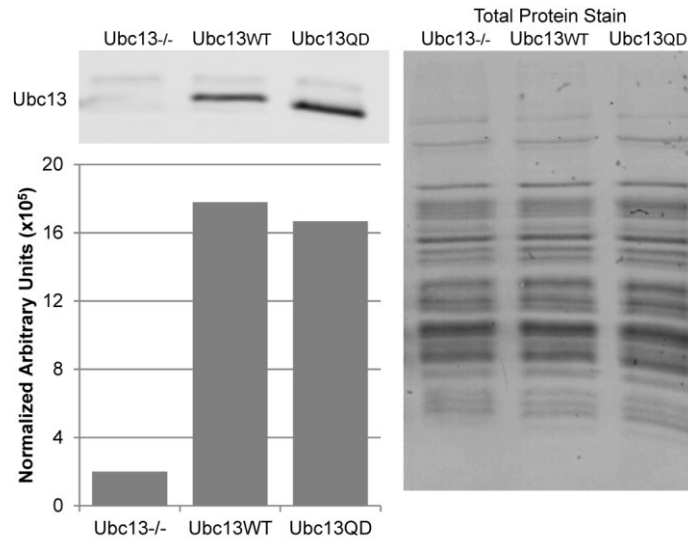


Figure 21. Ubc13 expression in Ubc13^{WT} and Ubc13^{QD} MEF cell lines is similar.

Whole cell extracts of Ubc13^{-/-}, Ubc13^{WT}, or Ubc13^{QD} MEF cells were prepared and Ubc13 was visualized using an anti-Ubc13 antibody via Western blot analysis (top left panel). Band intensities were quantified (bottom left panel) using a total protein stain as a loading control (right panel). Copper [II]Phthalocyanine 3,4,4',4''' TetraSulfonic acid tetrasodium salt (CPTS) was used for the total protein stain.

In the absence of inhibitor, both wild type and Ubc13^{QD} are able to induce nearly total translocation of p65 to the nucleus upon LPS stimulation (Figure 22a) and consistent with previous findings this translocation is greatly dependent upon Ubc13 (Figure 23a,b)⁶³. Treatment of WT reconstituted MEF cells with 2.5 μM NSC697923 inhibited the LPS-driven translocation of p65, so that a large amount remained in the cytoplasm. Treatment of Ubc13^{QD} reconstituted MEFs with 2.5 μM NSC697923 resulted in less overall inhibition (Figure 22b). These treatments did not significantly alter p65 expression in the MEF cell lines

(Figure 23c). Quantification of these results reveals that the average percentage of total p65 localized to the nucleus is reduced from $51 \pm 1\%$ to $33 \pm 1\%$ upon treatment with $2.5 \mu\text{M}$ NSC697923 in WT cells (Figure 22b,c). Given that $\sim 30\%$ of p65 is localized to the nucleus in these cells in the absence of NF- κ B activation, this represents an almost complete inhibition of LPS-inducible NF- κ B signaling. In contrast, in Ubc13^{QD} cells, the average percentage of nuclear p65 is only reduced from $51 \pm 1\%$ to $39 \pm 1\%$ upon NSC697923 treatment, which is well above the level of p65 translocation in the absence of LPS treatment ($\sim 30\%$). We find that this reflects a statistically significant reduction in inhibition in Ubc13^{QD} compared to Ubc13^{WT} cells (P-value = 0.02), and thus, the effects of NSC697923 on NF- κ B signaling are likely due, at least in part, to Ubc13 inhibition (Figure 22c).

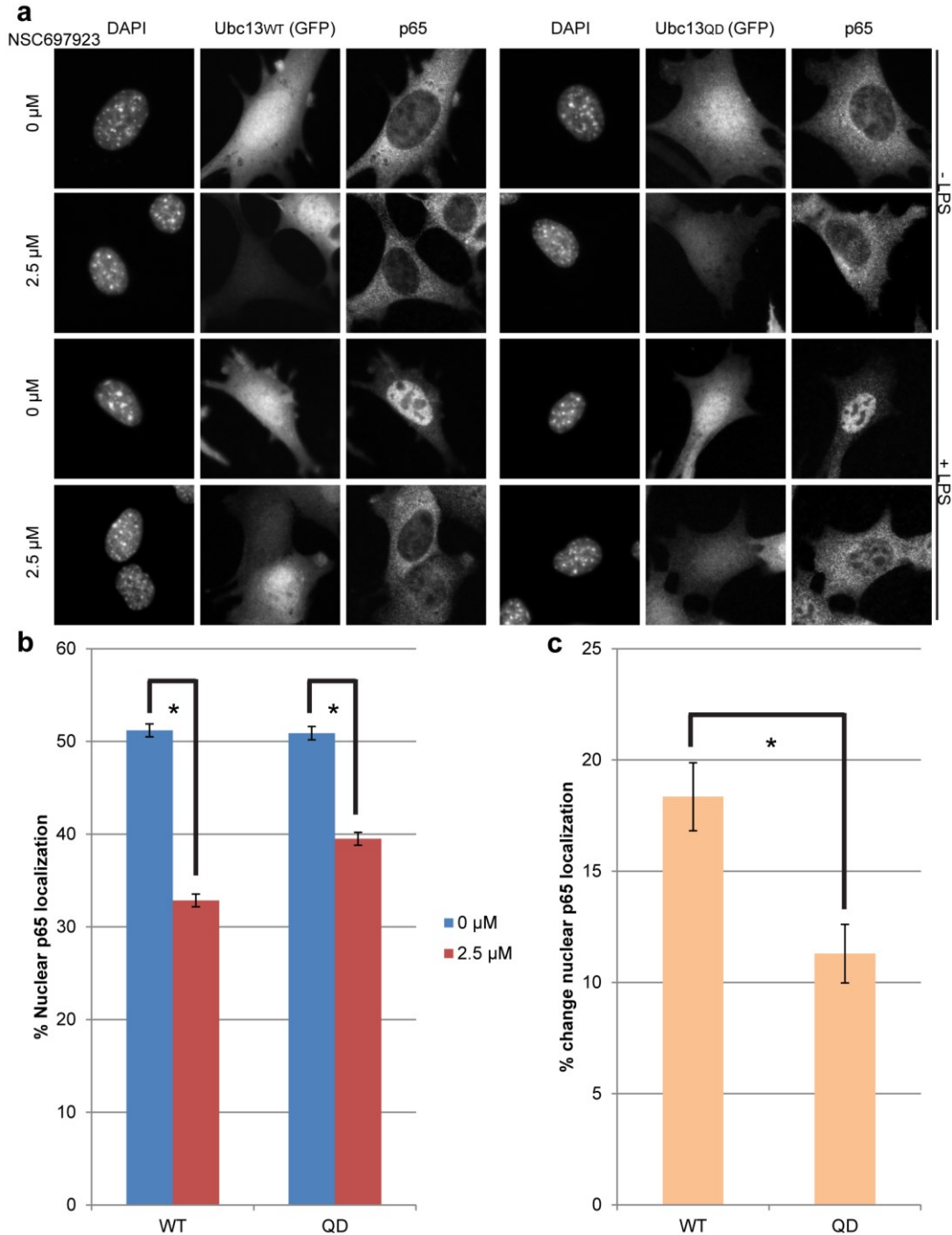


Figure 22. Inhibition of Ubc13 is required for significant disruption of cellular NF- κ B signalling by NSC697923.

(a) Representative images of Ubc13^{WT} (left) or Ubc13^{QD} (right) reconstituted Ubc13 knockout mouse embryonic fibroblast cells before and after lipopolysaccharide (LPS) stimulation, with and without NSC697923 treatment (2.5 μ M). (b) Quantitation of p65 translocation represented as percent of intensity localized to the nuclei and (c) the difference in p65

translocation between NSC697923-untreated and treated cells (P -value = 0.02). Unstimulated cells have approximately 30% background nuclear p65 translocation. Data from 3 independent experiments were pooled with at least 200 cells per condition, and standard error of image averages is included. The tonal range of whole images was rescaled from 0 to 255 in Photoshop to increase the overall contrast for display.

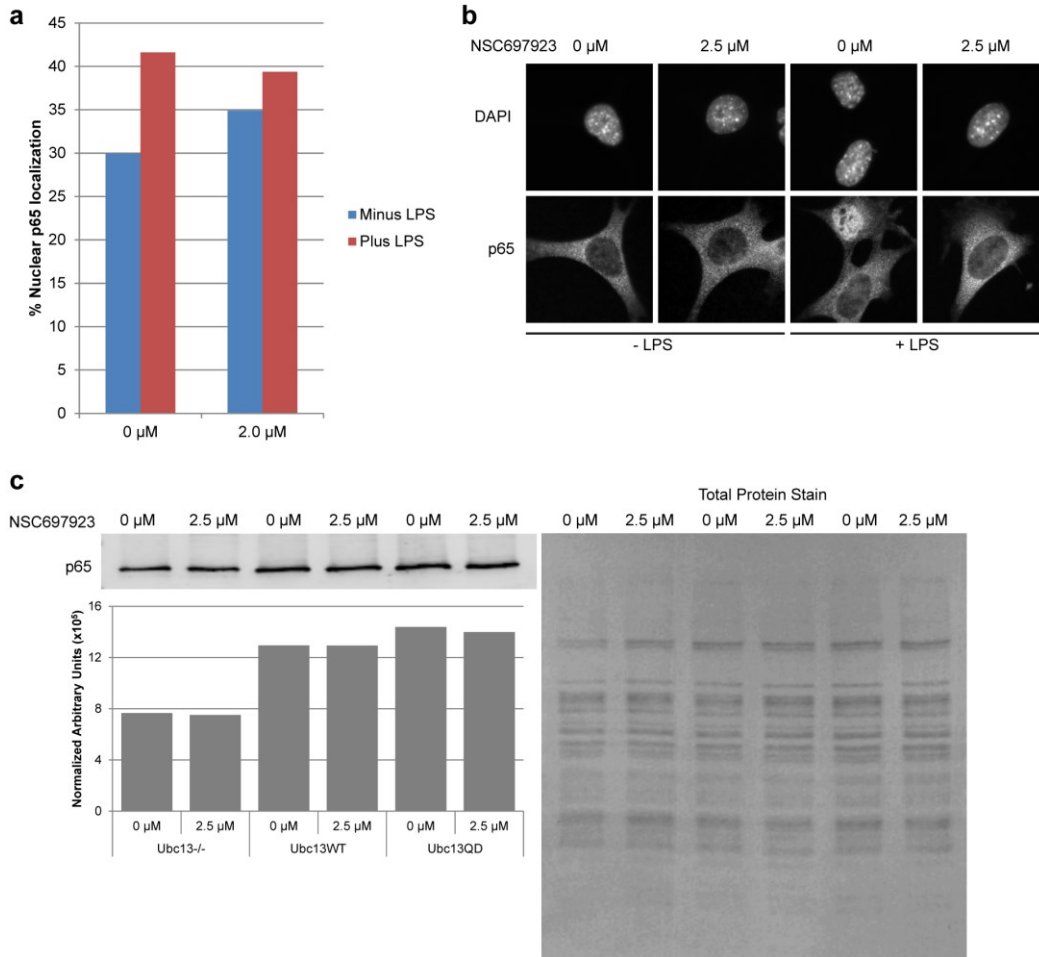


Figure 23. Ubc13^{-/-} MEF cells are deficient in p65 translocation and NSC697923 does not alter p65 expression in ^{-/-}, WT, or QD MEF cell lines.

(a) Quantitation of p65 translocation in Ubc13^{-/-} MEFs represented as percent of the total cellular intensity localized to the nuclei. Greater than 80 cells per condition were analyzed and averaged. 2 μ M of NSC697923 was used to treat these cells for quantitation, as 2.5 μ M causes many of the cells to round-up, rendering cytoplasm measurements inaccurate. (b)

Representative images of Ubc13^{-/-} MEFs with (right) or without LPS (left) stimulation, with and without NSC697923 treatment (2.5 μM). A small proportion of Ubc13^{-/-} MEFs were able to activate the LPS driven NF-κB translocation, of which the underlying mechanisms are not well-understood. This resulted in an approximate 10% increase of nuclear p65 localization due to LPS stimulation in the absence of NSC697923. The effect of NSC697923 in these cells was less pronounced. The tonal range of whole images was rescaled from 0 to 255 in Photoshop to increase the overall contrast for display. (c) Ubc13^{-/-}, Ubc13^{WT}, or Ubc13^{QD} MEF cell lines were treated with either DMSO (0 μM) or 2.5 μM NSC697923 for 30 minutes prior to LPS stimulation for 1 hour. Whole cell extracts were prepared and p65 was visualized using an anti-p65 antibody via Western blot analysis (top left panel). Band intensities were quantified (bottom left panel) using a total protein stain as a loading control (right panel). Copper [II]Phthalocyanine 3,4,4',4''' TetraSulfonic acid tetrasodium salt (CPTS) was used for the total protein stain.

To further assess the effect of NSC697923 on NF-κB signaling, we also analyzed the cellular cytokine release profile of the MEF cell lines (Figure 24) in response to LPS stimulation. Cytokines are small secreted signaling proteins that are extensively used by cells of the immune system, in particular macrophages, for intercellular communication and inflammation regulation in response to foreign particles/invaders¹³¹. As a major component of the connective tissue, fibroblasts are also known to secrete cytokines in response to stimulation via other cytokines or LPS^{131,132}.

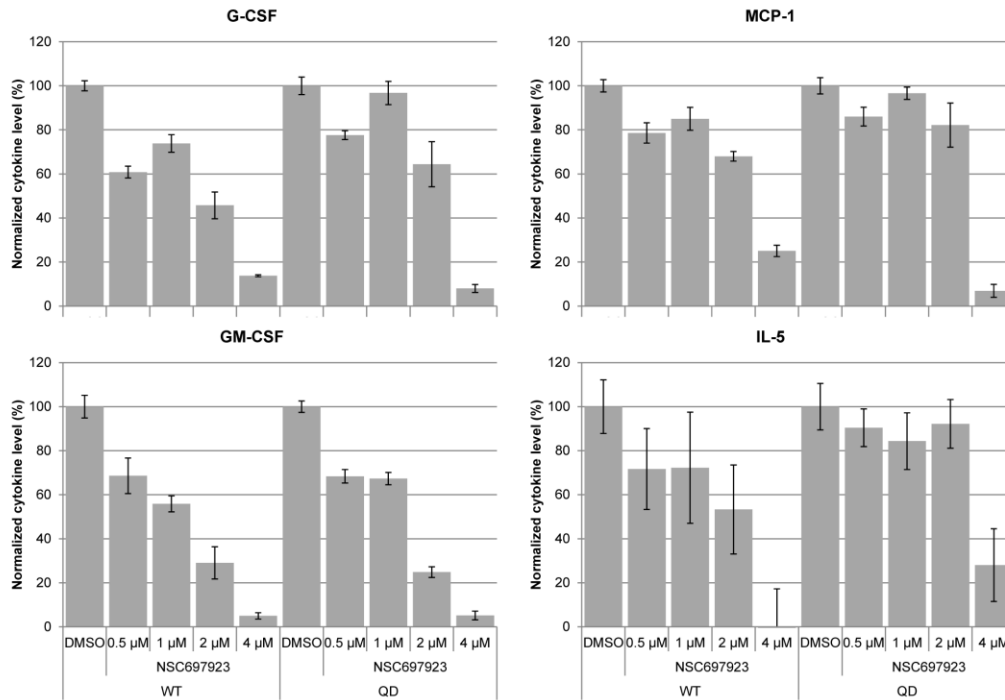


Figure 24. Normalized inhibition of Ubc13-dependent, NF- κ B-driven cytokine release by NSC697923.

Unstimulated (-LPS) or stimulated (+LPS) Ubc13^{WT} or Ubc13^{QD} MEF cells were treated with either DMSO, or increasing concentrations of NSC697923 from 0.5 μ M to 4 μ M and cytokine levels in the culture medium were quantified. The background unstimulated (-LPS) level was subtracted from each treatment (DMSO to 4 μ M NSC697923) and the stimulated (+LPS) DMSO treated level was normalized to 100% for optimal direct comparison of the two cell lines. The assay was done in triplicate, and the standard error of the mean for each treatment is included.

We found four cytokines that were responsive to LPS stimulation in a Ubc13-dependent manner suggesting that their expression levels are largely controlled by the NF- κ B pathway in our cells (Figure 25). We measured the levels of these secreted cytokines as a function of increasing NSC697923 concentration (Figure 24 and Figure 26). The

NSC697923-dependent reduction of the four cytokines, granulocyte-colony stimulating factor (G-CSF), monocyte chemoattractant protein 1 (MCP-1), granulocyte-macrophage-colony stimulating factor (GM-CSF), and interleukin-5 (IL-5)¹³¹⁻¹³⁴, was slightly more pronounced in the wild type cells compared to the Ubc13^{QD} cells. This is most notable when comparing the cytokine concentration differences between the DMSO control and the lower NSC697923 concentrations (0.5 to 2 μ M) as seen in the normalized data in Figure 24 (raw data in Figure 26). The longer incubation with NSC697923 (4.5 h) and the complex nature of the pathways contributing to cytokine secretion may explain the lower sensitivity of this experiment compared to the p65 translocation data (a more direct measure of NF- κ B signaling). Taken together, however, the cytokine secretion data are consistent with the p65 translocation data, which suggests that the effects on the NF- κ B signaling pathway are partially due to Ubc13 inhibition.

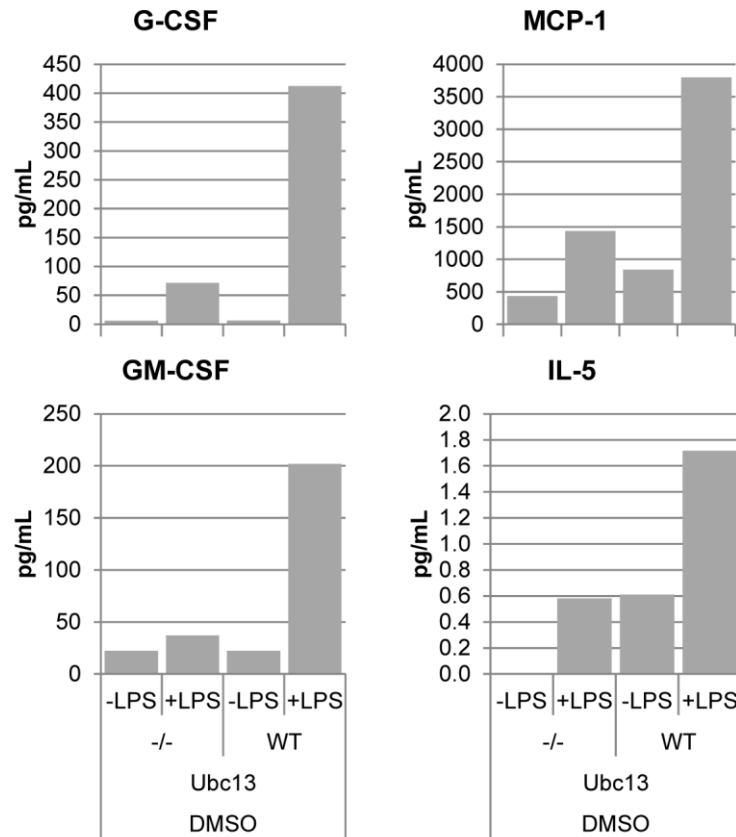


Figure 25. NF- κ B-driven cytokine release of -/- and WT Ubc13 MEFs upon stimulation with LPS.

The release of the cytokines G-CSF, MCP-1, GM-CSF, and, IL-5 are largely LPS and Ubc13-dependent in MEF cells.

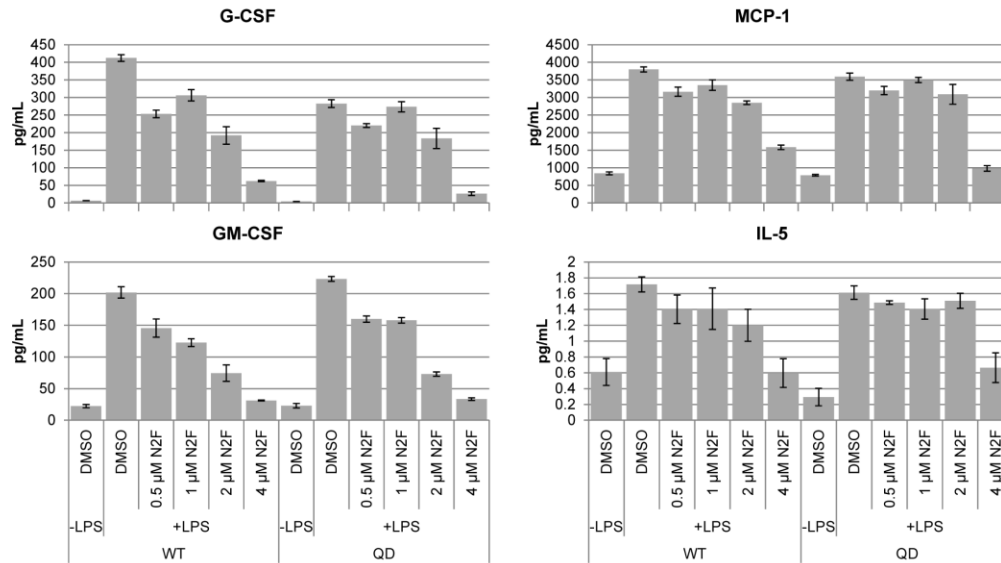
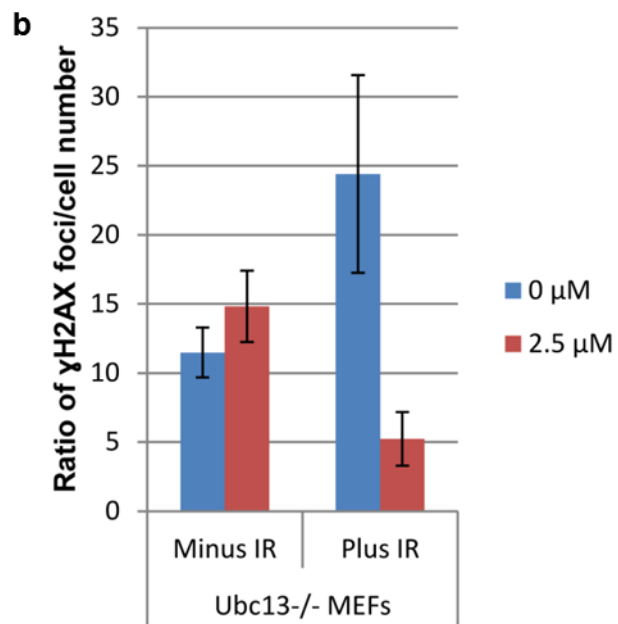
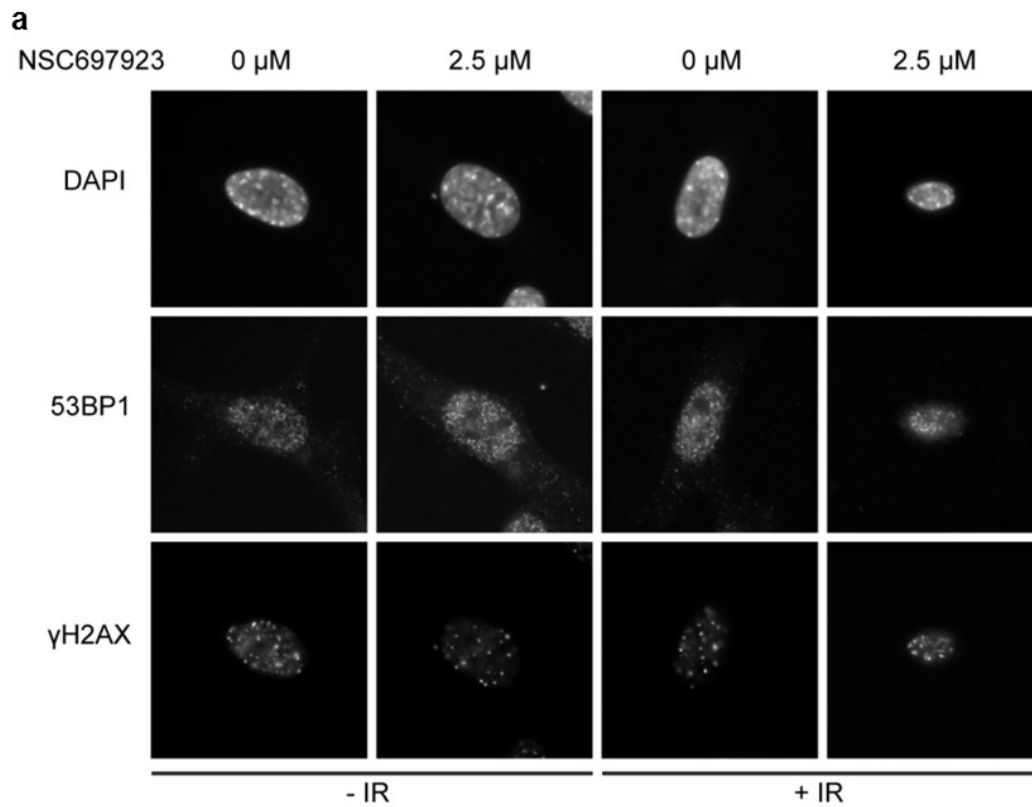


Figure 26. Inhibition of Ubc13-dependent, NF- κ B-driven cytokine release by NSC697923.

Unstimulated (-LPS) or stimulated (+LPS) Ubc13^{WT} or Ubc13^{QD} MEF cells were treated with either DMSO, or increasing concentrations of NSC697923 from 0.5 μ M to 4 μ M and cytokine levels in the culture medium were quantified. The assay was done in triplicate, and the standard error of the mean for each treatment is included. This raw data was used to derive the background-corrected, normalized data presented in Figure 24.

We utilized the same MEF cell lines to monitor the effects of NSC697923 on the cellular response to DNA damage signaling. DNA damage was induced with ionizing radiation and DNA lesions were monitored through the formation of γ H2AX foci, which form independent of Ubc13-dependent ubiquitin signaling^{18,19}. In the Ubc13 knockout MEFs, we observed a slight increase in γ H2AX foci upon ionizing radiation, which was decreased upon treatment with NSC697923, however neither effect was statistically significant (Figure 27a,b).



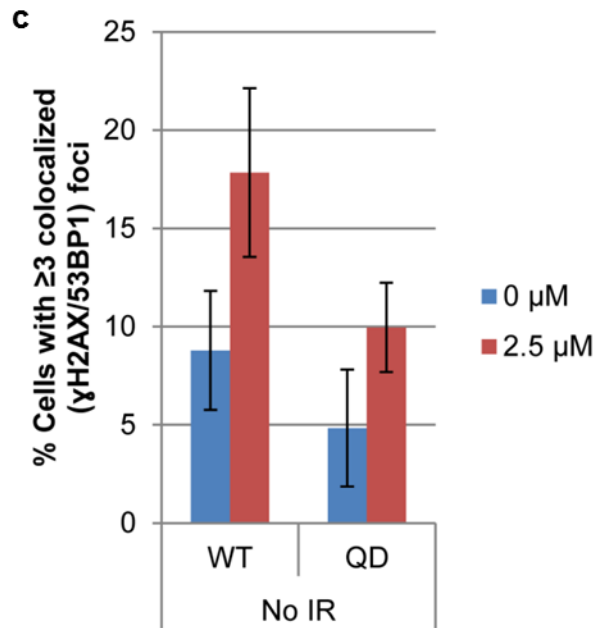
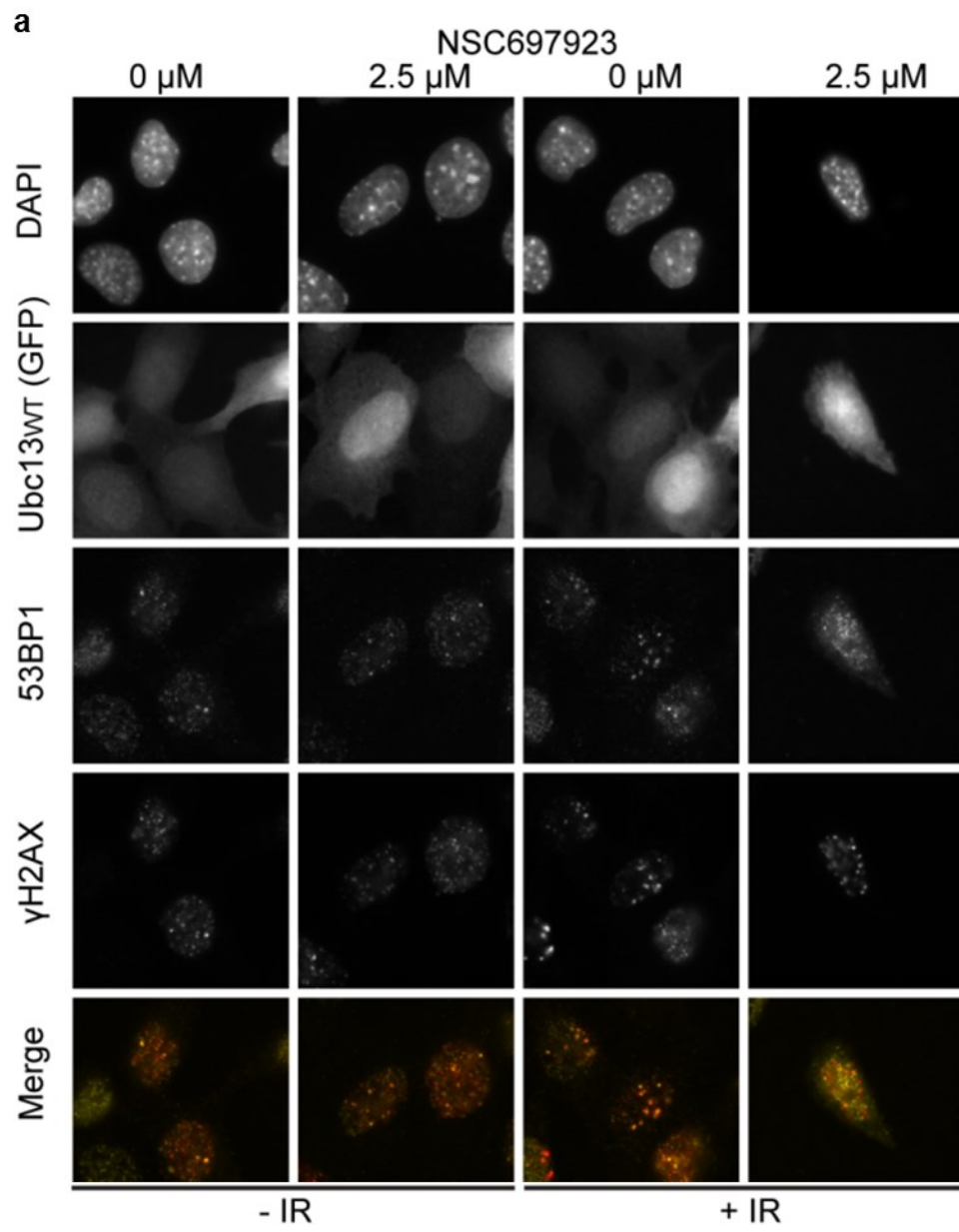
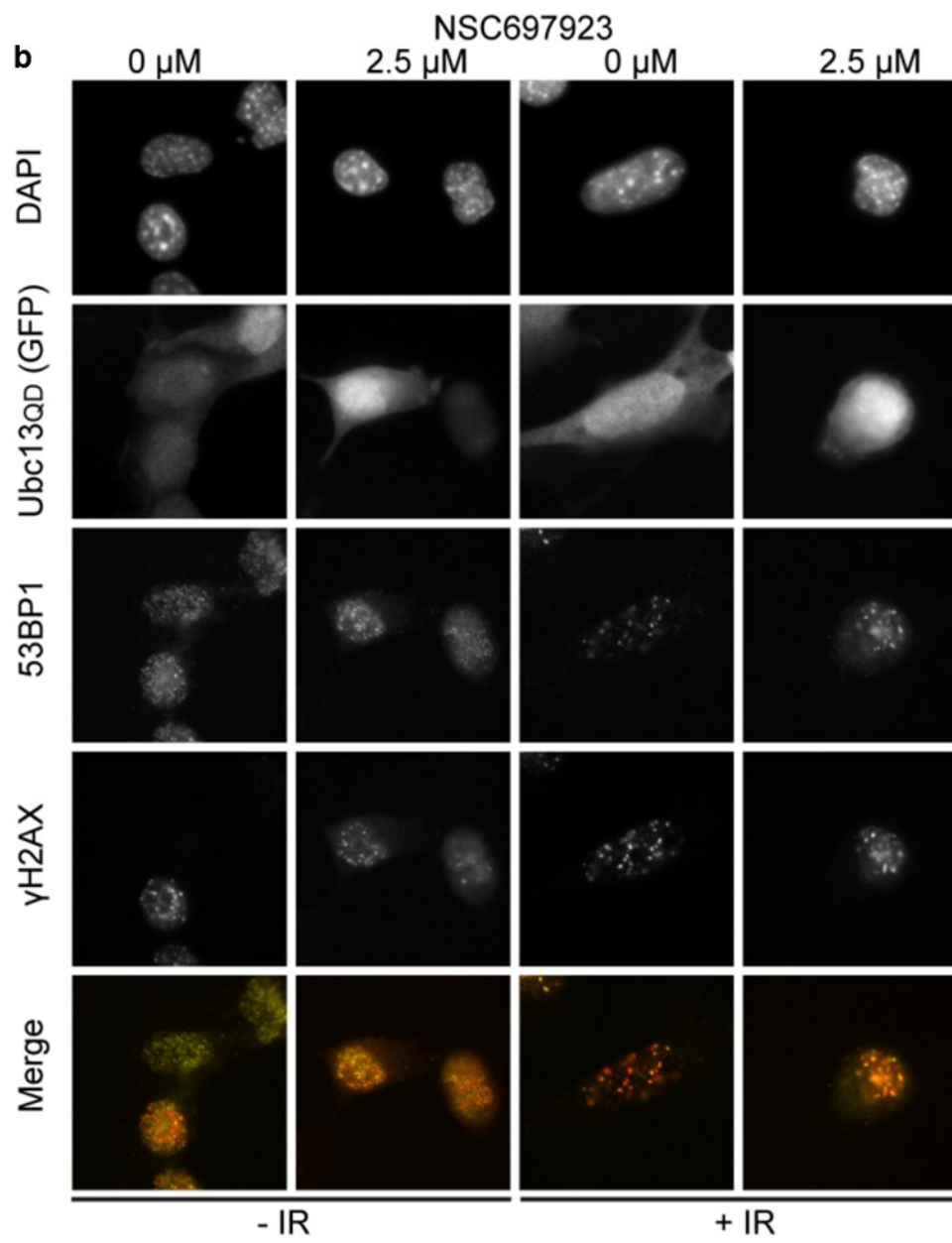


Figure 27. γ H2AX foci change in Ubc13^{-/-} MEFs with and without NSC697923 and IR, and γ H2AX/53BP1 foci localization in WT and QD Ubc13 MEFs in the absence of IR.

(a) Ubc13^{-/-} MEFs without (left) or with ionizing radiation (right), with and without NSC697923 treatment (2.5 μ M). (b) Quantitation of γ H2AX foci formation from (a) represented as a ratio of γ H2AX to cell number. There were no 53BP1 foci formed, therefore no colocalized foci. At least 25 cells per condition were analyzed and averaged. The standard error of image averages is included. Upon IR a non-statistically significant increase in γ H2AX foci formation was observed. Treatment with 2.5 μ M NSC697923 reduced the γ H2AX foci formation, however this was also not statistically significant. (c) Quantitation of 53BP1 localization represented as percentage of total cells positive (≥ 3 foci) for γ H2AX/53BP1 colocalization in the absence of ionizing radiation. At least 115 cells per condition were analyzed and averaged. The standard error of image averages is included. A small non-statistically significant increase in colocalization of γ H2AX and 53BP1 was observed for both WT and QD cell lines upon treatment with 2.5 μ M NSC697923. The tonal range of whole images was rescaled from 0 to 255 in Photoshop to increase the overall contrast for display.

To assess downstream signaling, we monitored the formation of 53BP1 foci, which are dependent on Ubc13 driven ubiquitination of chromatin^{34,135} (Figure 28a-c, Figure 27b). In both the wild type- and Ubc13^{QD}-expressing cells, we observed the colocalization of γ H2AX and 53BP1 foci in response to ionizing radiation, indicating that the Ubc13^{QD} mutant is competent to functionally replace the wild type protein in the DNA damage response. It should be noted that there was a small (not statistically significant) increase in colocalization of γ H2AX and 53BP1 (i.e., DNA damage) in the absence of ionizing radiation for both WT and QD cell lines upon treatment with NSC697923 (Figure 27c). This may be attributed to the reaction of NSC697923 with the natural cellular antioxidant glutathione, which could result in an increase in DNA damaging reactive oxygen species (ROS). Treatment of the irradiated cells with 2.5 μ M NSC697923 did not alter the appearance of the γ H2AX foci, but did significantly reduce the percentage of cells positive for colocalized γ H2AX/53BP1 foci in wild type Ubc13-expressing cells (P-value = 9.0^{-9} ; Figure 28a,c). There was no statistically significant inhibition of the γ H2AX/53BP1 colocalized-positive Ubc13^{QD}-expressing cells (P-value = 0.7) indicating that the effect of NSC697923 on the DNA damage response is largely due to the inhibition of Ubc13 (Figure 28b,c).





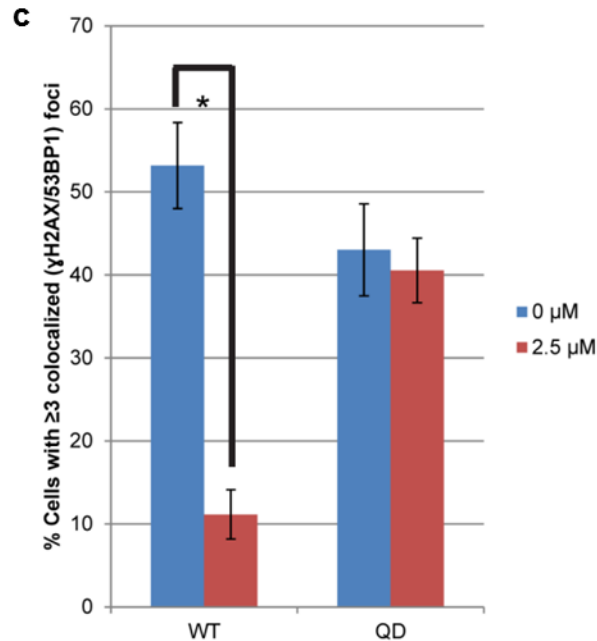


Figure 28. Inhibition of Ubc13 is required for disruption of cellular DNA damage signalling by NSC697923.

(a) Representative images of Ubc13^{WT} or (b) Ubc13^{QD} reconstituted mouse embryonic fibroblast cells plus/minus 3 Gy of ionizing radiation, with or without NSC697923 treatment (2.5 μM). (c) Quantitation of 53BP1 localization represented as percentage of total cells positive (≥3 foci) for γH2AX/53BP1 colocalization. Data from 3 independent experiments were pooled with at least 300 cells per condition, and standard error of image averages is included. The tonal range of whole images was rescaled from 0 to 255 in Photoshop to increase the overall contrast for display.

3.3 Discussion

Ubc13 is the ubiquitin-conjugating (E2) enzyme critical for the synthesis of Lys63-linked ubiquitin chains in both the homologous recombination DNA repair and NF-κB pathways, which have both been identified as targets for cancer therapy development. Here we have shown that two previously identified inhibitors of Ubc13 both covalently modify the

active site cysteine, forming sulfur adducts that dock into a unique groove adjacent to the catalytic cysteine. This groove is occluded by a loop opposing the active site cysteine in many E2 enzymes and therefore provides a route for the development of specific inhibitors of Ubc13. Mutations that block this groove but do not significantly impair catalytic activity afford resistance to one of the inhibitors *in vitro*. Using this resistant mutant, we show that the previously demonstrated inhibition of NF- κ B and DNA damage signaling attributed to this compound is predominantly due to the specific inhibition of Ubc13. However, we do note that the mutant only provides a partial reduction in the inhibition of the NF- κ B response. This raises the possibility that NSC697923, which is generally reactive to small molecule sulfhydryl compounds, may act on alternative targets that also inhibit the NF- κ B pathway or alternative related pathways that depend on Ubc13.

A comparison of the structure of free Ubc13 with the structure of Ubc13 with a ubiquitin covalently linked to the active site indicates that a UbcH5c-like conformation can be induced in the Ubc13 114-124 loop upon ubiquitin binding²⁸ (Figure 29). The ubiquitin-bound structure provides a view of the covalently bound donor ubiquitin, as well as an incoming acceptor ubiquitin (Figure 30). In the unbound state, Leu121 blocks the approach of the incoming lysine from the acceptor ubiquitin; however rearrangement of the 114-124 loop enables the access of ubiquitin Lys63 to the active site. This conformational rearrangement also shifts the

position of Ubc13 Asn123, which, in the free state, is hydrogen bonded to the main chain of His77, Pro78 and Val80. Upon ubiquitin binding and conformational change, Asn123 flips out and hydrogen bonds with the main chain of Lys63 of the acceptor ubiquitin and the adjacent Gln62 residue.

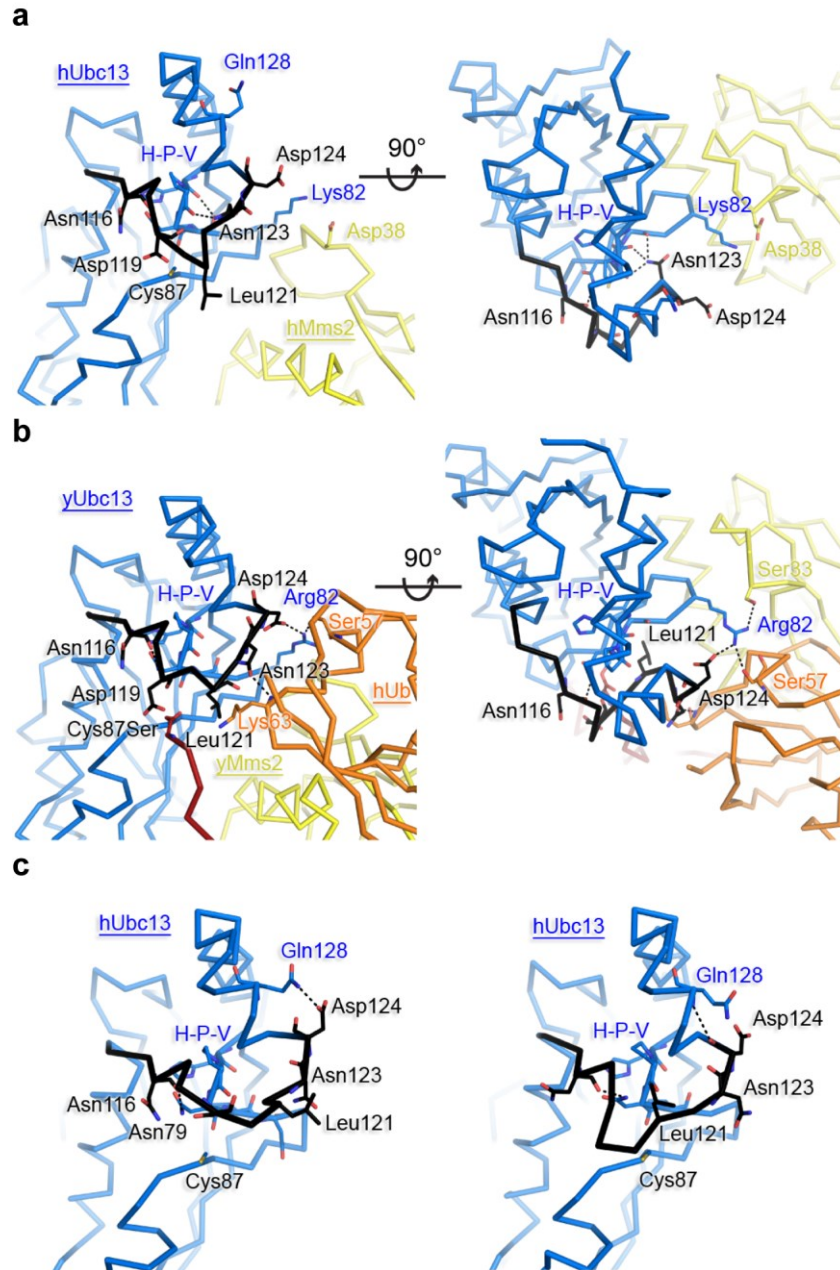


Figure 29. Ubc13 structures demonstrate loop 114-124 changes and pocket disruption upon acceptor ubiquitin binding.

(a) Asn123 mediated pocket formation by human Ubc13 in complex with Mms2 (PDB 1J7D). (b) Yeast Ubc13 loop shift and pocket disruption by human (acceptor) ubiquitin when bound to yeast Mms2. (c) Human Ubc13 in two different space groups (PDB 3HCT on left, 3HCU on right). Ubc13 is blue, Mms2 is yellow, and ubiquitin is orange. Loop 114-124 is highlighted black. H-P-V indicates Ubc13 residues His77 Pro78 and Val80, which together hydrogen bond with buried Asn123 in the absence of ubiquitin.

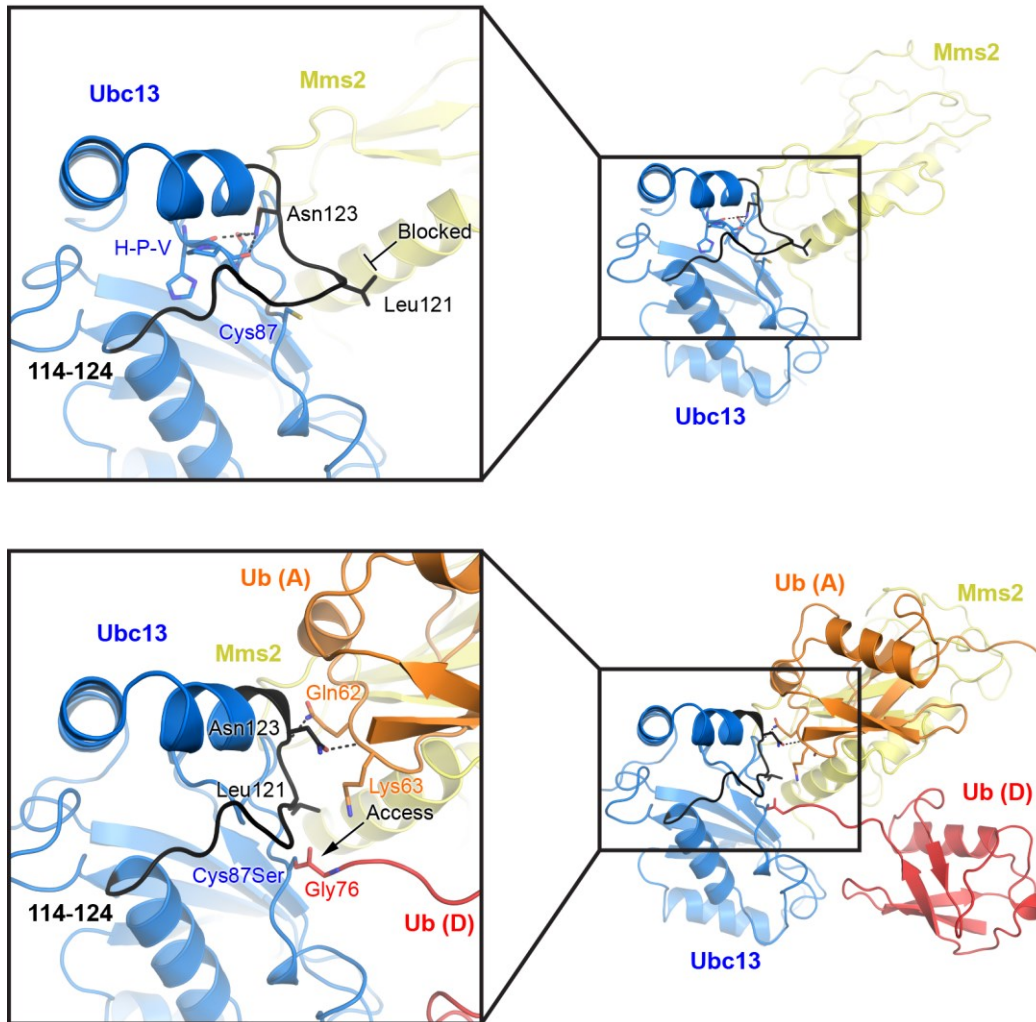


Figure 30. Conformational changes in Ubc13 loop 114-124 upon ubiquitin binding.

The top panel is hUbc13/hMms2 (PDB 1J7D) and the bottom panel is yUbc13~hUb/yMms2/hUb (2GMI). Ubc13 is blue, Mms2 is yellow, donor ubiquitin is red, and acceptor ubiquitin is orange for both panels, and the 114-124 loop is in black. The position of Leu121 in the unbound structure (top panel) is expected to block approach of Lys63 of the acceptor ubiquitin toward the active site cysteine.

The fact that an asparagine is only found at this position in Ubc13 among all the 34 known active human E2 enzymes suggests that this conformational rearrangement may be unique to Ubc13 (Figure 31). Flexibility of this loop is further suggested by the observation that the loop adopts still other conformations in complex with E3 ligases and other regulatory proteins (Figure 32). Indeed, through a collaboration with the Spyropoulos lab, we have recently shown the dynamics of this loop to be important for the catalytic activity of Ubc13¹³⁶. This is consistent with previous suggestions that E3 ligases may activate Ubc13 and other E2s by driving conformational change within the active site that propagates from the site of E3 binding^{74,75,137}.

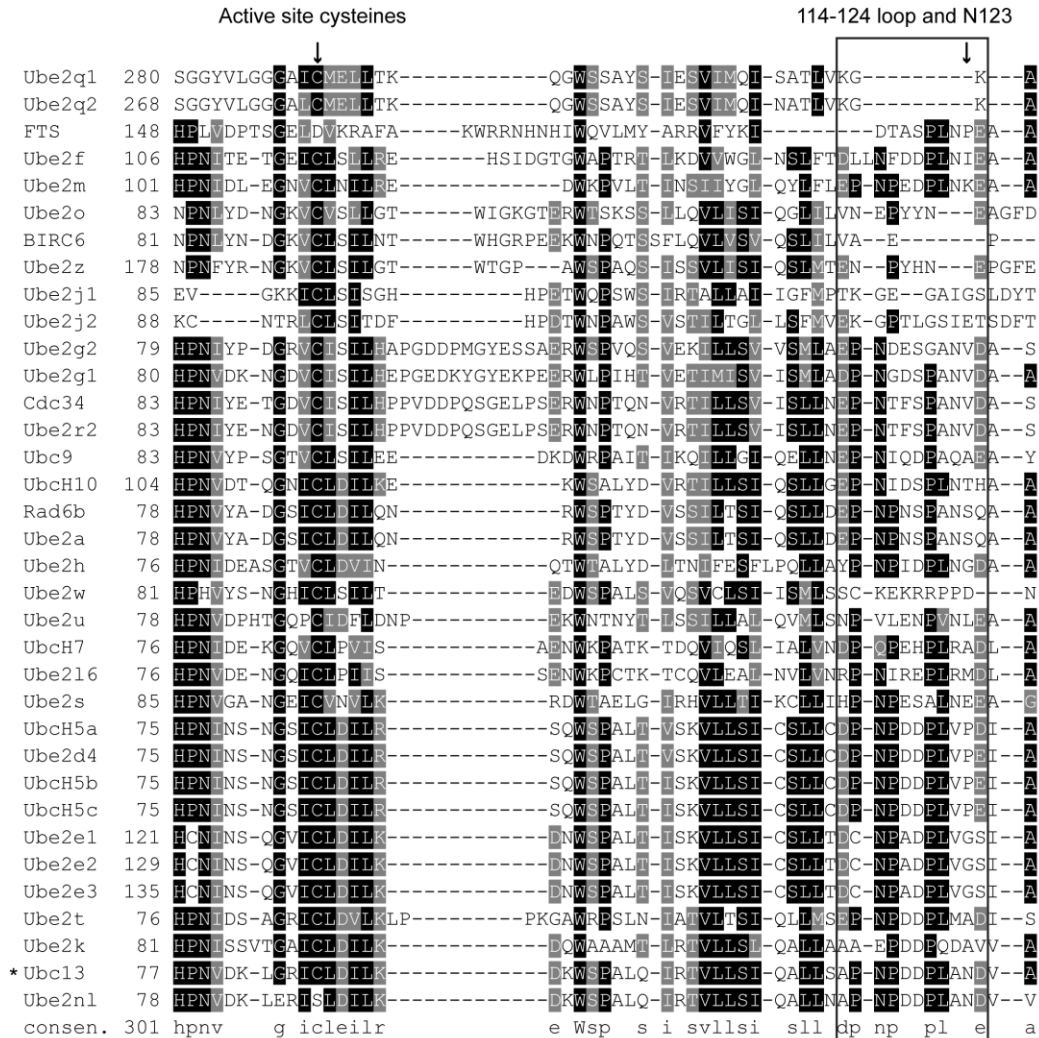


Figure 31. Multiple sequence alignment of all 34 known catalytically active E2 enzymes.

Conserved residues are shaded black, similar residues are shaded gray, and non-conserved residues are left unshaded. A box surrounds the alignment that corresponds to the Ubc13 loop 114-124 with an arrow enclosed indicating the position of Asn123. An arrow denotes the active site cysteines. An asterisk is placed beside Ubc13 in the alignment. Sequences were aligned using Clustal Omega, and shaded with BoxShade. Ube2n1 is likely not a functional E2 due to a Cys-Ser substitution at the predicted active site.

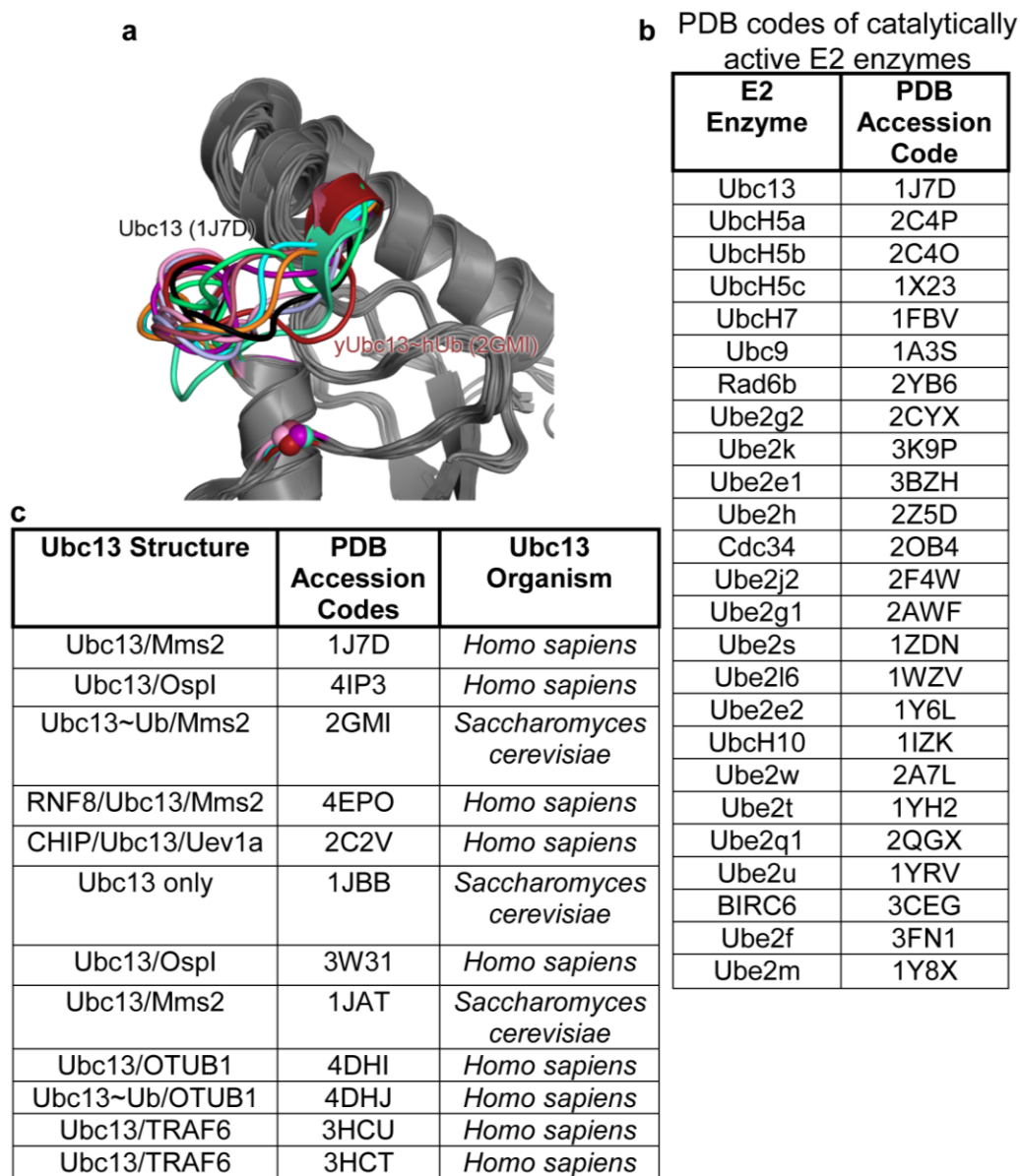


Figure 32. Superposition of Ubc13 structures and PDB codes of available E2 enzyme structures.

(a) Structural superposition of available human or yeast Ubc13-containing structures onto wild type human Ubc13 (black). The one structure (2GMI) of Ubc13 that adopts the UbcH5c-like loop conformation is shown in firebrick-red. All alpha carbons of active site cysteines are coloured the same as their corresponding loops; remaining parts of structures are gray. (b) PDB codes of all available catalytically active E2 enzymes. (c) All structures containing human or yeast Ubc13.

NSC697923 and BAY 11-7082 provide a starting point for future development of agents that act to covalently inhibit Ubc13. While covalent inhibitors were rarely utilized in the past for targeted drug discovery, many important drugs in current use act through a covalent mechanism, and there is renewed interest in covalent inhibitors¹³⁸. A key to lowering the toxicity of such inhibitors is to modulate their reactivity, so that their activation and reaction with a target is dependent upon stable and selective binding, termed binding-induced activation. Our work shows that the groove near the active site of Ubc13 can serve as a powerful selectivity determinant. The charged Asp119 near the active site could also be exploited as a hydrogen bond/salt bridge acceptor. Replacement of the nitro group in NSC697923 could offer a route to reduce the reactivity of the inhibitor, while potentially alleviating the well-known toxicities associated with nitrofuran-containing compounds¹³⁹. Our NMR experiments do not demonstrate specific prereaction binding of NSC697923 to Ubc13^{C87S}, arguing against the idea that the tosyl group, which is common to both inhibitors, directly contributes to Ubc13 binding. Nevertheless, next generation inhibitors could employ leaving groups that might enhance the precatalytic binding of the inhibitor to Ubc13. Interestingly, the predicted position of the tosyl group would be close to a groove that accepts the ubiquitin tail in E2-ubiquitin complex structures^{28,74}, and it is therefore possible that leaving groups or other modifications that target this groove could significantly improve binding.

BAY 11-7082 has been extensively used in studies of the NF- κ B pathway, and recently been shown to target protein tyrosine phosphatases^{125,140}. It has previously been demonstrated that BAY 11-7082 is toxic to multiple myeloma cells independent of its known effects on the NF- κ B pathway, indicating off-target effects¹⁴¹. This study did not, however, take into account the more recent report of the inhibition of protein tyrosine phosphatases by this compound¹⁴⁰. We found that the Ubc13^{QD} mutant was not resistant to BAY 11-7082, despite the predicted clash of Leu121 with the prop-2-enenitrile moiety. The smaller prop-2-enenitrile adduct may not dock as well into the active site pocket as the larger nitrofurans, and may exhibit greater mobility to evade the steric clash with Leu121. The ability of the Ubc13^{QD} mutant to discriminate between a bulkier, more specific compound and a smaller, more promiscuous one speaks to its potential utility as an effective active site binding inhibitor counter-screen.

In principle, noncovalent, allosteric inhibition could provide another route for the development of therapeutically useful Ubc13-targeted compounds. While E2 enzymes in general lack the deep, complex active site clefts that characterize traditionally druggable targets, an allosteric inhibitor of another E2 enzyme, Cdc34, has been developed¹⁴². The Cdc34 inhibitor, CC0651, binds and induces a conformational change in Cdc34 that opens the enzyme structure to accommodate the inhibitor and also distorts the active site to inhibit Cdc34 catalytic activity. The authors

suggest that this pocket could be exploited to develop similar inhibitors specific to a variety of different E2 enzymes, including Ubc13.

The importance of developing specific inhibitors of a critical, nonredundant enzyme such as Ubc13 that plays essential roles in pathways that are intimately associated with tumour cell viability and susceptibility to treatments cannot be underestimated. A recent study has shown Ubc13 to be among a number of genes that have increased expression in nasopharyngeal carcinoma cells resistant to cisplatin, which display a greater frequency of sister chromatid exchange via template switching¹⁴³. Depletion of Ubc13 in these cells suppresses sister chromatid exchange and resensitizes these cells to cisplatin. Another recent study demonstrated that increased Uev1A levels can drive human breast cancer cell invasion and metastasis in mouse xenograft models in a manner that is dependent on Ubc13¹⁴⁴. Ubc13 has also been shown to control breast cancer metastasis through the activation of a TAK1-p38 kinase¹⁴⁵. Chronic inflammation is often a precursor to cancer development, and the NF- κ B pathway is often constitutively activated in many cancers, which can, in part, lead to acquired chemo-resistance¹⁴⁶. An effective Ubc13 inhibitor could target chemo-resistant cancer cells through inhibition of the Ubc13-dependent template switching and NF- κ B pathways, aid in breast cancer metastasis prevention, and sensitize these cells to DNA damaging radiation/chemotherapy through inhibition of the Ubc13-dependent DDR.

3.4: Materials and Methods

3.4A: Protein production

Ubc13, Mms2, RNF8, and mUBA1 cloning, and protein production/purification was previously described^{29,147,148}. The Ubc13^{QD} mutant was made using PCR mutagenesis with Ubc13^{WT} as a template. The mUBA1 enzyme was produced according to a previously published protocol¹⁴⁸, however, the His-tag vector used was pET47b(+).

3.4B: Crystallization and structure determination

The Ubc13^{WT} (or Ubc13^{QD})/Mms2 heterodimeric complexes were concentrated to 6 mg/mL in crystallization buffer¹⁴⁷. Compounds for co-crystallization (NSC697923 from the National Cancer Institute Developmental Therapeutics Program, or BAY 11-7082 purchased from Sigma) were dissolved in 100% DMSO at a concentration of 100 mM and were mixed with Ubc13 at a 5-fold molar excess (for NSC697923) or a 10-fold molar excess (for BAY 11-7082) of protein:inhibitor. The complexes were incubated overnight at 4 °C prior to setting up crystallization trials. Crystals were grown using vapor diffusion in 100 mM sodium citrate, pH 7.4, and 15% (w/v) PEG 8000. Crystals grew within 2 days. Data were collected at both the Canadian Light Source 08B1-1 (Mms2/Ubc13~NSC697923 & Mms2/Ubc13~BAY 11-7082) and the Advanced Light Source 12.3.1 (Mms2/Ubc13^{QD}). The data sets were collected at 1.03321, 0.97947, and 1.03316 Å, respectively. Ramachandran statistics are 99%, 98%, and 97% preferred for

Mms2/Ubc13~NSC697923, Mms2/Ubc13~BAY 11-7082, and Mms2/Ubc13^{QD}, respectively. Structures were refined using PHENIX¹¹⁶.

Table 2. Data Collection and refinement statistics of mutant and inhibited Ubc13

	Ubc13~N2F	Ubc13~BY1	Ubc13^{QD}
Data Collection			
Space Group	P2(1)2(1)2(1)	P2(1)2(1)2(1)	P2(1)2(1)2(1)
Cell Dimensions			
a,b,c (Å)	44.5, 74.9, 91.3	44.7, 74.5, 91.5	43.9, 74.9, 92.0
α,β,γ (°)	90, 90, 90	90, 90, 90	90, 90, 90
Resolution (Å)	24.3-1.35	45.8-1.5	29.1-1.35
² R _{sym}	3.2 (61.5)*	4.3 (51.4)*	2.6 (52.7)*
I/σ	32.4 (1.97)*	19.2 (1.45)*	31.8 (2.23)*
Completeness (%)	99.5 (98.6)*	99.9 (99.9)*	98.9 (97.2)*
Redundancy	4.7 (4.0)*	3.5 (1.9)*	3.7 (3.5)*
Refinement			
No. Reflections	314,275	329,049	244,065
R _{work} /R _{free}	15.9/19.2	17.9/21.3	17.1/19.9
No. Atoms			
Protein	2,393	2,357	2,351
Ligand/ion	14	22	0
Water	212	183	197
Overall B-factor	25.1	28.9	24.1
Protein	24.4	28.3	23.5
Ligand/ion	26.9	37.8	0
Water	32.0	34.7	31.9
R.M.S. Deviations			
Bond Lengths (Å)	0.013	0.008	0.011
Bond Angles (°)	1.44	1.64	1.40

*Values in parentheses' are for highest resolution shell

3.4C: Ubiquitination inhibition assay

All ubiquitination assays were done in a buffer containing 50 mM Tris-HCl pH 7.5, 100 mM NaCl, 10 mM MgSO₄, and 1 μM ZnSO₄. The following concentrations of components were added when necessary: 0.5 μM mUBA1, 0.2 μM Ubc13 (WT or QD), 0.2 μM Mms2, 1 μM RNF8, 100 μM ubiquitin, 3 mM ATP. Appropriate dilutions of the compounds (NSC697923 or BAY 11-7082) were made from a 100 mM stock dissolved in 100% DMSO. The total volume of each reaction was 50 μL. The reactions were run for 1.5 hours at 37 °C and quenched with SDS-PAGE loading buffer and the results were visualized by Western blotting. The primary antibody was mouse anti-ubiquitin (Santa Cruz), and the secondary was goat anti-mouse-FITC (Sigma-Aldrich).

3.4D: *In vitro* inhibition absorbance assay

Reactions were done in a buffer containing 50 mM HEPES pH 7.5, 75 mM NaCl. The reactions contained 200 μM NSC697923, and 200 μM of Ubc13 (WT, QD, or C87S). The experimental absorbance data was baseline corrected using the intrinsic absorbance of the non-reactive C87S mutant. The second-order rate constant for reaction with NSC697923 was determined by numerically integrating the following coupled differential equations,

$$\frac{d[\text{Ubc13} \sim \text{NSC697923}]}{dt} = k_2 [\text{Ubc13}][\text{NSC697923}]$$

$$\frac{d[\text{Ubc13}]}{dt} = -k_2 [\text{Ubc13}][\text{NSC697923}]$$

$$\frac{d[\text{NSC697923}]}{dt} = -k_2 [\text{Ubc13}][\text{NSC697923}]$$

at various values of k_2 and a scaling factor (used to convert absorbance readings to protein concentration). Values of the k_2 and the scaling factor were chosen using an in-house simulated annealing algorithm and the squared differences between the generated curves and the experimental data points were calculated to find the values that best fit the experimental data. All reactions were performed at room temperature. The average k_2 values of three independent experiments were reported with their standard error.

3.4E: NMR of ^{15}N -Ubc13^{C87S} and NSC697923

BL21 DE3 *E.coli* cells harbouring a Ubc13^{C87S} expression plasmid were grown and uniformly ^{15}N -labeled according to the published protocol¹⁴⁹ and as previously described for wild-type Ubc13¹⁵⁰.

$[\text{U-}^{15}\text{N}]\text{-Ubc13}^{\text{C87S}}$ was expressed as a GST fusion protein, and cleaved and purified (see Protein production). The 600 μL NMR sample contained 0.21 mM $[\text{U-}^{15}\text{N}]\text{-Ubc13}^{\text{C87S}}$ in PBS, pH 7.4 and 10% D2O in a standard 5 mm NMR tube. $^1\text{H-}^{15}\text{N}$ sensitivity enhanced HSQC spectra¹⁵¹ were acquired at 25°C on a Varian Unity INOVA 600 MHz spectrometer

equipped with a room temperature 5 mm triple resonance probe. Spectra were processed using NMRPipe¹⁵².

¹H and ¹⁵N chemical shift changes relative to the free protein sample were measured in the presence of 83 μM, 250 μM, and 1.88 mM of NSC697923. As the NSC697923 stock solution was dissolved in DMSO, these chemical shift changes were also compared to those upon addition of DMSO alone to [*U*-¹⁵N]-Ubc13^{C87S}, as a control. Chemical shift changes were analyzed using Sparky¹⁵³.

3.4F: Generation of stably integrated Ubc13 MEFs

The generation of Ubc13 knockout mouse embryonic fibroblasts has previously been reported¹³⁵. Re-introduction of either WT or QD Ubc13 was accomplished using retroviral transduction. 293T cells were transiently transfected with 0.9 μg gag/pol expression vector, 0.1 μg VSV-G envelope vector, and 1 μg of pBABE-GFP-Ubc13 transfer vector using Qiagen Effectene for viral production. Viral supernatant was collected at 24, 48, and 72 hours post transfection. Knockout MEFs were infected twice with the viral supernatants. GFP expressing cells were sorted via flow cytometry.

3.4G: Assay for NF-κB signaling and DNA damage localization in MEFs

Transduced MEF cells or knockouts were seeded to $\sim 8.57 \times 10^4$ cells the day before using a hemacytometer. The next day they were incubated with

NSC697923 for 30 minutes, then stimulated with 0.1 $\mu\text{g}/\text{mL}$ LPS for 1 hour or irradiated with 3 Gy ionizing radiation and left to recover for 2 hours, then fixed in 4% (w/v) paraformaldehyde. The 0 μM controls contained an equivalent concentration of DMSO as that found in the NSC697923 treated cells. Fixed cells were permeabilized with PBS-0.5% (v/v) Triton X-100 and rinsed with PBS. Cells were incubated with either an anti-p65 antibody (Santa Cruz, sc-372), or anti-53BP1 (Santa Cruz, sc-22760) and anti- γH2AX (Millipore, 05-636) antibodies. Slides were mounted in a glycerol-based media containing 4',6-diamidino-2-phenylindole (DAPI) to stain the nuclei. Invitrogen (37-1100) anti-Ubc13 antibody was used for Western blotting. MetaMorph was used to acquire single-plane images. Images were independently scaled in Photoshop CS3 (Adobe) for Windows, to best represent the subcellular distribution of the fluorescent stain. Further technical details are described in Supporting Information.

3.4H: Multiplex Mouse Cytokine Array

MEF conditioned medium was assayed by Eve Technologies (Calgary, Alberta, Canada) using Multiplexing LASER bead technology. Briefly the method entails the addition of different coloured fluorescent beads coupled with specific cytokine-specific antibodies to the medium, which can be discriminated via a bead analyzer. A biotinylated antibody is used to detect the cytokine, which is then quantified using a fluorescent streptavidin-phycoerythrin conjugate. The target analyte is directly proportional to the amount of conjugate detected by the bead analyzer. The

cytokines/chemokines contained in the array from Eve Technologies were: Eotaxin, G-CSF, GM-CSF, IFN γ , IL-1 α , IL-1 β , IL-2, IL-3, IL-4, IL-5, IL-6, IL-7, IL-9, IL-10, IL-12 (p40), IL-12 (p70), IL-13, IL-15, IL-17A, IP-10, KC, LIF, LIX, MCP-1, M-CSF, MIG, MIP-1 α , MIP-1 β , MIP-2, RANTES, TNF α , VEGF.

3.4I: CellProfiler and Statistical Analyses

CellProfiler was used to find and measure nuclei, cytoplasm, and foci of the MEF cells in the 16-bit TIFF files, for which the Otsu thresholding method was chosen¹⁵⁴⁻¹⁵⁶. Statistical significance was determined using a two-tailed Student's *t* test and significance level of *P<0.05 (unless otherwise specified) using Microsoft Excel 2010.

3.4J: Accession codes

Ubc13~NSC697923: **4ONM**. Ubc13~BAY 11-7082: **4ONN**. Ubc13^{QD}: **4ONL**.

3.5 Acknowledgments

The authors thank P. Grochulski, K. Janzen, and M. Fodje at the Canadian Light Source and S. Classen at the Advanced Light Source (SIBYLS) for crystallographic data collections support. They also thank the Flow Cytometry Units and Cellular Imaging Facility at the Cross Cancer Institute for the use of flow cytometers and microscopes and S. Baksh for helpful discussions. This work was performed with support from Canadian Cancer Society/Canadian Breast Cancer Research Alliance (to J.N.M.G.), the

Canadian Institutes of Health Research (CIHR114975 to J.N.M.G.; CIHR119515 to M.J.H.), the National Institutes of Health (CA92584 to J.N.M.G.), and the Alberta Innovates Health Solutions.

Chapter 4

¹The DNA damage response requires E2-ubiquitination enzyme stimulation by RING E3

¹A version of this chapter is in preparation for submission as: Hodge, C. D., Edwards, R. A., Hura, G., Tainer, J. A., Hendzel, M. J., & Glover, J. N. M. The DNA damage response requires E2-ubiquitination enzyme stimulation by RING E3.

4.1 Introduction

A major method of intracellular communication is accomplished through protein ubiquitination, whereby a target molecule is tagged with ubiquitin or ubiquitin chains to confer a specific signal⁵⁶. An E1 activating enzyme uses ATP to initiate ubiquitin chain synthesis by the formation of a covalent linkage to the C-terminal glycine of ubiquitin^{54,57}. The ubiquitin molecule is subsequently transferred to the active site cysteine of an E2 conjugating enzyme, via a trans-thiolation reaction^{52,57}. One of many possible E3 ligases can bind the E2~Ub complex to both provide the target and to possibly stimulate the conjugating activity of the E2 enzyme (RING E3s) or to act as an intermediate to the substrate through the use of an active site cysteine (HECT and RBR E3s)^{29,73-76}.

An important RING E3 ligase that functions in the DNA Damage Response (DDR) is RNF8, which binds and activates the E2, Ubc13, to create Lys63-linked ubiquitin chains^{29,32}. These chains act as scaffolds for proteins that contain ubiquitin-interacting motifs (UIMs), such as RAP80, or motifs interacting with ubiquitin (MIUs) such as the RING E3 ligase RNF168, which directly bind ubiquitin^{20,37,157,158}. Both RING E3 ligases RNF8 and RNF168 are recruited to the sites of double strand break (DSB) DNA damage, although it is not completely clear as to the order of recruitment. Initially, broken DNA ends are recognized by the Mre11-Rad50-Nbs1 (MRN) complex that subsequently recruit and activate ATM, which phosphorylates H2AX (γ H2AX) within chromatin surrounding the

lesion^{21,22}. The scaffolding protein MDC1 binds γ H2AX through its BRCT domain, and is also phosphorylated by ATM²³⁻²⁵. This allows association of RNF8 through its N-terminal FHA domain^{30,36}. It is likely that RNF8 then poly-Lys63 ubiquitinates an unknown substrate, which recruits RNF168 through its MIUs to amplify the signal and monoubiquitinate histones H2A/H2AX on K13-15^{20,32,33}. RNF8 and RNF168 then cooperate to extend these Lys63 polyubiquitin chains allowing for the eventual recruitment of RAP80, BRCA1, and 53BP1, resulting in DSB repair^{2,35}. RNF8 and RNF168 both serve as recruitment factors for Ubc13, however work with the purified E3 RING domains and Ubc13 have shown that while the RNF8 RING tightly binds and activates Ubc13, RNF168 interacts much more weakly with Ubc13 and does not significantly stimulate its catalytic activity²⁹.

The mechanism by which RING E3s stimulate E2~Ub conjugating activity was largely uncharacterized until recent studies (2012) demonstrated that a hydrophobic-mediated interaction between the E2-linked donor ubiquitin and the RING domain of the RING E3 ligase position the ubiquitin C-terminus in an E2 groove, which likely enforces a catalytically favorable orientation for attack of the thioester by the incoming acceptor lysine^{74-76,159}. Despite these characterized roles of RING E3 ligases, it has yet to be determined if both the E2-stimulating activity and the E2-targeting activity of RING E3 ligases are required for proper functioning of an E2-E3 pair. Here, we demonstrate through structural and

biochemical studies that the recently proposed RING E3-mediated E2-stimulating mechanism holds true for the RNF8 - Ubc13 E3 – E2 pair. Using an RNF8 mutant specifically deficient in its E2-stimulating activity, we demonstrate that the RNF8 E2-stimulating activity is required for proper functioning of the DNA damage response, and that the recruitment of the RNF8 mutant to the sites of DNA DSBs is insufficient for repair. Our results indicate that the direct stimulation of Ubc13 polyubiquitination by RNF8 is required for the formation of Lys63-linked ubiquitin chains at sites of DNA DSBs and for the downstream recruitment of 53BP1.

4.2 Results

4.2A: The crystal structure of RNF8/Ubc13~Ub reveals an activated ubiquitin conformation

E3 RNF4 can stimulate the ubiquitination activity of the E2 UbcH5a by directly interacting with the donor ubiquitin linked to the UbcH5a active site (UbcH5a~Ub)^{74,160}. To stabilize the UbcH5a~Ub complex for structural studies, the thioester linkage between the ubiquitin C-terminus and the UbcH5a active site cysteine was replaced with an isopeptide linkage via mutation of the active site cysteine to a lysine. To test if a similar mechanism acts in the RNF8/Ubc13 system, we used the same technique to covalently tether the ubiquitin C-terminus to Ubc13 and crystallized this complex bound to an RNF8 construct encompassing its RING domain and coiled-coil (RNF8₃₄₅₋₄₈₅). We previously solved the X-ray crystal structure of RNF8₃₄₅₋₄₈₅ bound to Ubc13/Mms2²⁹. Although efforts to crystallize a

complex of RNF8₃₄₅₋₄₈₅/Ubc13~Ub/Mms2 were unsuccessful, we were able to crystallize the RNF8₃₄₅₋₄₈₅/Ubc13~Ub complex in the absence of Mms2 and determine its structure at 8.3 Å resolution by molecular replacement using our RNF8/Ubc13 and free ubiquitin as search models (Methods; Figure 33a,b).

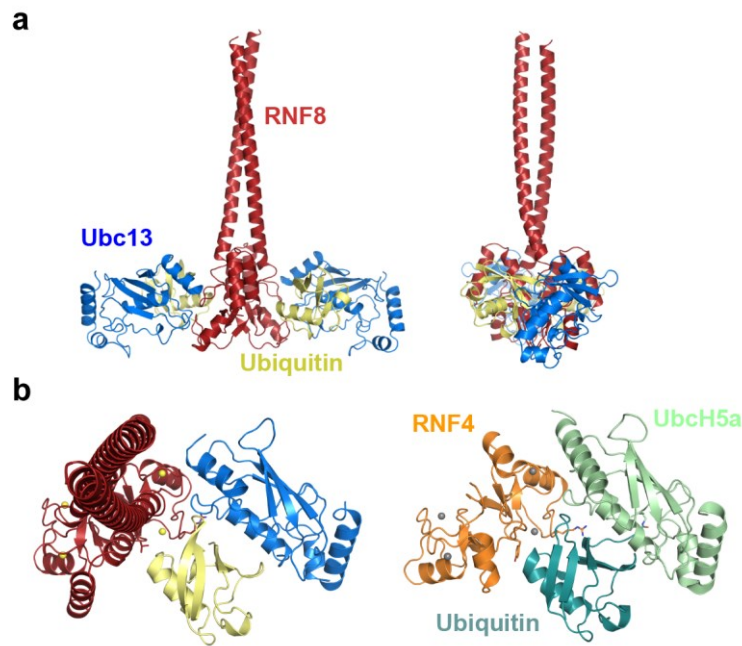


Figure 33. RNF8/Ubc13~Ub structure and comparison to RNF4/UbcH5a~Ub.

(a) Overview of RNF8/Ubc13~Ub structure (Protein Data Bank accession 4WHV). RNF8 dimers are firebrick red, Ubc13s are blue, ubiquitins are yellow. (b) Top-down view of singly loaded (one Ubc13 and one ubiquitin) RNF8 dimer (left) and singly loaded (one UbcH5a and one ubiquitin) RNF4 dimer (right; PDB: 4AP4). RNF4 dimer is orange, UbcH5a is pale green, and ubiquitin is aqua green.

The resolution was limited due to long distance crystallization contacts mediated by the RNF8 coiled-coil domain, which adopts different

orientations relative to the RING domain in the two complexes in the asymmetric unit (Figure 34a,b). Despite the low resolution, the difference density after molecular replacement with a RNF8-RING/Ubc13 model was sufficient for Phaser to place one ubiquitin molecule, and the other ubiquitins were placed using symmetry operations and rigid body refinement (Methods, Figure 35). The structure shows that both RNF8 protomers in the dimer can simultaneously bind a Ubc13~Ub (i.e. the RNF8 dimer is doubly-loaded), which supports and extends our previous determination of the stoichiometry of the complex in solution²⁹ (Figure 33a).

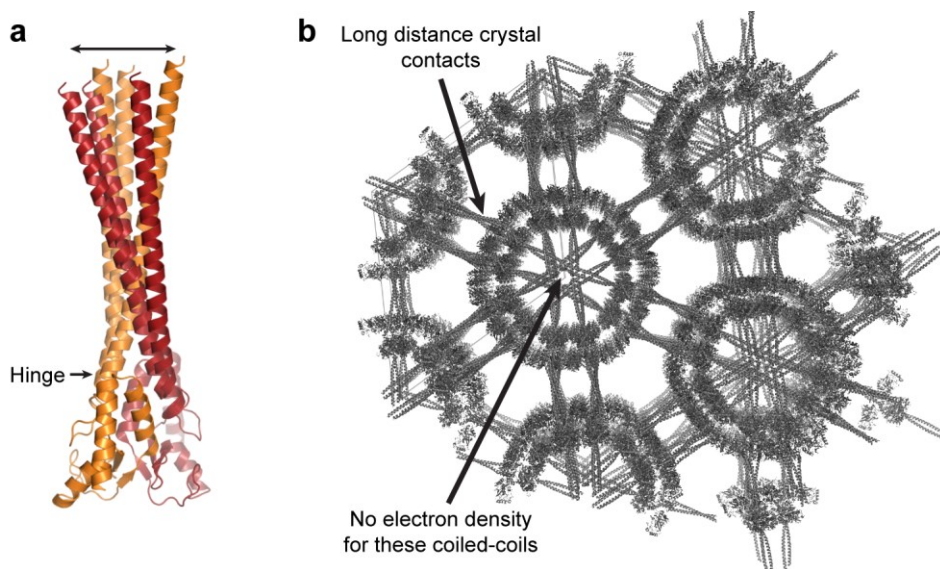


Figure 34. RNF8 coiled-coils have flexibility and make long distance crystallization contacts in the RNF8/Ubc13~Ub crystal lattice.

(a), Superposition of the RING domains (393-480) of RNF8 from the RNF8/Ubc13~Ub structure and two RNF8 dimers in the asymmetric unit of the RNF8/Ubc13/Mms2 structure (PDB: 4ORH). One set of protomers is colored orange and the other firebrick red. (b), Symmetry related complexes of the RNF8/Ubc13~Ub structure showing long distance crystal contacts mediated by the RNF8 coiled-coils.

The structure reveals a closed ubiquitin conformation that makes contacts with both protomers of the RNF8 RING dimer (Figure 33a). The orientation of the ubiquitin resembles that seen in the high resolution RNF4/UbcH5a~Ub structure (Figure 33b). The closest contact between RNF8 and the ubiquitin is between the C-terminal end of the ubiquitin alpha-helix and the distal RNF8 protomer L451. RNF8 H420 may hydrogen bond with ubiquitin E34 at the alpha helix C-terminus, as there is an analogous interaction between RNF4 H160 and ubiquitin⁷⁴. The canonical hydrophobic I44 patch on ubiquitin, which mediates many ubiquitin interactions with protein partners⁸⁵, likely makes contact with the Ubc13 central crossover helix (α 2). The C-terminal tail of ubiquitin is not modeled, due to weak electron density, but is likely tethered to Ubc13 via an isopeptide bond with the amino group of the Cys to Lys active site mutation (C87K) formed by an *in vitro* reaction (see 4.4 Methods). The asymmetric unit contains two doubly-loaded complexes, and the RNF8 coiled-coils are only partially modeled in one of these complexes, likely due to a lack of crystal contacts at their N-terminal end (see Figure 34). However, the closed ubiquitin conformation is clear.

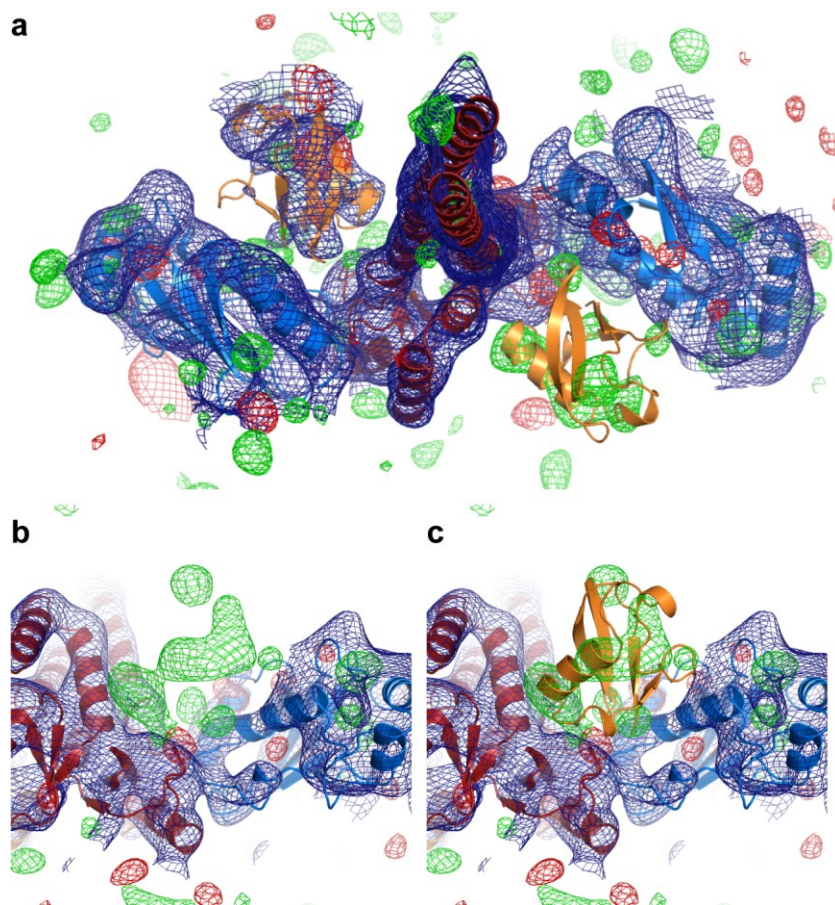


Figure 35. Electron density of the RNF8/Ubc13~Ub complex at 8.3 Å resolution.

(a), Electron density maps for an RNF8/Ubc13~Ub complex in which one of the ubiquitins (lower right side, orange) was omitted from the phase calculation. $F_o - F_c$ difference density contoured at $\sigma = 3$ is shown in green and red, and $2F_o - F_c$ contoured at $\sigma = 1$ is shown in blue. (b) and (c), The same model and maps are shown in a view rotated 180° about the horizontal axes compared with panel (a). In panel (b), the omitted ubiquitin chain is removed, while in panel (c) the omitted ubiquitin is shown in orange. RNF8 is red and Ubc13 is blue.

4.2B: RNF8 L451 is required for full stimulation of Ubc13 catalytic activity in vitro

We sought to uncover mutations that destabilize the ubiquitin-RNF8 interface to test its importance for ubiquitination. An alignment of the low resolution RNF8/Ubc13~Ub structure with the RNF4/UbcH5a~Ub structure allowed us to infer important residues in RNF8 that mediate the contact with ubiquitin, despite the limited resolution (Figure 36a). We reasoned that two residues could be largely responsible for stabilizing ubiquitin in the closed conformation. RNF8 L451 makes hydrophobic contacts with the C-terminus of the ubiquitin alpha-helix (Figure 36a). The RNF4/UbcH5a~Ub structure makes an analogous contact between RNF4 Y193 and the ubiquitin alpha-helix⁷⁴. RNF4 Y193 not only contacts ubiquitin but also forms part of the E3 dimer interface¹⁶⁰, however our structure predicts that L451 in RNF8 does not participate in the RNF8 dimer interface. The second residue is RNF8 R441, which we predict makes extensive hydrogen bonds with both Ubc13 and ubiquitin based on the analogous RNF4 R181 of the RNF4/UbcH5a~Ub structure⁷⁴ (Figure 36a). Mutation of RNF4 R181 to alanine severely impairs RNF4/UbcH5a catalytic activity in a single-turnover assay¹⁶⁰.

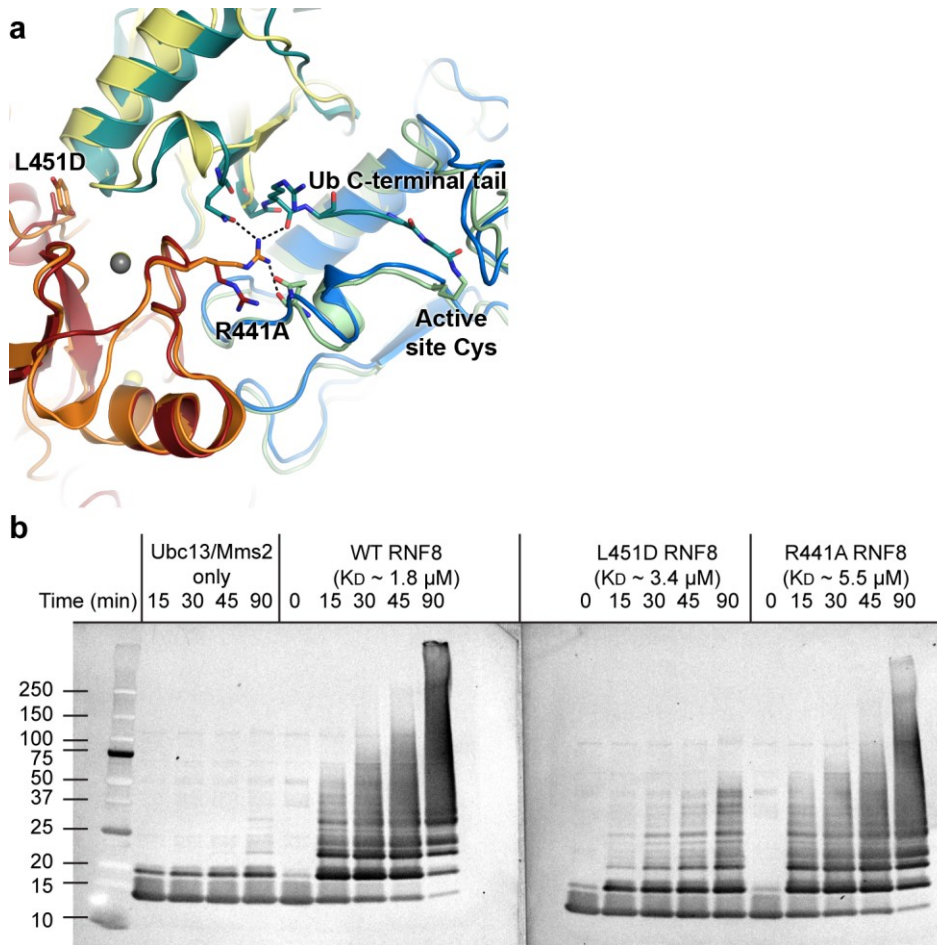


Figure 36. RNF8 mutations affect Ubc13 catalytic activity.

(a) Close-up view of an alignment of the RNF8/Ubc13~Ub structure (RNF8 is firebrick red, Ubc13 is blue, ubiquitin is yellow) with the RNF4/UbcH5a~Ub structure (PDB: 4AP4; RNF4 is orange, UbcH5a is pale green, and ubiquitin is aqua green). Residues proposed to be important for interactions with E2s and ubiquitin are shown in sticks. (b) *In vitro* ubiquitination assays in which purified RNF8 (WT, L451D, or R441A) was incubated with Ubc13/Mms2, ubiquitin, ATP, and E1 enzyme, for the indicated time before quenching. Results were visualized via Western blotting using an anti-ubiquitin antibody. The apparent equilibrium dissociation constants (K_D) for the interactions of each of the RNF8 proteins with Ubc13 is indicated.

To test our hypothesis that RNF8 residues L451 and R441 are largely responsible for stable ubiquitin binding and stimulation of Ubc13

catalytic activity, we made the RNF8 mutations L451D and R441A. The L451D mutation introduces a negative charge in place of the hydrophobic leucine, which is predicted to clash with the carbonyl oxygens at the C-terminus of the ubiquitin alpha-helix to disfavour the closed conformation of the ubiquitin. The R441A mutant is predicted to disrupt interactions between RNF8, Ubc13 and ubiquitin. We tested the ability of these mutants to stimulate Lys63-linked ubiquitin chain formation by Ubc13/Mms2 compared to wild type RNF8 in an *in vitro* assay using purified proteins (Figure 36b). Under these reaction conditions, Ubc13/Mms2 is able to drive formation of di-ubiquitin; however, addition of wild type RNF8 stimulated the formation of longer poly-ubiquitin chains. The L451D mutation caused a drastic decrease in the ability of RNF8 to stimulate Ubc13: ubiquitin chain formation is only marginally better than Ubc13/Mms2 alone (Figure 36b, right panel). Surprisingly the R441A mutant had little effect on ubiquitin chain formation. To ensure that the mutations only affect ubiquitin conformational selection and not binding to Ubc13, we measured the steady state affinities of the WT and mutant RNF8 proteins for Ubc13 by surface plasmon resonance (Figure 37 and Figure 38). The results demonstrate that the L451D mutation has little effect on the apparent equilibrium dissociation constant ($K_{D,WT} \sim 1.8 \mu\text{M}$; $K_{D,L451D} \sim 3.4 \mu\text{M}$), and the R441A mutation had a very minor effect ($K_{D,R441A} \sim 5.5 \mu\text{M}$). The bivalent binding capability of the RNF8 RING dimer likely increased the apparent on-rate of binding to Ubc13, which

suggests that the true affinities are likely lower. This would make the affinities more consistent with other E2:E3 RING pairs such as the monomeric gp78 RING:Ube2g2 complex with a $K_D \sim 144 \mu\text{M}$ ¹⁶¹. Taken together, these results indicate RNF8 L451D selectively abrogates Ubc13 polyubiquitination through disruption of RNF8-ubiquitin interactions.

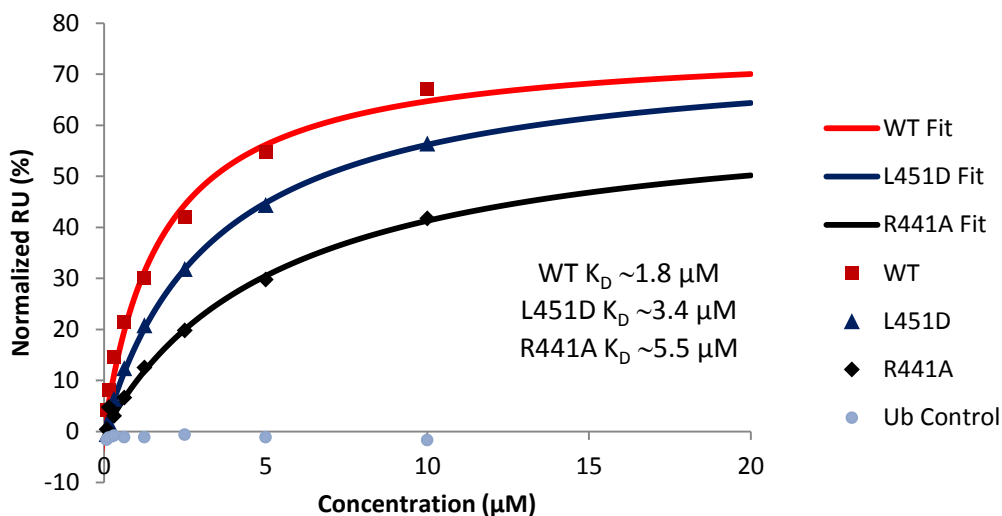


Figure 37. RNF8-ubiquitin interface mutations do not significantly affect binding to Ubc13.

Steady state affinity analysis of the RNF8 surface plasmon resonance (SPR) curves of WT, L451D, and R441A demonstrating binding to chip-conjugated Ubc13. Ubiquitin was run as a negative control. The saturation point for wild type, L451D, and R441A RNF8 binding to Ubc13 was estimated from a hyperbolic non-linear regression fit to duplicate data sets. The estimated apparent equilibrium constants (K_D) were determined using a fractional saturation analysis¹⁶² in SigmaPlot.

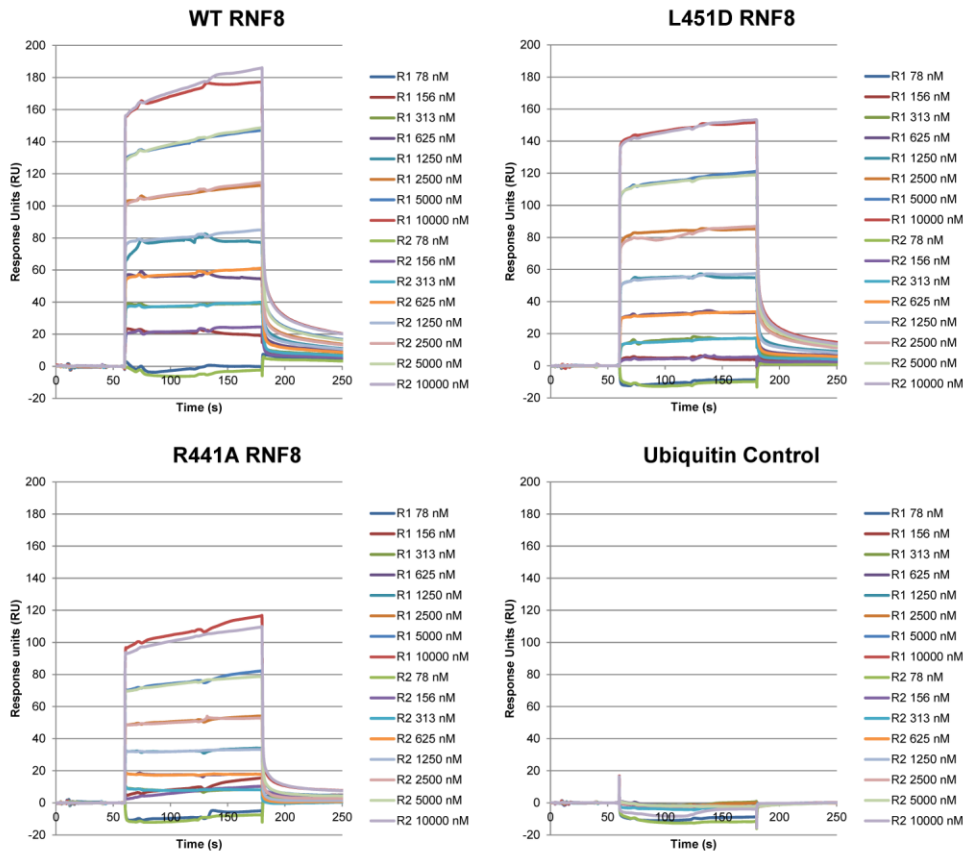


Figure 38. Raw SPR curves for RNF8 constructs.

Surface plasmon resonance curves of WT, L451D, and R441A demonstrating binding to chip-conjugated Ubc13. Ubiquitin was run as a negative control.

4.2C: SAXS analysis of the RNF8/Ubc13~Ub complex show ubiquitin conformational selection in solution

Having demonstrated that the RNF8 L451D mutation abrogates Ubc13 ubiquitination stimulation, we wished to determine whether the closed ubiquitin conformational selection seen in our RNF8/Ubc13~Ub crystal structure is also present in solution and compare this to the conformational selection of the L451D RNF8/Ubc13~Ub complex. To do this we used small angle X-ray scattering (SAXS) to assess the solution

structure and dynamics of the purified WT (top panel) and L451D (bottom panel) RNF8₃₄₅₋₄₈₅/Ubc13~Ub complexes (Figure 39). Guinier analysis of the scattering of the wild type (Figure 40a) and L451D (Figure 41a) complexes indicate well-behaved samples with no significant aggregation and a radius of gyration (R_g) of 41.4 Å and 41 Å, respectively. To assess the degree of flexibility of the complexes in solution, we used a method based on the Porod-Debye law that has been developed to assess the relative electron density contrast between the scattering particle and the solution and can give information on the flexibility of complexes¹⁶³, (Figure 40b and Figure 41b). The SAXS profiles of WT and L451D are similar and indicate flexibility within the RNF8/Ubc13~Ub complexes. The degree of flexibility is correlated to the rate of decay of the SAXS curve as a function of the scattering angle, q ¹⁶³. A plateau region is observed in the Sibyls plots when plotting the SAXS curves as $q^3 \times I(q)$ vs q indicating a q^3 decay. This is between the q^4 decay typical of a compact particle and q^2 decay of an unfolded one. The degree of flexibility is consistent with discrete elements of conformational flexibility within the complexes. We reasoned that this motion may reflect movement of the covalently bound ubiquitin, as has been reported for E4BU/UbcH5c~Ub^{75,137}.

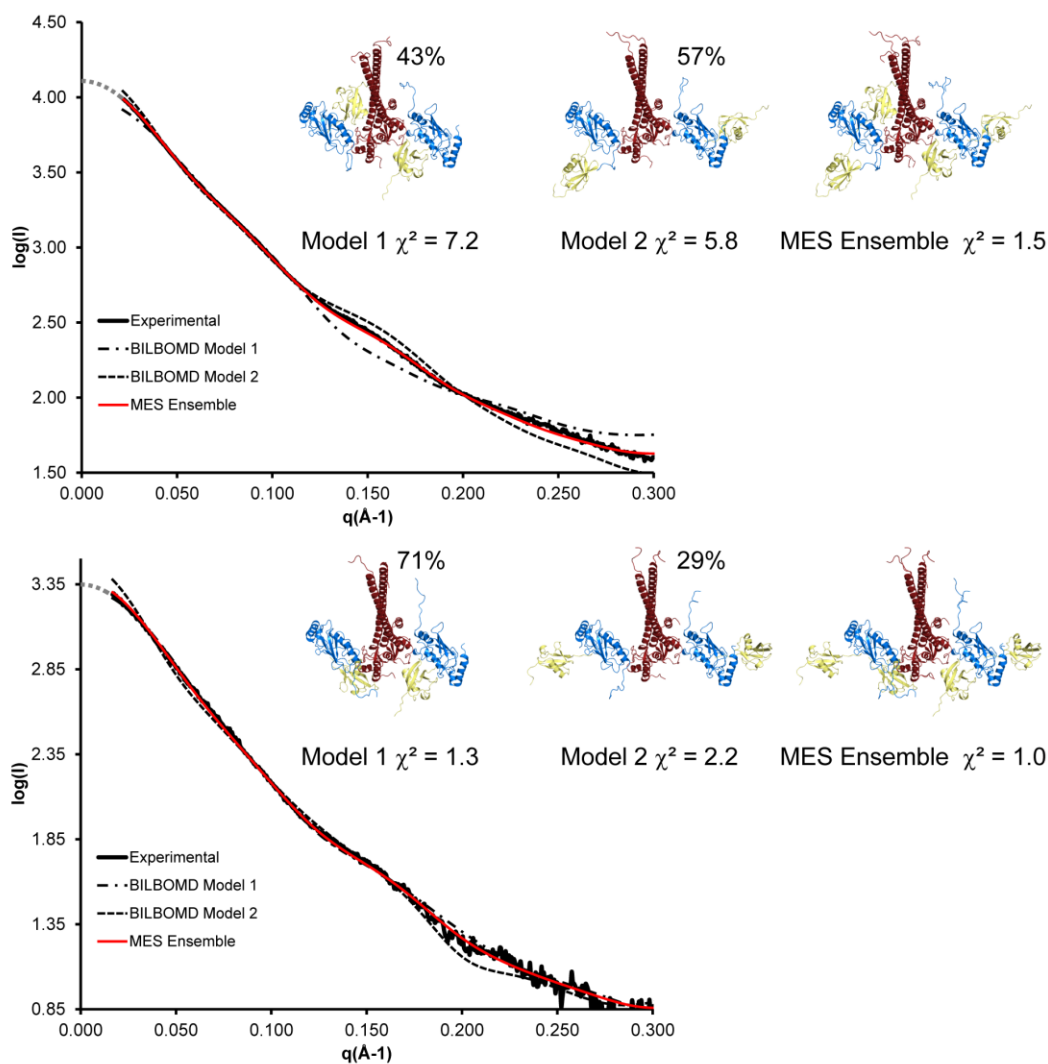


Figure 39. SAXS analysis and defining a minimal RNF8/Ubc13~Ub ensemble.

A plots of the experimental SAXS curves for WT RNF8/Ubc13~Ub (top panel) and L451D RNF8/Ubc13~Ub (bottom panel) are shown as black solid lines. The two models selected in the MES procedure as well as an overlay of the two models are shown with the same colors as Figure 33. The calculated scattering curves of the individual models (black, dashed), their relative weighting in MES, and their goodness of fit (χ^2) to the experimental data are indicated. In red is the calculated scattering curve of the MES ensembles, as well as their associated goodness of fit to the experimental data.

To test the idea that the complex flexibility might be due to the reorientation of the tethered ubiquitin relative to the rest of the complex, we utilized a minimal ensemble search (MES) to identify a minimal set of RNF8/Ubc13~Ub conformations that represent the distributions of structures in solution and best fit the SAXS data. We created a library of stereochemically reasonable RNF8₃₄₅₋₄₈₅/Ubc13~Ub models using molecular dynamics as implemented in BILBOMD¹¹⁴. The RNF8 dimer and both Ubc13 molecules were fixed during the simulation, while the Ubc13-tethered ubiquitin was allowed to sample conformational space. FoXS^{164,165} was used to calculate theoretical scattering curves for each of the 9599 models in the library and to perform the minimal ensemble search. MES for the WT RNF8/Ubc13~Ub complex found a minimal ensemble of two models, one of which corresponds to a model in which both ubiquitins are in the closed conformation, resembling the crystal structure, and a second in which the ubiquitins are in an extended conformation. Notably, neither of these models provide a good fit to the data alone ($\chi^2 = 7.2$ for the closed conformation, $\chi^2 = 5.8$ for the open), however a weighted average of the two models gives an excellent fit to the experimental data ($\chi^2 = 1.5$; Figure 39 – top panel).

MES for the L451D RNF8/Ubc13~Ub complex also selected a minimal ensemble of two models; however neither of these correspond to the fully closed state of the crystal structure. One model has a partially closed state where one ubiquitin is in the closed conformation and the

other ubiquitin is in a “down” extended conformation close to the bottom of the RNF8 RING. The other model resembles the wild type open model with the ubiquitins in an extended conformation. These models provide a reasonably good fit to the data alone ($\chi^2 = 1.3$ for the half-closed conformation, $\chi^2 = 2.2$ for the open), however a weighted average of the two models gives an enhanced fit to the experimental data ($\chi^2 = 1.0$; Figure 39 – bottom panel). Overall, this suggests that the mutant data are functionally similar to the wild type, within the limits of SAXS discrimination. Thus the SAXS analysis indicates that while the tethered ubiquitin is likely flexible, it samples the closed conformation in both wild type and L451D RNF8/Ubc13~Ub complex. The flexibility of the complexes can be accurately modeled by reorientation of the tethered ubiquitins.

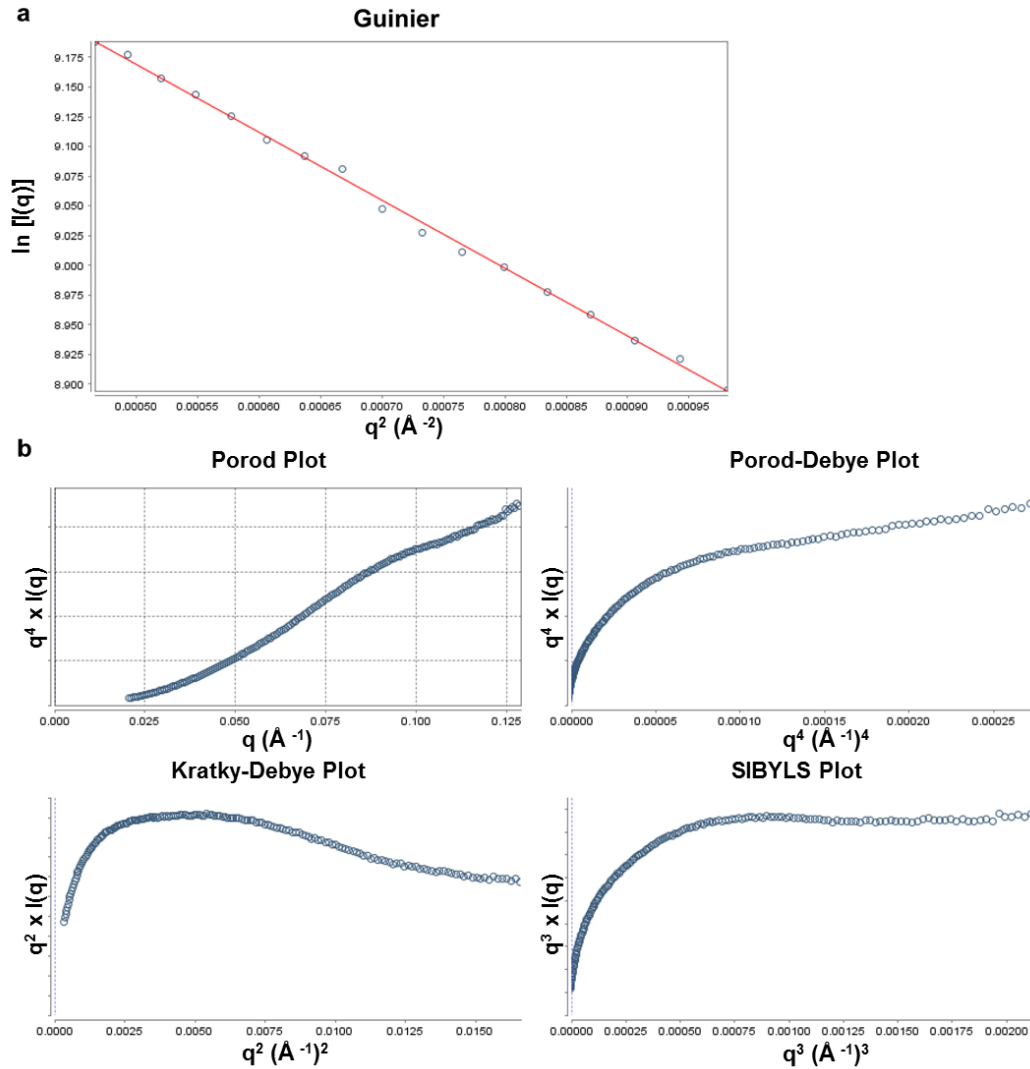


Figure 40. Guinier and flexibility plots of the WT RNF8/Ubc13~Ub complex derived from SAXS.

(a) Linear Guinier analysis of the RNF8/Ubc13~Ub complex shows no sample aggregation¹¹³. (b) The lack of a plateau in the Porod-Debye plot indicates significant conformational flexibility, while a plateau in the SIBYLS plot indicates a high likelihood of a non-disordered complex of discrete elements that account for the flexibility¹⁶³.

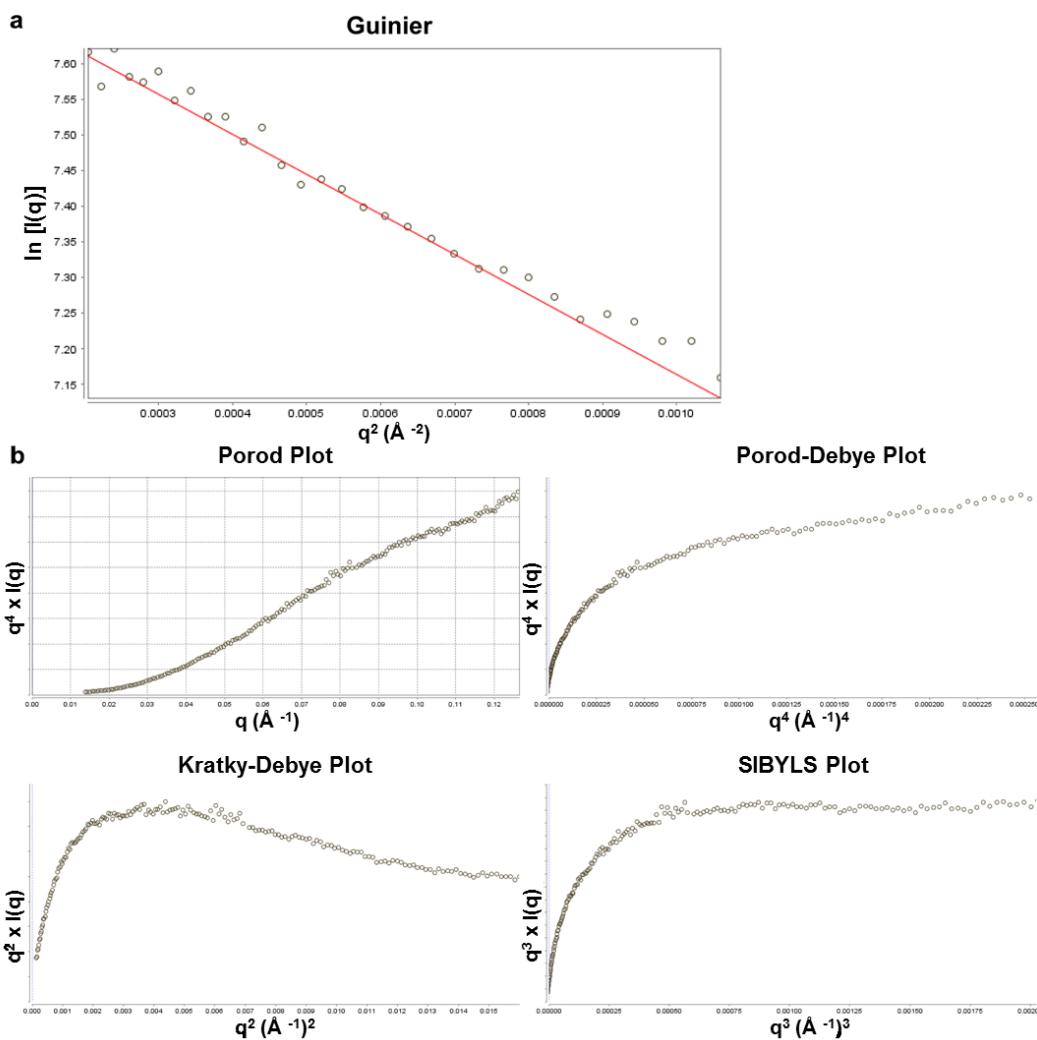


Figure 41. Guinier and flexibility plots of the L451D RNF8/Ubc13~Ub complex derived from SAXS.

(a) Linear Guinier analysis of the L451D RNF8/Ubc13~Ub complex shows no sample aggregation¹¹³. (b) The lack of a plateau in the Porod-Debye plot indicates significant conformational flexibility, while a plateau in the SIBYLS plot indicates a high likelihood of a non-disordered complex of discrete elements that account for the flexibility¹⁶³.

4.2D: The RNF8 L451D mutation severely impairs Lys63-linked polyubiquitin DNA damage signaling

The RNF8 L451D mutant provides an excellent opportunity to specifically test the role of the Ubc13-stimulating activity of RNF8 in mammalian cells, since the other functions of RNF8, specifically its FHA-dependent recruitment and Ubc13 binding activities, should be unaffected in the mutant. To test the impact of decreased RNF8-dependent catalytic stimulation of Ubc13 on DNA damage signalling, we retrovirally reintroduced full length WT or L451D hemagglutinin tagged (HA-) RNF8 into RNF8 knockout mouse embryonic fibroblasts (MEFs), subjected the cells to ionizing radiation to induce DNA damage, and imaged protein localization in the DNA damage response by immunofluorescence. The RNF8 proteins produced in these stable cell lines were expressed at similar levels (Figure 42) and colocalized with γ H2AX (Figure 43) demonstrating that the L451D mutation does not impair RNF8 recruitment to sites of DNA damage.

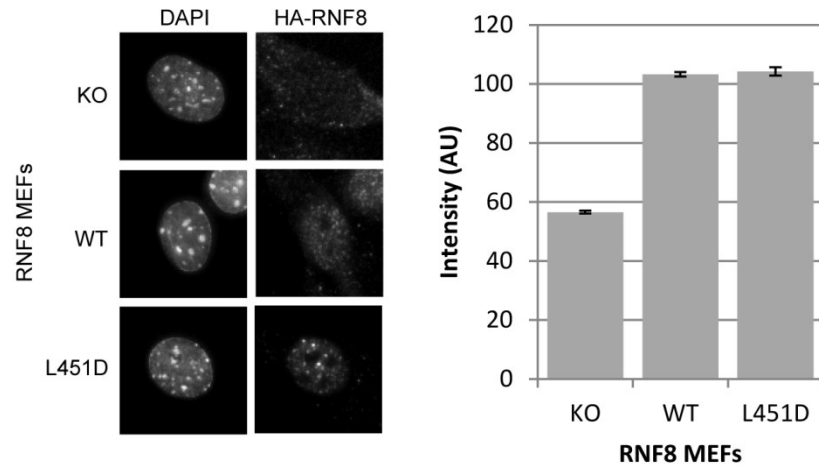


Figure 42. RNF8 levels are similar in the WT and L451D MEF populations.

An anti-HA antibody was used to stain RNF8 knockout (KO), WT, and L451D MEFs (left panel). The nuclear intensity of HA-RNF8 was quantified in arbitrary units (AU) (right panel). The nonspecific nuclear HA-stain of the KO cells was used to determine a threshold to filter out any non-reconstituted cells, and the nuclear intensity of HA-RNF8 was quantified for the remaining WT and L451D MEFs. The tonal range of cell images was rescaled from 0 to 255 in Photoshop to increase the overall contrast for display in the representative image.

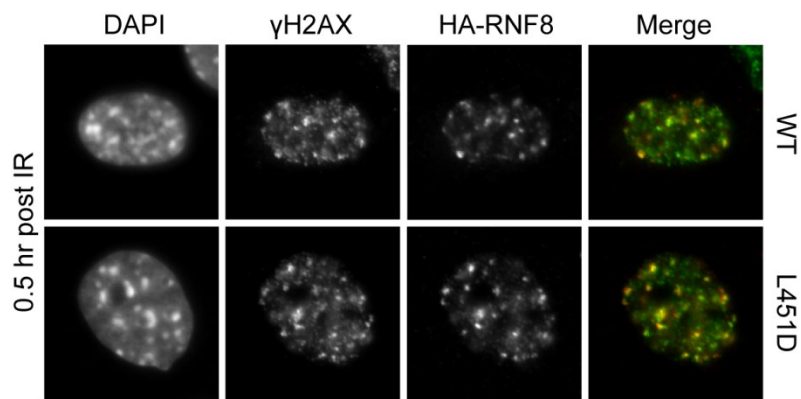
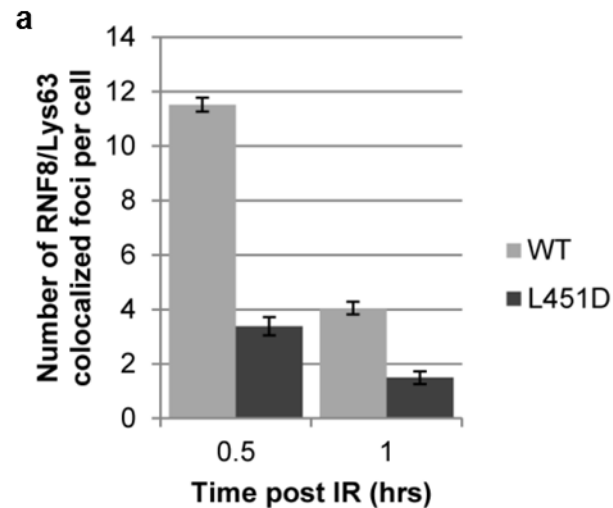


Figure 43. RNF8 colocalization with γ H2AX foci after ionizing radiation.

γ H2AX/RNF8 colocalized foci 0.5 hours after ionizing radiation in both wild type and L451D RNF8 reconstituted MEFs. RNF8 foci are red and γ H2AX are green in the merged images. The tonal range of whole images was

rescaled from 0 to 255 in Photoshop to increase the overall contrast for display.

To test the effects on Lys63-linked ubiquitin chain formation of the L451D mutation, we performed immunofluorescence in these cells with antibodies specific to Lys63-linked polyubiquitin and hemagglutinin tagged RNF8. The results indicate that while the WT RNF8 and Lys63-linked polyubiquitin associated with DNA damage foci, the degree of colocalization of these foci was dramatically reduced in the L451D mutant due to a large decrease in Lys63-linked polyubiquitin (Figure 44). These results indicate that while the RNF8 L451D mutant is able to localize to DNA damage foci, it markedly reduces the formation of Lys63-linked polyubiquitin within these foci.



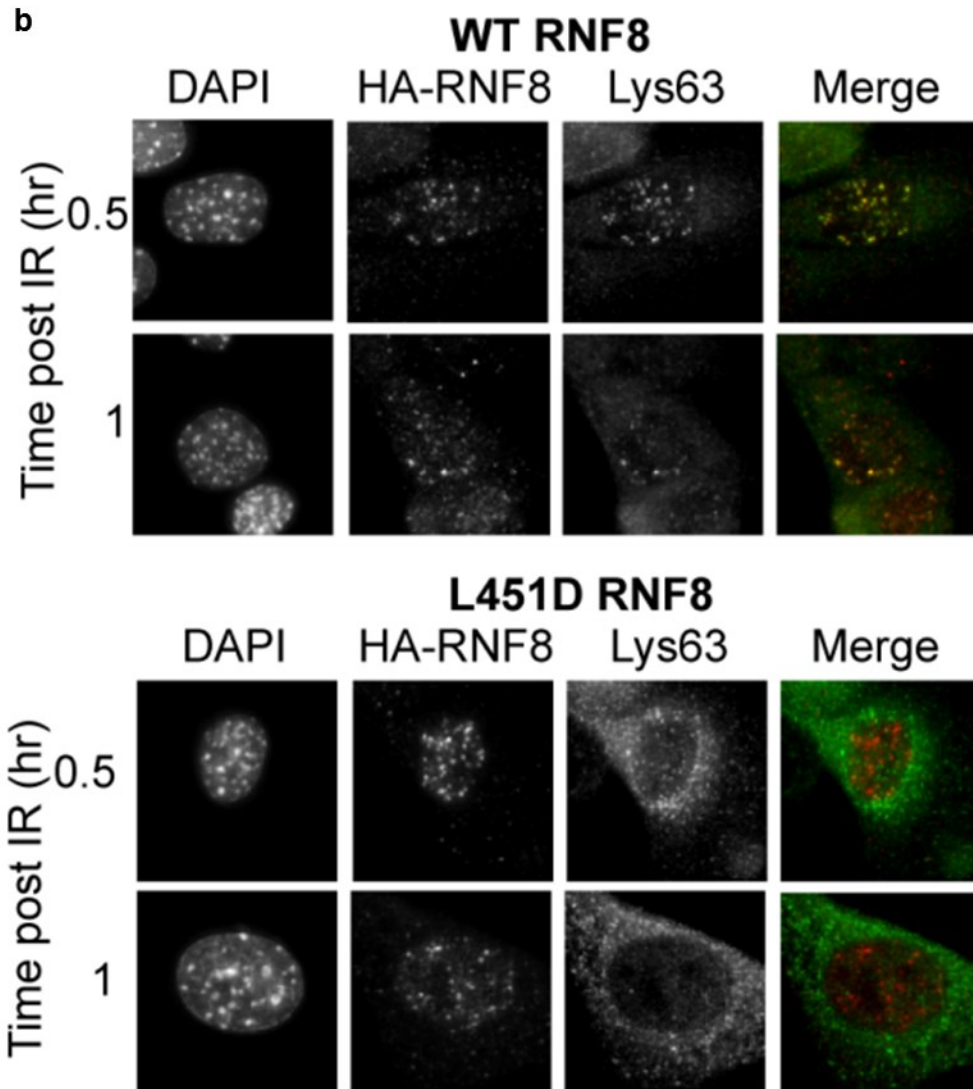
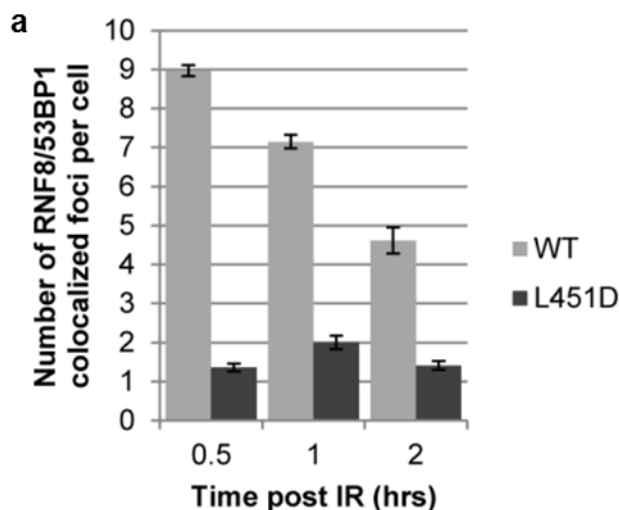
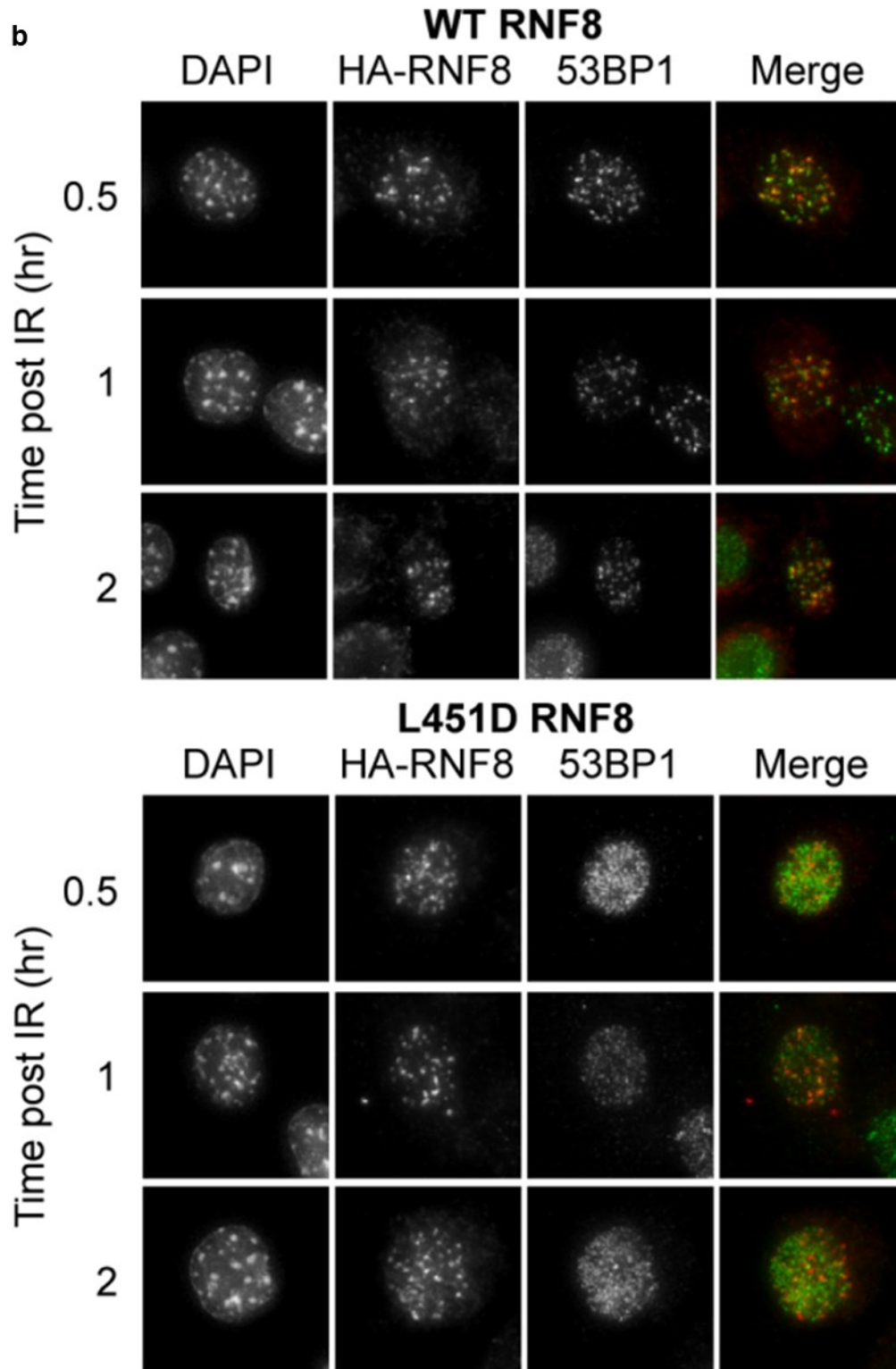


Figure 44. RNF8 L451D mutation sharply reduces Lys63-linked polyubiquitin chain formation in MEF cells.

(a) The RNF8/Lys63 colocalized foci per cell for WT or L451D cells from 0.5 to 1 hour post 3 Gy of ionizing radiation. (b) Representative image of the RNF8 L451D mutation on DNA DSB repair via a RNF8/Lys63 IRIF time-course. Wild type RNF8 reconstituted MEFs are in the top panel and L451D RNF8 MEFs are in the bottom panel. RNF8 is red and Lys63 is green in the merged images. The tonal range of cell images was rescaled from 0 to 255 in Photoshop to increase the overall contrast for display. Cells with ≥ 20 RNF8 foci per cell were examined to insure only RNF8 positive cells were analyzed, to avoid inclusion of spurious non-IR induced foci, and increased diffuse background stain in later time points. The experiment was done in triplicate and data were pooled with at least 200 cells per time point and standard error of the mean is included.

To further test the biological importance of the Ubc13-stimulating activity of RNF8, we probed the effects of the inhibition of RNF8-dependent polyubiquitination on the downstream DNA damage signalling factor, 53BP1, by monitoring the association of this protein with IR-induced DNA damage foci by immunofluorescence (Figure 45)^{36,135}. The WT RNF8 MEFs have substantial RNF8/53BP1 foci colocalization; however, there is very little in the L451D RNF8 MEFs for all time points. This indicates a severe defect in the RNF8-dependent recruitment of 53BP1 to the sites of DNA DSBs in the L451D, but not the WT RNF8 MEFs. In support of this, the RNF8 L451D MEFs have increased RNF8 foci per cell, likely indicating more unrepaired DSBs at the time points examined, compared with WT MEFs (Figure 45b,c). Taken together these data suggest that not only does RNF8 target Ubc13 to DNA damage foci, but that its E2-stimulating function is critical for subsequent Lys63 polyubiquitin signalling in the DNA damage response.





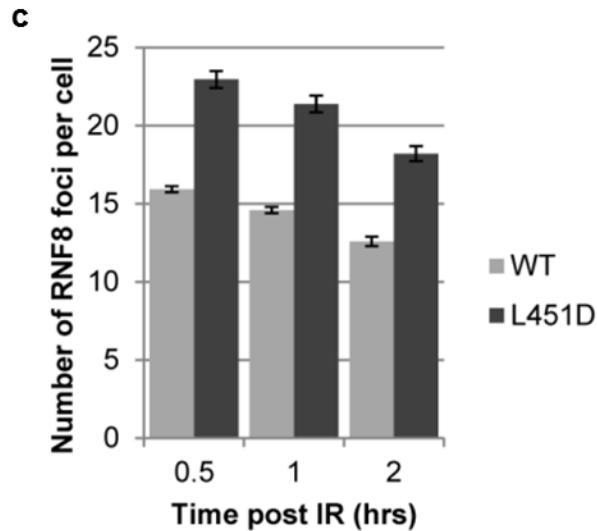


Figure 45. The effects of the RNF8 L451D mutation on DNA DSB repair via a RNF8/53BP1 IRIF time-course.

(a) The RNF8/53BP1 colocalized foci per cell for WT or L451D cells from 0.5 to 2 hours post 3 Gy of ionizing radiation. (b) Representative image of the RNF8 L451D mutation on DNA DSB repair via a RNF8/53BP1 IRIF time-course. Wild type RNF8 reconstituted MEFs are in the top panel and L451D RNF8 MEFs are in the bottom panel. RNF8 is red and 53BP1 is green in the merged images. The tonal range of cell images was rescaled from 0 to 255 in Photoshop to increase the overall contrast for display. (c) Individual assessment of the RNF8 foci per cell of WT and L451D cells. Cells with ≥ 10 RNF8 foci per cell were examined to insure only RNF8 positive cells were analyzed, to avoid inclusion of spurious non-IR induced foci, and increased diffuse background stain in later time points. The experiment was done in triplicate and data were pooled with at least 120 cells per time point and standard error of the mean is included.

4.3 Discussion

4.3A: RNF8 stimulates Ubc13 catalytic activity by stabilizing ubiquitin in a closed conformation

The nature and importance of activation of E2 enzymes by RING E3 ligases has been enigmatic. Here, combined structural and mutation

results support the hypothesis that RING E3 ligases activate E2 enzymes by altering the population distribution of the E2~Ub conjugate so that the ubiquitin molecule occupies a catalytically active conformation more frequently^{74,75,137}. The crystal structure of RNF8/Ubc13~Ub furthermore reveals that the RNF8 dimer can be doubly loaded with an Ubc13~Ub, and that both ubiquitin molecules in such a complex can exist in the closed conformation.

The Ubc13~Ub conjugate alone was previously studied via both NMR and SAXS¹⁶⁶. This study demonstrated that in the absence of an E3 ligase, the tethered ubiquitin occupies many conformations including an extended conformation, a folded-back (towards Mms2 binding site) conformation, and a closed conformation. A MES analysis of these data resulted in a 20 member ensemble showing that the complex is highly dynamic in solution. The ensemble included many extended conformations, with a $\chi^2 = 2.75$. In comparison, our minimal ensemble of two models including both an extended and closed ubiquitin conformation satisfied our SAXS curve with a $\chi^2 = 1.5$ suggesting a less dynamic complex in the presence of RNF8. This is consistent with our *in vitro* ubiquitination data, which shows that the Ubc13/Mms2 heterodimer alone can make ubiquitin chains, but that this activity is dramatically enhanced by RNF8. Although the SAXS data from Pruneda et al.¹⁶⁶ was analyzed using different software than our analysis, which may produce slight data-independent variations in χ^2 values, there is a striking difference revealed

by the SAXS data from the added RNF8. The greater noise in the L451D RNF8/Ubc13~Ub SAXS data compared to the wild type (Figure 39; compare top and bottom panels) likely explains the overall lower χ^2 values of all the fitted models in the mutant data set compared to wild type. This may affect discrimination of subtle differences between the wild type and mutant curves. Importantly, SAXS data has limitations because each SAXS curve represents the population-weighted average of all possible conformations in solution¹⁶⁷. It is therefore possible that the RNF8 L451D mutation reorients the ubiquitin in the closed position so that its C-terminal tail is no longer in the optimal conformation in the Ubc13 active site for catalysis. This would likely also influence the Ubc13 active site loop, which we know to be important for its catalytic activity^{136,168}. The observation that mutations that change conformational sampling without otherwise distorting the fold or assembly can selectively alter biological outcomes was also recently found for the multifunctional DNA double-strand break repair ATPase RAD50¹⁶⁹, suggesting that this strategy of altering the average conformational state offers a promising approach for dissection of function mutations in protein complexes.

4.3B: The RNF8 residue L451 is critical to the E2-stimulation mechanism, while R441 is not

Based upon our RNF8/Ubc13~Ub structure, we hypothesized that two residues, L451 and R441, would be important for the ability of RNF8 to stimulate the Ubc13 conjugating activity, and indeed the L451D

mutation severely abrogates RNF8 E2-stimulating activity. This supports and extends results from analogous mutations in the RNF4/UbcH5a (Figure 36a) and RING/U-box:UbcH5c systems^{75,137,160}. A superposition of multiple RING E3 ligase dimers/heterodimers onto the RING of RNF8 in the RNF8/Ubc13~Ub structure suggests that both hydrophobic and positively charged basic residues may mediate the E2-stimulation mechanism of these E3s (Figure 46). BARD1/BRCA1¹⁷⁰, TRAF6¹⁷¹, E4B⁷⁵ and CHIP^{172,173} all stimulate E2s to make polyubiquitin chains *in vitro*. These superpositions suggest that TRAF6 may utilize an Arg to stimulate the E2s. There are two negatively charged acidic residues at the end of the ubiquitin alpha helix, D32 and E34, which, together with the negative helix dipole, are suitable to provide an electrostatic interaction for a positively charged residue contact in the E3. TRAF6 may additionally engage the ubiquitin with a His on its first zinc finger domain, which makes a close approach to the ubiquitin D32 in our model. Similar to RNF8, it is likely that a Leu in the U-box E3 CHIP mediates ubiquitin contact, while BRCA1 probably engages with a Thr, and possibly a Ser (Figure 46).

Interestingly the R441A mutation had little effect on the E3 ligase activity of RNF8, with a slight decrease in binding to Ubc13 ($K_{D,WT} \sim 1.8 \mu\text{M}$ vs. $K_{D,R441A} \sim 5.5 \mu\text{M}$; Figure 37). This is different from mutational analysis of other RING E3s. For example, Pruneda et al.^{75,137} found that in the E4B/UbcH5c~Ub system, mutation of the analogous Arg to an Ala (R1143A) in mouse E4B reduced the rate of E2~Ub oxyester hydrolysis

and autoubiquitination⁷⁵. Similarly Plechanovová et al found that the analogous Arg to Ala mutation in RNF4 was severely impaired in a single-turnover substrate-ubiquitination assay with UbcH5a¹⁶⁰. This difference suggests that the conserved Arg proposed to be a “linchpin” residue in RING E3-mediated E2-stimulation does not play a similar role in RNF8⁷⁵. A possible explanation for the lack of effect of the Arg mutation in RNF8 compared to E4B is that RNF8 forms a stable homodimer, whereas E4B is a monomer in solution. The L451 residue in RNF8 resides on the opposite dimer-mediated protomer, which is absent in E4B due to the lack of dimerization. This may have led to more evolutionary selective pressure on other residues in monomeric RING/U-box E3s, such as E4B, to mediate activation of an E2-ubiquitin conjugate.

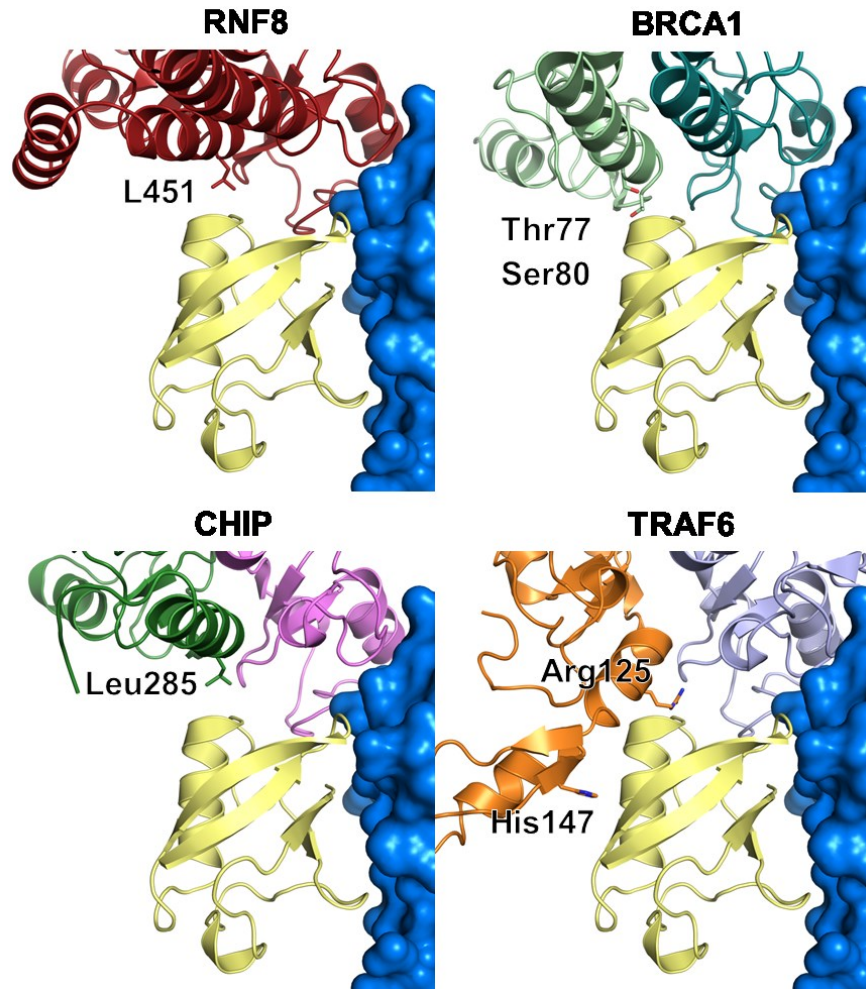


Figure 46. Models of RING E3 dimers and heterodimers relative to E2~Ub.

The RING domains of the E3s BARD1/BRCA1 (teal/green; PDB:1JM7), CHIP (green/violet; PDB:2C2V), and TRAF6 (orange; PDB:3HCS) were superimposed on the RNF8 RING (red) in the RNF8/Ubc13~Ub crystal structure. Possible interacting residues are labeled. The TRAF6 structure includes a zinc finger connected to its RING. In all images Ubc13 is blue with surface representation and ubiquitin is yellow.

4.3C: The E2-stimulating role of RNF8 is vital to the DNA damage response

It is known that E3 ligases are critical to cellular ubiquitination, and that this is dependent on an interaction with E2-conjugation enzymes. The RING and structurally similar U-box E3 ligase interaction with E2 conjugating enzymes has been characterized^{29,76,171,172,174-177}, and E3-mediated ubiquitin transfer is established¹⁷⁸. The observation that E2 conjugating activity is stimulated by RING/U-box E3 binding has also been extensively demonstrated. Examples include the E3 TRAF6 with Ubc13/Uev1A¹⁷¹, RNF8 and RNF168 with Ubc13/Mms2 or UbcH5c^{29,32}, RNF4 with UbcH5a^{74,160}, and the U-box E3 CHIP with UbcH5a or Ubc13/Uev1A^{74,172,173}. A primary role of target presentation is implicated for some RING E3s, such as Bmi1/RING1b, which requires fully assembled nucleosomes for monoubiquitination with the E2, UbcH5c¹⁷⁴. The E2 Rad6b can make extensive *de novo* chains without an E3 ligase through a ubiquitin binding site on its “backside”, and the addition of the RING E3 Rad18 actually prevents this activity and provides specificity for monoubiquitination of PCNA¹⁷⁶. Dimerization mutations of several of the RING/U-box E3s capable of *de novo* ubiquitin chain synthesis demonstrate a dimer-dependence of many of these E3s on their ability to stimulate an E2 enzyme, which is likely due to the contact of both RING/U-box protomers with an E2-linked donor ubiquitin^{29,74,75,137,159,160,171,179}, (Figure 46).

Here we show that a single point mutation in RNF8, which specifically abrogates its E2 stimulating activity but not its ability to bind to the sites of DNA damage, blocks DNA damage-associated Lys63-linked ubiquitination and downstream signaling. It is likely that the necessity for RING E3 E2-stimulating activity extends to other RING E3 ligases (Figure 46), and that this activity is required for their individual roles in the cell. This combined observation and concept has implications for potential therapeutic strategies. Inhibitors that block protein-protein interactions are notoriously challenging and are actively being pursued. Our work presents a novel avenue for blocking RING E3-mediated E2-stimulation, which we show to be critical for the DNA damage response, and likely for many other pathways that involve RING E3s.

There is a great degree of interest in inhibiting ubiquitination pathways, as they play a pivotal regulatory role in many cellular functions¹⁸⁰, and in the pathogenicity of human diseases including cancer and chronic inflammation. While significant effort has been directed toward inhibiting E2:E3 interactions, the difficulties associated with the inhibition of the rather flat and fairly well conserved E2:E3 interface has limited progress in this area¹⁸⁰. We propose here that a more promising approach may be to target the ubiquitin-docking cleft at the E2:E3 interface. Such inhibitors could allosterically inhibit polyubiquitination associated with cellular processes driven by specific E2:E3 complexes. As there are approximately 34 active E2 enzymes and over 600 RING-like E3 enzymes

in mammalian cells⁷³, this allosteric approach presents an attractive prospect for targeting specific ubiquitination events in many different pathways. A related direction also implied by the results presented here is to target the E2 enzymes themselves. Indeed, a lead Ubc13 inhibitor has recently been uncovered that could indicate a route for the selective regulation of Ubc13 that takes advantage of the unique Ubc13 active site architecture¹⁶⁸. In addition, an inhibitor of the E2 Cdc34 has been discovered and shown to act through binding-mediated distortion of the E2¹⁴². In this context of controlling Ub pathways, here we bridge the gap from crystal structures to biological outcomes by showing that the Ubc13-stimulating activity of RNF8 may be driven by the shift of the population distribution of bound Ub and that this stimulation is essential for DSB signaling in mammalian cells.

4.4 Methods

4.4A: Protein production

Ubc13, Mms2, and RNF8 cloning, and protein production/purification was previously described^{29,147}. The RNF8 L451D and R441A and Ubc13C87K mutants were made using PCR mutagenesis from wild type RNF8 and Ubc13 templates. The mUBA1 enzyme was produced according to a previously published protocol¹⁴⁸, however, the His-tag vector used was pET47b(+).

4.4B: Crystallization

The formation of a stable E2~Ub isopeptide bond has previously been described⁷⁴. The RNF8/Ubc13C87K~Ub complexes were concentrated to 10 mg/mL in a buffer containing 20 mM HEPES pH 6.8, 20 mM NaCl, 10 μ M ZnSO₄, and 1 mM DTT. Crystals were grown using vapor diffusion in 0.1 M imidazole pH 8.0, 1.04 M (NH₄)₂HPO₄. Crystals grew within one to two weeks.

4.4C: Structure solution and refinement

Both SAXS and crystallography X-ray data were collected at the SIBYLS beamline (12.3.1) at the Advanced Light Source¹⁸¹. Both experiments were performed at an X-ray wavelength of 1.03321 Å. The data was processed in HKL2000, and structure solution was accomplished using PHENIX¹¹⁶. A model for molecular replacement was created from a modified version of the previously determined RNF8/Ubc13 structure (PDB: 4ORH). The RING domain (392-485) of RNF8 was used and a second Ubc13 molecule was added using two-fold symmetry to create a dimer complex. Phaser^{182,183} was used to place two copies of this model within the crystallographic asymmetric unit. Next, a ubiquitin (PDB: 4AP4) with a truncated C-terminal tail was used as a second search model. Phaser was able to place a single ubiquitin into this model (Z-score = 6.2) onto a region with significant positive difference density (Figure 35b). Alignment of the RNF8/Ubc13~Ub structure with the RNF4/UbcH5a~Ub (PDB: 4AP4) structure revealed that the ubiquitins are in the same relative

orientation relative to the E2:E3. Weaker difference density was also observed at each of the other potential ubiquitin positions predicted by noncrystallographic symmetry. NCS was used to position these ubiquitins, and the validity of the placement of each ubiquitin was monitored via reduction in R_{free}. Portions of each of the RNF8 coiled-coils were placed through alignments with 4ORH. In one complex the positive difference density enabled placement of the entire coiled-coil (342/345-392), creating crystal contacts between adjacent helical arrays of complexes running down the 6-fold axis of the cell (Figure 34). In the second complex 180° to the first, the coiled-coils are pointing into a large solvent channel running down the interior of the helical filament and the positive difference density for these coiled-coils only justified modeling a small section of the coiled-coil corresponding to residues 380-392. The junction where the coiled-coil C-terminal residue (392) was linked to the N-terminal RING residue (393) was real-space refined in Coot using Ramachandran restraints to maintain the bonds and angles. The resulting RNF8/Ubc13 complexes were kept as one rigid body to maintain the RNF8/Ubc13 binding interface, while the ubiquitin molecules were each treated as a separate rigid body in rigid body refinements. This allowed the ubiquitin molecules to move as rigid bodies relative to the RNF8/Ubc13 complexes.

4.4D: SAXS data collection and analysis

The wild type RNF8/Ubc13C87K~Ub complexes were concentrated to 6 and 4 mg/mL, and the L451D to 8, 6, and 4 mg/mL. The flow-through

buffer was collected after sample concentration and used for buffer subtraction. SAXS data were collected as previously described^{184,185}. ScÅtter was used to determine which data sets of various exposure times were best for merging (i.e. showed no aggregation or interparticle interference). The 6.14 mg/mL concentration for wild type and 6 and 4 mg/mL concentration for L451D complexes provided the best data. 0.5 and 5 second, and 1 and 2 second exposure data sets were merged for wild type and L451D, respectively. The short exposure provided better low scattering angle $q(\text{\AA}^{-1})$ data, while the longer exposure provided better large scattering angle $q(\text{\AA}^{-1})$ data. BILBOMD¹¹⁴ was used to generate models and FoXS^{164,165} for calculating theoretical scattering curves and a minimal ensemble search (MES), which is further discussed in the Results section.

4.4E: Surface Plasmon Resonance

0.19 pmol/mm² of Ubc13 was coupled to a CM5 Biacore sensor chip using an Amine Coupling Kit. Briefly this included activation with N-hydroxysuccinimide/N-ethyl-N'-(3-dimethylaminopropyl)-carbodiimide hydrochloride for seven minutes at a flow rate of 5 $\mu\text{Ls}/\text{min}$, conjugation of 1 μM of purified Ubc13 in 10 mM sodium acetate pH 5 at a flow rate of 5 $\mu\text{Ls}/\text{min}$, and blocking with 1 M ethanolamine at pH 8.5 for seven minutes at a flow rate of 5 $\mu\text{Ls}/\text{min}$. The purified RNF8 proteins were diluted to 10 μM in 10 mM HEPES pH 7.4, 150 mM NaCl, 0.005% NP-40 at a flow rate of 30 $\mu\text{Ls}/\text{min}$, and a titration series from 0 to 10,000 nM was performed

on a Biacore 3000 SPR biosensor. Control samples of buffer only were used for blank subtraction. Due to the rapid kinetics, estimated apparent equilibrium dissociation constants (K_D) were determined using a fractional saturation analysis in SigmaPlot. The response used for the steady state affinity calculation was four seconds before the injection stop.

4.4F: Ubiquitination assay

All ubiquitination assays were done essentially as previously described¹⁶⁸. The reactions were run for 15, 30, 45, and 90 minutes at 37 °C and quenched with SDS-PAGE loading buffer and the results were visualized by Western blotting. The primary antibody was mouse anti-ubiquitin (Santa Cruz), and the secondary was goat anti-mouse-FITC (Sigma-Aldrich).

4.4G: Generation of stably integrated RNF8 MEFs

The generation of RNF8 knockout mouse embryonic fibroblasts have previously been described¹⁸⁶. Re-introduction of either WT or L451D RNF8 was accomplished using retroviral transduction. 293T cells were transiently transfected with 0.9 µg gag/pol expression vector, 0.1 µg VSV-G envelope vector, and 1 µg of pBABE-Hygromycin-HA~RNF8 transfer vector using Qiagen Effectene for viral production. Viral supernatant was collected at 24, 48, and 72 hours post transfection. Knockout MEFs were infected twice with the viral supernatants. HA~RNF8 expressing cells were selected with 400 µg/mL hygromycin.

4.4H: DNA damage localization assay

Transduced MEF cells or knockouts were seeded to 1×10^4 cells per well in a 96 well glass bottom plate the day before using a hemacytometer. The next day cells were irradiated with 3 Gy ionizing radiation and were allowed to recover for 0.5, 1, and 2 hours before fixation and immunofluorescence. The primary antibodies used were anti-HA (Covance), anti-Lys63 ubiquitin chains (Millipore, 05-1308) and anti-53BP1 (Santa Cruz, sc-22760). Images were acquired using a High Content Instrument (Molecular Devices MetaXpress XLS). A z-stack was taken for each image using either 1 or 0.6 μm steps. Image analysis was accomplished using a foci count and colocalization module in CellProfiler^{154,155}, with restraints optimized to detect empirically determined foci, while minimizing false positives from background stain. Data were analyzed using Microsoft Excel 2010.

4.4I: Accession codes

The RNF8/Ubc13C87K~Ub crystal structure has been deposited at the Protein Data Bank with the accession code **4WHV**.

4.4J: Acknowledgements

The authors thank S. Classen at the Advanced Light Source (SIBYLS) for crystallographic data collections support. They also thank the Cellular Imaging Facility at the Cross Cancer Institute for the use of microscopes. We thank X. Yu, Division of Molecular Medicine and Genetics, University of Michigan Medical School, Ann Arbor, MI for the gift of the RNF8

knockout MEFs. This work was performed with support from Canadian Cancer Society/Canadian Breast Cancer Research Alliance (to J.N.M.G.), the Canadian Institutes of Health Research (CIHR114975 to J.N.M.G.; CIHR119515 to M.J.H.), the National Institutes of Health (CA92584 to J.N.M.G.), and the Alberta Innovates Health Solutions.

Table 3. X-Ray diffraction data collection and refinement statistics of RNF8/Ubc13~Ub

		RNF8/Ubc13~Ub
Data Collection		
Space Group		P6422
Cell Dimensions		
	a,b,c (Å)	341.4, 341.4, 113.4
	α,β,γ (°)	90, 90, 120
Resolution (Å)		49.3-8.2 (8.5-8.2)*
	R_{sym}^2	11.7 (83.4)*
	I/ σ I	24.3 (6.6)*
Completeness (%)		99.8 (97.9)*
Redundancy		21.8 (24.2)*
Refinement		
No. Reflections		89,114
$R_{\text{work}}/R_{\text{free}}$		32.9/33.7
No. Atoms		
	Total	9,620
	Protein	9,612
	Ligand/ion	8
	Water	0
Overall B-factor		522.7
	Protein	522.7
	Ligand/ion	498.9
R.M.S. Deviations		
	Bond Lengths (Å)	0.007
	Bond Angles (°)	1.09

*Values in parentheses' are for highest resolution shell

Chapter 5

Discussion and Conclusions

5.1 Overview of findings

The work presented in this thesis provides a detailed examination of the modulation of Ubc13 through both small-molecule inhibitors and protein-protein interaction with RNF8. This work on Ubc13 and RNF8 began with contributions to an initial study in which Campbell et al.²⁹ solved the X-ray crystal structure of the RNF8 RING domain dimer with a novel extended coiled-coil bound to the E2 heterodimer Ubc13/Mms2. The importance of this complex for K63 ubiquitin chain formation *in vitro* was also demonstrated. To confidently assign the positions of the amino acids in the extended coiled-coil, the structure of a selenomethionine derivative of RNF8 in complex with Ubc13/Mms2 was determined.

Armed with further support that Ubc13 is a very important E2 enzyme, the discovery of Ubc13 small molecule inhibitors by Pulvino et al.¹²⁶ and Strickson et al.¹²⁵ provided an opportunity to investigate these inhibitors at a detailed molecular and cellular level. We uncovered the mechanism of Ubc13 inhibition by both compounds, and discovered unique aspects of the Ubc13 active site important for its specific *in vitro* inhibition by NSC697923. We designed a NSC697923 resistant mutant Ubc13 and used it to test the specificity of NSC697923 in the cellular NF- κ B and DNA damage signaling pathways. The selective inhibition of Ubc13 by NSC697923 was primarily responsible for the inhibition of cellular ubiquitin signaling in these pathways. Our work provides an excellent body of data to develop selective small molecule inhibitors of

Ubc13, which is a critical regulator of key cancer-associated signaling pathways.

A rational continuation of the research detailed in Chapter 2 was the investigation of the RING E3 ligase RNF8 and its role in activating/increasing the catalytic conjugating activities of the E2 enzyme Ubc13. In fact this continuation preceded the Ubc13 inhibitor work temporally, and data was accumulated in parallel, despite the publication of the inhibitor work first. We hypothesized that RNF8 stimulates the ubiquitination abilities of Ubc13/Mms2 by stabilizing ubiquitin in a closed conformation that is believed to optimize the orientation of the thioester linkage for nucleophilic attack by an incoming ubiquitin lysine, resulting in increased catalysis. The crystal structure of RNF8/Ubc13~Ub solved to 8.3 Å resolution supported our hypothesis. Conformational selection was further demonstrated in solution through small-angle X-ray scattering (SAXS) data. The contribution of RING E3-mediated E2-stimulation in the DNA damage response was enabled by our creation of a point mutation to RNF8 that severely disrupts its ability to stimulate Ubc13 conjugating activity. Characterization of this mutation *in vitro* was performed to ensure the RNF8/Ubc13 binding was maintained. We show that the DDR is dependent on the RNF8 ability to stimulate Ubc13 E2 conjugating activity through the donor ubiquitin conformational selection.

5.2 Concerning RNF8 coiled-coil

The study that required the selenomethionine derivative of RNF8 has already been published²⁹. It is unlikely that this method will be needed for further studies of RNF8 specifically, although the coiled-coil very likely extends beyond residue 345, as predicted in Figure 9. Paircoil2 predicts that another RNF8 coiled-coil (or extension of the known one) exists approximately between residues 301-333 (if the threshold is set to 0.4), Figure 47. Harbury et al¹⁸⁷ studied coiled-coils and theorized (with experimental examples of wild type/mutant GCN4 leucine zipper structures) that the primarily hydrophobic coiled-coil register position “a” and “d” dictate the oligomerization state of a given coiled-coil. In short, they found that leucine at “d” forms parallel dimers and at “a” forms a parallel tetrameric α -helical bundle in a left-handed superhelix. β -branched residues (primarily isoleucine) at position “d” disfavors dimer, at “a” disfavors tetramers, and at both “a” and “d” favors parallel trimers due to residue packing¹⁸⁷. They also note that positions “e” and “g” often contain charged residues that form salt bridges, and the remaining positions can also contribute to packing preferences. As shown in Figure 47, there are leucines at positions “d, a, and d,” residue numbers 313, 324, and 327, respectively. This indicates that this sequence is more likely to favor a parallel dimer, which is further supported by a single β -branched valine at position “a” (310) that disfavors tetramers. It may be interesting to experimentally probe this predicted coiled-coil region, as well as the

potential break in between it and the known 345-400 coiled-coil (see prediction in Figure 9).

301 – AEQAQQARVEQLEKTFQEEEQHLQGLEIAQGE – 333
fgabcdefgabcdefgabcdefgabcdefgabc

Figure 47. Amino acid sequence and predicted coiled-coil register of RNF8₃₀₁₋₃₃₃.

Primary amino acid sequence of RNF8 from residues 301 to 333. Residues in the “a” and “d” positions are highlighted green. The coiled-coil heptad repeat register alternates from highlighted turquoise to colorless below the primary amino acid sequence.

The method of using selenomethionine derivatives to help place residues in low resolution structures may increasingly become necessary, as the complexity of crystallography targets increases, so may the number of low resolution structures. It is evident that the scientific community has been solving and depositing more structures with greater complexity each year, as detailed by Berman et al¹⁸⁸. Application of our strategy for solution of novel low resolution structures for which full molecular replacement is not an option may prove useful going forward.

5.3 Concerning Ubc13 inhibition with small-molecule inhibitors

The reasons for the desire to develop small-molecule inhibitors of Ubc13 have previously been described in Chapter 3. Very recent studies have linked this E2 enzyme to the pathogenicity of a number of cancers,

as well as the development of resistance to conventional chemotherapies¹⁴³⁻¹⁴⁶. Ubc13 possesses a number of desirable traits as a target for inhibition. It is a nonredundant enzyme in humans, meaning there are no other proteins able to fulfill its role. It plays a major role in the signalling of two pathways, the NF- κ B and DNA damage response, which are both critical for cancer proliferation and survival^{15,146,189}. The other characteristic of Ubc13 that currently makes it a desirable target for chemical inhibition in the treatment of cancers is our discovery of its unique active site. As mentioned in Chapter 3, E2 enzymes are not classically druggable, because they do not have deep complex active site clefts traditionally targeted by small molecule inhibitors¹⁶⁸. In addition a subset (17 E2s) of the ~34 active human E2 enzymes share a great degree of similarity in overall fold and residue conservation. This makes our discovery of a unique active site loop conformation and small pocket crucial to its specific successful inhibition, as it sets Ubc13 apart from the other E2s.

One very desirable characteristic that it either lacks, or may not have been discovered yet is a synthetic lethal relationship with another gene. The principle of synthetic lethality is powerful, and has been demonstrated through the development of poly (ADP-ribose) polymerase (PARP) inhibition^{189,190}. The idea behind it is that a relationship between two genes exists whereby cells can survive a loss/inhibition of one, but not both at the same time¹⁹⁰. The previous example of PARP is that hereditary

breast and ovarian cancers in particular have a tendency for loss of BRCA1/BRCA2, while normal cells retain functional proteins. This results in a repair defect in the HR DNA repair pathway, so that the cancer cells cannot repair DNA damage that requires HR¹⁸⁹. The inhibition of PARP, involved in single-strand break repair, results in DNA lesions that require HR for repair. This results in specificity for cancer cells over normal cells. This is particularly important because traditional chemotherapy targets highly proliferating (or dividing) cells, which causes severe side-effects such as a dangerously compromised immune system through bone marrow destruction¹⁴⁶. The other issue with this mode of targeting is that solid tumors are thought to have a gradient of proliferation rates with stagnant non-dividing cells at the core, and proliferating cells on the outer surface. This is likely a result of a unique tumor microenvironment characterized by hypoxia, decreased diffusion rates of nutrients and acidity¹⁴⁶. It remains to be seen whether Ubc13 possesses the highly desirable trait of synthetic lethality. Thomson et al.¹⁹⁰ provides a review of strategies to identify synthetic lethal partners, which involves different types of inhibitory screens (siRNA, chemical, etc.), which should be applied to Ubc13 in future studies.

The development of NSC697923 is a valid option to create specific inhibitors of Ubc13 for therapeutic use. There are two interrelated hurdles to this, which must be overcome in next generation inhibitors. The first is the nitrofuranyl moiety. It both binds in the small Ubc13 active site pocket

(contributing to the current selectivity), and is known to be toxic to mammals and potentially carcinogenic¹³⁹. The second is that the covalent reaction results in the loss of the tosyl group, which is undesirable. As previously mentioned in Chapter 3, a route for designing more selective covalent inhibitors of Ubc13, is to target the groove adjacent to the active site cysteine that accepts the ubiquitin C-terminal tail when a donor ubiquitin is bound. Our data that demonstrates a critical dependence of the DDR on the E3-mediated E2-stimulation relies on this groove (see Figure 33a), so an inhibitor that blocks this groove is highly desirable for more selective high-affinity inhibitors. One way to potentially achieve this is to use a crotonamide moiety, which results in a Michael addition without the loss of additional desirable chemical groups (Figure 48). An example where this has been successfully used is in the tyrosine kinase domain of the epidermal growth factor receptor (EGFR) inhibitor, neratinib (HKI-272), which is in late stage clinical trials for treatment of breast cancer^{138,191}. This type of approach may prove fruitful in the further development of small molecule inhibitors of Ubc13.

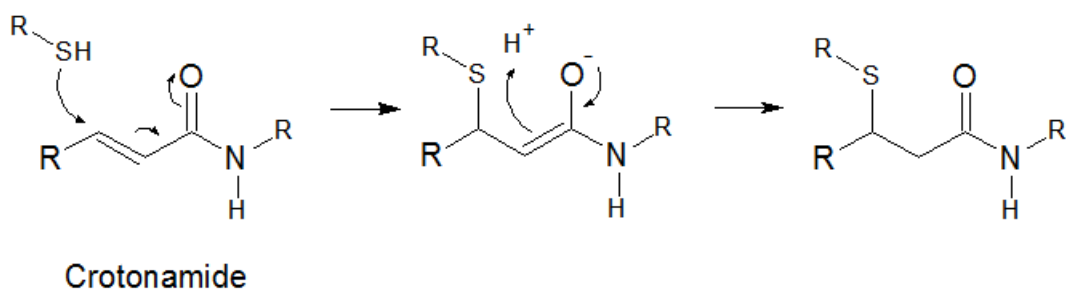


Figure 48. Crotonamide Michael addition mechanism.

A reaction of the active site cysteine sulfur with a crotonamide moiety would result in a Michael addition without loss of additional chemical groups.

5.4 Concerning RNF8-dependent Ubc13 conjugation stimulation

Our demonstration that Ubc13 requires RNF8 RING E3-mediated stimulation, in addition to targeting is important, as it distinguishes two functions that are difficult to separate experimentally. The RNF8 L451D mutation is quite interesting as it provides a route for further investigation of RNF8 function in cells. The current cellular data investigating RNF8 has largely been accomplished through very drastic modifications, including RNF8 gene deletion/silencing, RING domain deletions, dimerization domain deletions and dimer-disrupting point mutations, or RING/dimerization domain point mutations that disrupt proper folding^{27,30,192}. With the RNF8 L451D mutant, we can now study RNF8 in a capacity where it still localizes to sites of DNA damage through its FHA domain, maintains a structured RING domain for binding and targeting E2 enzymes, and contains the region between the N-terminal FHA and C-

terminal RING. This inter-domain region of RNF8 is already known to contain the previously mentioned CDK1 phosphorylation site (T198), and Paircoil2 predicts an additional or extended coiled-coil that is currently unexplored (Figure 9 and Figure 47). There is, however, a caveat to the use of the RNF8 L451D mutation, which is that RNF8 can bind other E2 enzymes in addition to Ubc13. An example of this is the possible Ubc13-independent role of RNF8 in Lys48-linked ubiquitination of Ku on chromatin,⁵¹ therefore care must be taken to discriminate between the multiple roles of RNF8 when the L451D mutant is used in future studies.

RNF8 has indeed been shown to function with another E2, UbcH8, to form Lys48-linked ubiquitin chains, which may be important in the proteasomal turnover of RNF8 itself¹⁹². Interestingly, a point mutation (I405A) on RNF8 selectively disrupted its interaction with UbcH8, but maintained interaction with Ubc13. We also previously tested this RNF8 mutation and found that it abolished binding to Ubc13, as monitored via size exclusion chromatography, but maintained some degree of stimulation of Ubc13 conjugating activity²⁹. Computational analyses of RING E3:E2 pairs led Scheper et al.¹⁹³ to conclude that the selectivity for binding of a RING E3:E2 pair is largely dictated by residues in the E3 RING. Interestingly, this study found three residues important for E2 selectivity in two different RING E3s, RNF11 and RNF103. A small hydrophobic residue at RNF11 position 103 results in less selectivity for E2s, whereas polar residues at RNF103 positions 649-650 results in more

W430, which likely participates in binding to the S-P-A motif, possibly through perpendicular pi stacking with Ubc13 Pro97. This interaction is absent in the RNF168 RING (Figure 50b), possibly because the analogous residue in RNF168 is a threonine (T43), which our lab previously found not to have stable binding to Ubc13 on a size exclusion column²⁹. Interestingly, both RNF11 and RNF103, which also interact with Ubc13, have a tryptophan in that position, just like RNF8 (Figure 49). It may be that both the I405 and W430 positions dictate the binding affinity of RING E3s to many E2 enzymes. Perhaps the RNF8 I405 mutation to alanine, which still bound Ubc13 in pulldown assays, reduced the kinetic stability of the interaction, which was tolerable to Ubc13 to retain activity (as with RNF168), but not to Ubch8. It may be other residues in Ubch8 that cause a less stable interaction in the absence of RNF8 I405. Contributions to lower stability could be from the difference in the Ubc13 S-P-A motif, which is a Lys-Pro-Cys in Ubch8, and perhaps from the more conservative Ubch8 phenylalanine in the analogous Ubc13 M64 position (Figure 50).

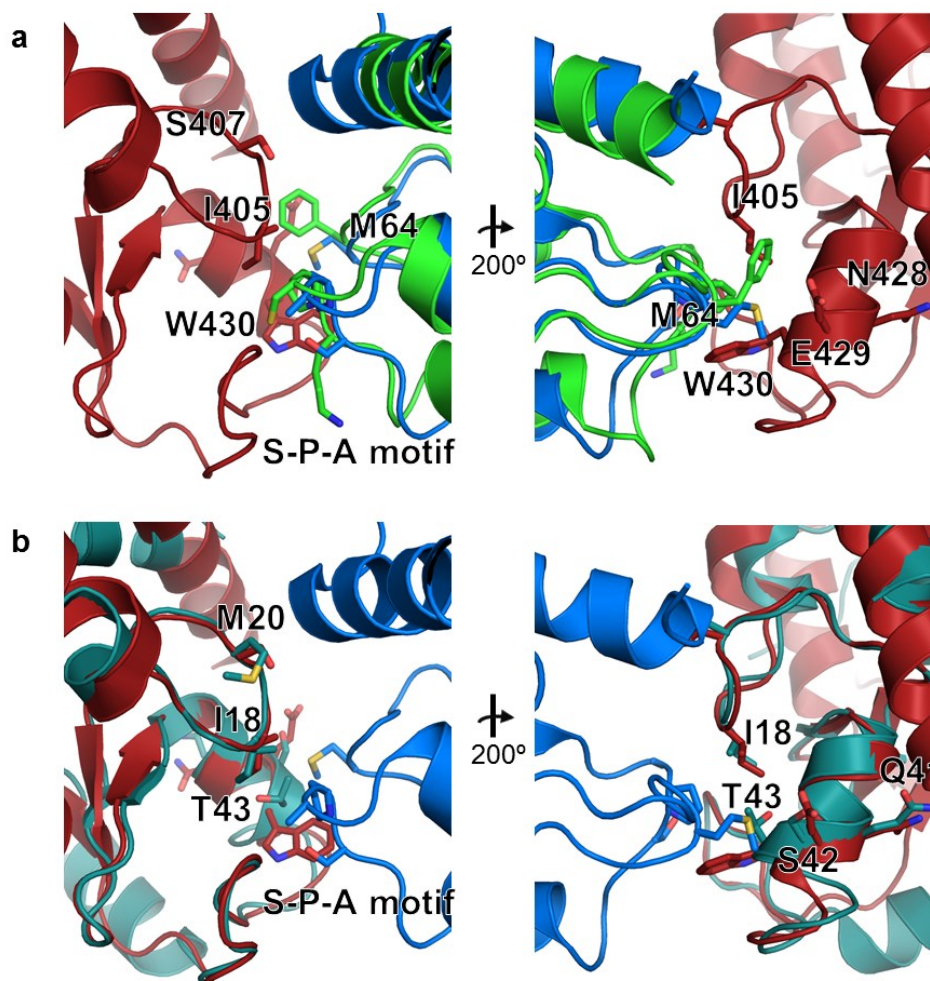


Figure 50. RNF8 and RNF168 selectivity of E2 enzymes.

(a) Ubch8 superposed onto Ubc13 in the RNF8/Ubc13 structure (PDB:4ORH). Labels correspond to important residues in RNF8 and Ubc13. (b) RNF168 (PDB: 3L11) superposed onto RNF8 in the RNF8/Ubc13 structure. Labels correspond to potentially important residues in RNF168. Ubch8 is green, Ubc13 is blue, RNF8 is red, and RNF168 is deep teal.

Further future investigations into the function of RNF8 should include study of its other potential PTMs. As predicted by a PTM curation site called PhosphoSitePlus¹⁹⁴, there are a number of possible PTMs in

the RNF8 inter-domain region, such as a possible acetylation site in the RNF8 coiled-coil at residue Lys370 (Figure 10). This PTM, in particular, was found in mice liver tissue via mass spectrometry, and upon further investigation could suggest a role in regulation through the RNF8 coiled-coil. Many of the potential PTMs are found through proteomics studies using mass spectrometry, which require experimental validation using other methodologies.

5.5 Cancer-associated mutations in Ubc13 and RNF8

cBioPortal is a database of sequenced cancer genomes, which will conveniently map all known mutations for a given protein onto its structure if one is available¹⁹⁵. The functional impact of a given mutation in a cancer is largely based on residue conservation in protein families, and mutations are rated low, medium, or high, with medium/high ranked being possible driver mutations¹⁹⁶. Ubc13 cancer mutations in positions likely to disrupt the active site structure are T73I (liver), I75M (uterine), P78L (melanoma), and R85I/K (lung adenocarcinoma/multiple myeloma). Ubc13 mutations that could destabilize the loop that opposes the active site (114-124, Figure 30) are S113T (liver) and A126V (colorectal). Active site structure-disrupting mutations and active site loop mutations would likely hinder proper transfer of the covalently linked donor ubiquitin from the E2 to an acceptor lysine on a substrate or another ubiquitin. As seen in Chapter 4, this would likely lead to impairment of DDR factor recruitment to the sites of DNA DSBs to some degree. It is possible then, that these particular

cancers may have inefficient HR repair, which could possibly be exploited in treatment strategies, such as a synthetic-lethality or sensitivity to PARP inhibitors. Ubc13 R70L/C (lung/stomach adenocarcinoma) mutations likely affect Mms2 binding, as R70 hydrogen bonds to the main chain carbonyl of Mms2 M41. These mutations may cause Ubc13 to be less specific for creating K63-linked ubiquitin chains, and likely disrupt ubiquitin chain formation altogether. The Ubc13 mutation R7S is found in liver hepatocellular carcinoma and small cell lung cancer. It is predicted to have a high functional impact, which is likely true because R7 makes two important hydrogen bonds. The first hydrogen bond is an internal one with the main chain carbonyl oxygen of L99, which is the first C-terminal residue after the conserved Ubc13 S-P-A motif important for RNF8 binding²⁹. Ubc13 R7 also likely hydrogen bonds with the main chain carbonyl oxygen of RNF8 I405, which may be a major E2 selectivity determinant (see earlier discussion above and Figure 50). The effects of the Ubc13 R7S mutation would likely entail deficient E3 binding, which would likely cause major defects in DDR repair factor recruitment and possibly other pathways where K63-linked ubiquitin chains are necessary.

Several cancers harbour RNF8 mutations according to cBioPortal. Disease-associated mutations in the RNF8 coiled-coil are K376N, E378Q, and K379R, which are in coiled-coil heptad positions “e, g, and a,” respectively (Figure 10). These changes are fairly conservative, have a medium predicted functional impact, and may somewhat destabilize the

RNF8 coiled-coil. A destabilized coiled-coil may present issues with the function of the E3 at sites of DNA DSBs, as the coiled-coils may be necessary to bridge gaps in space where the ubiquitination activities of the RING-E2 are active at a separate site from where the FHA is bound to a phospho-motif. There are many disease-associated mutations in and near the RNF8 RING domain, which may affect its ability to bind Ubc13 to make Lys63-linked ubiquitin chains important for the DDR (see Chapter 4). These are: Q402H (liver hepatocellular carcinoma), I405S (uterine), N417F (ovarian), A419N (small cell lung), I427V (pancreatic adenocarcinoma), R433L (liver), and P438L (melanoma). Notably, I405 and P438 are both residues predicted to be important for E2-selectivity of RNF8 (Figure 49 and Figure 50), and we previously showed that I405 is vital to stable Ubc13 binding (Figure 5b)²⁹. The I405 and P438 mutations may therefore cause improper targeting of Ubc13 to sites other than DNA DSBs by other RING E3 ligases. This would likely be disastrous to many pathways, including those that require K63-linked ubiquitin chains. Taken together, mutations to the E2:E3 pair, Ubc13/RNF8 are likely to cause defects in proper Lys63-linked ubiquitin signaling, which could contribute to DDR dysregulation and genome instability.

5.6 Impact of Results and Future Studies

The results presented in this thesis have implications for understanding ubiquitination, E2 enzyme inhibitor development, DNA DSB repair, and cancer biology. The process of ubiquitination is clearly a critical

form of signalling in cellular processes. It is also evident that the pervasiveness of ubiquitination in most major cellular processes is crucial to the physiology and function of mammals on a whole organism level. The identification of a mode of specific inhibition of a vital non-redundant, E2 enzyme, Ubc13, is likely to have a widespread impact on human-intervention of disease such as cancer. Battling cancer is essentially a strategy game, with very high stakes in the balance. Cancer is characterized by genome instability, but also the ability to proliferate indefinitely. This combination allows for microevolution, because the cancer genomes can have such variety, and replicate with such speed, that current therapeutics merely become acute evolutionary selective pressures to the cancer cell population. Due to these characteristics, therapies have a higher probability of hitting all cancer cells if they target multiple non-redundant proteins relied upon by these cells for survival. These characteristics also make a cure-all therapy highly improbable. Perhaps one day a biological therapy with the ability to adapt or evolve itself to match that of the cancer cells may be developed, but unfortunately such a therapy is likely a long way from fruition. The only way to get to the point of an adaptable therapy is through basic research on cellular processes from all angles and at all levels.

The inhibitor work on Ubc13 fits into the aforementioned scheme as a possible avenue for the development of more targeted therapies to be used in combination with others. Our discovery of a way to specifically

discriminate Ubc13 from the other homologous E2 enzymes using small-molecule inhibitors means that it should be seriously considered as a therapeutic anti-cancer target because it is also a non-redundant enzyme in multiple critical cellular processes important for cancer proliferation and survival. The future studies on this should include in-depth pharmacology, combined with X-ray crystallography, biochemistry, and cellular studies. Upon the development of serious pharmacological candidates, these should be tested against a wide spectrum of different cancer cell types to identify those most responsive to Ubc13 inhibition. The candidates should further be tested on mammalian models, alone and in combination with other chemo- and radio-therapies to identify the most potent anti-cancer regime. Although these studies represent many years of future work, the risk of drug development should be considered offset by the researchers because of the potential for learning more about ubiquitination, DNA repair, and cancer biology through these studies.

The work in this thesis on how the RING E3 ligase RNF8 interacts with and activates the E2 conjugating enzyme Ubc13 expands our current understanding of the DNA damage response pathway that responds to DNA double strand breaks. The impact of this work is not likely to be limited to the HR pathway, as RNF8 is also likely involved in NHEJ, as previously noted. Further, the knowledge gained from these studies may help inform ubiquitination, DNA repair, aging research, and cancer biology in the future. One day possessing a complete understanding of a

ubiquitous process such as ubiquitination may present the possibility of specifically manipulating the function of one or multiple pathways concomitantly to produce a very particular outcome. A step toward this is the realization that a manipulation, such as inhibition with small molecules, can be made much more specific if a particular E2:E3 pair is considered a single target. This is due to the fact that E2s can function with multiple E3s, which as a pair function in specific ubiquitination events. The targeting of an E2:E3 pair instead of an E2 or E3 alone means that inhibitors will discriminate between various roles of each individual protein alone or in an unrelated E2:E3 pair. Achieving such powerful control over such a ubiquitous cellular process could have widespread implications for many human diseases, which may not have been thought of yet. Future studies should further this idea, and aim to develop a small-molecule to target the RNF8/Ubc13 complex, which would set precedence for a potentially very powerful method of intervention in human disease. These studies may also require the development of a functional shortened RNF8 construct, so that high resolution X-ray crystallography studies can be employed in the development of the previously mentioned small molecule.

Collectively our work presents significant contributions to understanding ubiquitination, and cancer-associated pathways such as DNA repair and inflammation signalling. There are still many intriguing possibilities surrounding RNF8, Ubc13, and ubiquitination E2-E3s in

general, and the future may have many more interesting things to show us about the finer details of our own biology.

References

- 1 Hoeijmakers, J. H. DNA damage, aging, and cancer. *The New England journal of medicine* **361**, 1475-1485, doi:10.1056/NEJMra0804615 (2009).
- 2 Ciccia, A. & Elledge, S. J. The DNA damage response: making it safe to play with knives. *Mol. Cell* **40**, 179-204, doi:10.1016/j.molcel.2010.09.019 (2010).
- 3 De Bont, R. & van Larebeke, N. Endogenous DNA damage in humans: a review of quantitative data. *Mutagenesis* **19**, 169-185 (2004).
- 4 Predonzani, A., Cali, B., Agnellini, A. H. & Molon, B. Spotlights on immunological effects of reactive nitrogen species: When inflammation says nitric oxide. *World J Exp Med* **5**, 64-76, doi:10.5493/wjem.v5.i2.64 (2015).
- 5 Boal, A. K., Grove, T. L., McLaughlin, M. I., Yennawar, N. H., Booker, S. J. & Rosenzweig, A. C. Structural basis for methyl transfer by a radical SAM enzyme. *Science* **332**, 1089-1092, doi:10.1126/science.1205358 (2011).
- 6 Lindahl, T. Instability and decay of the primary structure of DNA. *Nature* **362**, 709-715, doi:10.1038/362709a0 (1993).
- 7 Jackson, A. L. & Loeb, L. A. The contribution of endogenous sources of DNA damage to the multiple mutations in cancer. *Mutat. Res.* **477**, 7-21 (2001).
- 8 Kim, Y. & He, Y. Y. Ultraviolet radiation-induced non-melanoma skin cancer: Regulation of DNA damage repair and inflammation. *Genes Dis* **1**, 188-198, doi:10.1016/j.gendis.2014.08.005 (2014).
- 9 Brash, D. E. Sunlight and the onset of skin cancer. *Trends Genet.* **13**, 410-414, doi:http://dx.doi.org/10.1016/S0168-9525(97)01246-8 (1997).
- 10 Bui, E., Joseph, B., Rhee, P., Diven, C., Pandit, V. & Brown, C. V. Contemporary management of radiation exposure and injury. *J Trauma Acute Care Surg* **77**, 495-500, doi:10.1097/TA.0000000000000297 (2014).
- 11 NRC. (ed National Research Council (US) Committee on Health Effects of Exposure to Low Levels of Ionizing Radiations (BEIR VII).) (The National Academies Press, Washington, D.C., 1998).
- 12 NRC. (ed National Research Council (US) Committee on Health Risks of Exposure to Radon (BEIR VI)) (The National Academies Press, Washington, D.C., 1999).
- 13 Frankenberg-Schwager, M. Induction, repair and biological relevance of radiation-induced DNA lesions in eukaryotic cells. *Radiat. Environ. Biophys.* **29**, 273-292 (1990).
- 14 Aguilera, A. & Garcia-Muse, T. Causes of genome instability. *Annu. Rev. Genet.* **47**, 1-32, doi:10.1146/annurev-genet-111212-133232 (2013).
- 15 Jackson, S. P. & Bartek, J. The DNA-damage response in human biology and disease. *Nature* **461**, 1071-1078, doi:10.1038/nature08467 (2009).

- 16 Tian, H., Gao, Z., Li, H., Zhang, B., Wang, G., Zhang, Q., Pei, D. & Zheng, J. DNA damage response--a double-edged sword in cancer prevention and cancer therapy. *Cancer Lett.* **358**, 8-16, doi:10.1016/j.canlet.2014.12.038 (2015).
- 17 Fell, V. L. & Schild-Poulter, C. The Ku heterodimer: function in DNA repair and beyond. *Mutat Res Rev Mutat Res* **763**, 15-29, doi:10.1016/j.mrrev.2014.06.002 (2015).
- 18 Fernandez-Capetillo, O., Lee, A., Nussenzweig, M. & Nussenzweig, A. H2AX: the histone guardian of the genome. *DNA Repair (Amst)* **3**, 959-967, doi:10.1016/j.dnarep.2004.03.024 (2004).
- 19 Lukas, J., Lukas, C. & Bartek, J. Mammalian cell cycle checkpoints: signalling pathways and their organization in space and time. *DNA Repair (Amst)* **3**, 997-1007, doi:10.1016/j.dnarep.2004.03.006 (2004).
- 20 Doil, C., Mailand, N., Bekker-Jensen, S., Menard, P., Larsen, D. H., Pepperkok, R., Ellenberg, J., Panier, S., Durocher, D., Bartek, J., Lukas, J. & Lukas, C. RNF168 binds and amplifies ubiquitin conjugates on damaged chromosomes to allow accumulation of repair proteins. *Cell* **136**, 435-446, doi:10.1016/j.cell.2008.12.041 (2009).
- 21 Polo, S. E. & Jackson, S. P. Dynamics of DNA damage response proteins at DNA breaks: a focus on protein modifications. *Genes Dev.* **25**, 409-433, doi:10.1101/gad.2021311 (2011).
- 22 Williams, R. S., Williams, J. S. & Tainer, J. A. Mre11-Rad50-Nbs1 is a keystone complex connecting DNA repair machinery, double-strand break signaling, and the chromatin template. *Biochem. Cell Biol.* **85**, 509-520, doi:10.1139/O07-069 (2007).
- 23 Spycher, C., Miller, E. S., Townsend, K., Pavic, L., Morrice, N. A., Janscak, P., Stewart, G. S. & Stucki, M. Constitutive phosphorylation of MDC1 physically links the MRE11-RAD50-NBS1 complex to damaged chromatin. *J. Cell Biol.* **181**, 227-240, doi:10.1083/jcb.200709008 (2008).
- 24 Stucki, M., Clapperton, J. A., Mohammad, D., Yaffe, M. B., Smerdon, S. J. & Jackson, S. P. MDC1 directly binds phosphorylated histone H2AX to regulate cellular responses to DNA double-strand breaks. *Cell* **123**, 1213-1226, doi:10.1016/j.cell.2005.09.038 (2005).
- 25 Lee, M. S., Edwards, R. A., Thede, G. L. & Glover, J. N. Structure of the BRCT repeat domain of MDC1 and its specificity for the free COOH-terminal end of the gamma-H2AX histone tail. *J. Biol. Chem.* **280**, 32053-32056, doi:10.1074/jbc.C500273200 (2005).
- 26 Melander, F., Bekker-Jensen, S., Falck, J., Bartek, J., Mailand, N. & Lukas, J. Phosphorylation of SDT repeats in the MDC1 N terminus triggers retention of NBS1 at the DNA damage-modified chromatin. *J. Cell Biol.* **181**, 213-226, doi:10.1083/jcb.200708210 (2008).
- 27 Huen, M. S., Grant, R., Manke, I., Minn, K., Yu, X., Yaffe, M. B. & Chen, J. RNF8 transduces the DNA-damage signal via histone ubiquitylation and checkpoint protein assembly. *Cell* **131**, 901-914, doi:10.1016/j.cell.2007.09.041 (2007).
- 28 Eddins, M. J., Carlile, C. M., Gomez, K. M., Pickart, C. M. & Wolberger, C. Mms2-Ubc13 covalently bound to ubiquitin reveals the structural basis of linkage-specific polyubiquitin chain formation. *Nat. Struct. Mol. Biol.* **13**, 915-920, doi:10.1038/nsmb1148 (2006).
- 29 Campbell, S. J., Edwards, R. A., Leung, C. C., Neculai, D., Hodge, C. D., Dhe-Paganon, S. & Glover, J. N. Molecular insights into the function of

- RING finger (RNF)-containing proteins hRNF8 and hRNF168 in Ubc13/Mms2-dependent ubiquitylation. *J. Biol. Chem.* **287**, 23900-23910, doi:10.1074/jbc.M112.359653 (2012).
- 30 Kolas, N. K., Chapman, J. R., Nakada, S., Ylanko, J., Chahwan, R., Sweeney, F. D., Panier, S., Mendez, M., Wildenhain, J., Thomson, T. M., Pelletier, L., Jackson, S. P. & Durocher, D. Orchestration of the DNA-damage response by the RNF8 ubiquitin ligase. *Science* **318**, 1637-1640, doi:10.1126/science.1150034 (2007).
- 31 Wang, B. & Elledge, S. J. Ubc13/Rnf8 ubiquitin ligases control foci formation of the Rap80/Abraxas/Brca1/Brcc36 complex in response to DNA damage. *Proc. Natl. Acad. Sci. U. S. A.* **104**, 20759-20763, doi:10.1073/pnas.0710061104 (2007).
- 32 Mattioli, F., Vissers, J. H., van Dijk, W. J., Ikpa, P., Citterio, E., Vermeulen, W., Marteijn, J. A. & Sixma, T. K. RNF168 ubiquitinates K13-15 on H2A/H2AX to drive DNA damage signaling. *Cell* **150**, 1182-1195, doi:10.1016/j.cell.2012.08.005 (2012).
- 33 Stewart, G. S., Panier, S., Townsend, K., Al-Hakim, A. K., Kolas, N. K., Miller, E. S., Nakada, S., Ylanko, J., Olivarius, S., Mendez, M., Oldreive, C., Wildenhain, J., Tagliaferro, A., Pelletier, L., Taubenheim, N., Durandy, A., Byrd, P. J., Stankovic, T., Taylor, A. M. & Durocher, D. The RIDDLE syndrome protein mediates a ubiquitin-dependent signaling cascade at sites of DNA damage. *Cell* **136**, 420-434, doi:10.1016/j.cell.2008.12.042 (2009).
- 34 Fradet-Turcotte, A., Canny, M. D., Escibano-Diaz, C., Orthwein, A., Leung, C. C., Huang, H., Landry, M. C., Kitevski-LeBlanc, J., Noordermeer, S. M., Sicheri, F. & Durocher, D. 53BP1 is a reader of the DNA-damage-induced H2A Lys 15 ubiquitin mark. *Nature* **499**, 50-54, doi:10.1038/nature12318 (2013).
- 35 Xie, A., Hartlerode, A., Stucki, M., Odate, S., Puget, N., Kwok, A., Nagaraju, G., Yan, C., Alt, F. W., Chen, J., Jackson, S. P. & Scully, R. Distinct roles of chromatin-associated proteins MDC1 and 53BP1 in mammalian double-strand break repair. *Mol. Cell* **28**, 1045-1057, doi:10.1016/j.molcel.2007.12.005 (2007).
- 36 Mailand, N., Bekker-Jensen, S., Faustrup, H., Melander, F., Bartek, J., Lukas, C. & Lukas, J. RNF8 ubiquitylates histones at DNA double-strand breaks and promotes assembly of repair proteins. *Cell* **131**, 887-900, doi:10.1016/j.cell.2007.09.040 (2007).
- 37 Sato, Y., Yoshikawa, A., Mimura, H., Yamashita, M., Yamagata, A. & Fukai, S. Structural basis for specific recognition of Lys 63-linked polyubiquitin chains by tandem UIMs of RAP80. *EMBO J.* **28**, 2461-2468, doi:10.1038/emboj.2009.160 (2009).
- 38 Daley, J. M., Kwon, Y., Niu, H. & Sung, P. Investigations of homologous recombination pathways and their regulation. *Yale J Biol Med* **86**, 453-461 (2013).
- 39 Sung, P. & Roberson, D. L. DNA strand exchange mediated by a RAD51-ssDNA nucleoprotein filament with polarity opposite to that of RecA. *Cell* **82**, 453-461 (1995).
- 40 Wang, C. & Lees-Miller, S. P. Detection and repair of ionizing radiation-induced DNA double strand breaks: new developments in nonhomologous end joining. *Int. J. Radiat. Oncol. Biol. Phys.* **86**, 440-449, doi:10.1016/j.ijrobp.2013.01.011 (2013).

- 41 Mimori, T., Hardin, J. A. & Steitz, J. A. Characterization of the DNA-binding protein antigen Ku recognized by autoantibodies from patients with rheumatic disorders. *J. Biol. Chem.* **261**, 2274-2278 (1986).
- 42 Paillard, S. & Strauss, F. Analysis of the mechanism of interaction of simian Ku protein with DNA. *Nucleic Acids Res.* **19**, 5619-5624 (1991).
- 43 Ono, M., Tucker, P. W. & Capra, J. D. Production and characterization of recombinant human Ku antigen. *Nucleic Acids Res.* **22**, 3918-3924 (1994).
- 44 Weinfeld, M., Mani, R. S., Abdou, I., Aceytuno, R. D. & Glover, J. N. Tidying up loose ends: the role of polynucleotide kinase/phosphatase in DNA strand break repair. *Trends Biochem. Sci.* **36**, 262-271, doi:10.1016/j.tibs.2011.01.006 (2011).
- 45 Chappell, C., Hanakahi, L. A., Karimi-Busheri, F., Weinfeld, M. & West, S. C. Involvement of human polynucleotide kinase in double-strand break repair by non-homologous end joining. *EMBO J.* **21**, 2827-2832, doi:10.1093/emboj/21.11.2827 (2002).
- 46 Bahmed, K., Seth, A., Nitiss, K. C. & Nitiss, J. L. End-processing during non-homologous end-joining: a role for exonuclease 1. *Nucleic Acids Res.* **39**, 970-978, doi:10.1093/nar/gkq886 (2011).
- 47 Xie, A., Kwok, A. & Scully, R. Role of mammalian Mre11 in classical and alternative nonhomologous end joining. *Nat. Struct. Mol. Biol.* **16**, 814-818, doi:10.1038/nsmb.1640 (2009).
- 48 Weterings, E., Verkaik, N. S., Keijzers, G., Florea, B. I., Wang, S. Y., Ortega, L. G., Uematsu, N., Chen, D. J. & van Gent, D. C. The Ku80 carboxy terminus stimulates joining and artemis-mediated processing of DNA ends. *Mol. Cell. Biol.* **29**, 1134-1142, doi:10.1128/MCB.00971-08 (2009).
- 49 Kusumoto, R., Dawut, L., Marchetti, C., Wan Lee, J., Vindigni, A., Ramsden, D. & Bohr, V. A. Werner protein cooperates with the XRCC4-DNA ligase IV complex in end-processing. *Biochemistry* **47**, 7548-7556, doi:10.1021/bi702325t (2008).
- 50 Ahel, I., Rass, U., El-Khamisy, S. F., Katyal, S., Clements, P. M., McKinnon, P. J., Caldecott, K. W. & West, S. C. The neurodegenerative disease protein aprataxin resolves abortive DNA ligation intermediates. *Nature* **443**, 713-716, doi:10.1038/nature05164 (2006).
- 51 Feng, L. & Chen, J. The E3 ligase RNF8 regulates KU80 removal and NHEJ repair. *Nat. Struct. Mol. Biol.* **19**, 201-206, doi:10.1038/nsmb.2211 (2012).
- 52 Komander, D. & Rape, M. The ubiquitin code. *Annu. Rev. Biochem.* **81**, 203-229, doi:10.1146/annurev-biochem-060310-170328 (2012).
- 53 Al-Hakim, A., Escribano-Diaz, C., Landry, M. C., O'Donnell, L., Panier, S., Szilard, R. K. & Durocher, D. The ubiquitous role of ubiquitin in the DNA damage response. *DNA Repair (Amst)* **9**, 1229-1240, doi:10.1016/j.dnarep.2010.09.011 (2010).
- 54 Haas, A. L. & Siepmann, T. J. Pathways of ubiquitin conjugation. *FASEB J.* **11**, 1257-1268 (1997).
- 55 Hershko, A. & Ciechanover, A. The ubiquitin system. *Annu. Rev. Biochem.* **67**, 425-479, doi:10.1146/annurev.biochem.67.1.425 (1998).
- 56 Pickart, C. M. & Eddins, M. J. Ubiquitin: structures, functions, mechanisms. *Biochim. Biophys. Acta* **1695**, 55-72, doi:10.1016/j.bbamcr.2004.09.019 (2004).

- 57 Dye, B. T. & Schulman, B. A. Structural mechanisms underlying posttranslational modification by ubiquitin-like proteins. *Annu. Rev. Biophys. Biomol. Struct.* **36**, 131-150, doi:10.1146/annurev.biophys.36.040306.132820 (2007).
- 58 Peng, J., Schwartz, D., Elias, J. E., Thoreen, C. C., Cheng, D., Marsischky, G., Roelofs, J., Finley, D. & Gygi, S. P. A proteomics approach to understanding protein ubiquitination. *Nat. Biotechnol.* **21**, 921-926, doi:10.1038/nbt849 (2003).
- 59 Xu, P., Duong, D. M., Seyfried, N. T., Cheng, D., Xie, Y., Robert, J., Rush, J., Hochstrasser, M., Finley, D. & Peng, J. Quantitative proteomics reveals the function of unconventional ubiquitin chains in proteasomal degradation. *Cell* **137**, 133-145, doi:10.1016/j.cell.2009.01.041 (2009).
- 60 Nishikawa, H., Ooka, S., Sato, K., Arima, K., Okamoto, J., Klevit, R. E., Fukuda, M. & Ohta, T. Mass spectrometric and mutational analyses reveal Lys-6-linked polyubiquitin chains catalyzed by BRCA1-BARD1 ubiquitin ligase. *J. Biol. Chem.* **279**, 3916-3924, doi:10.1074/jbc.M308540200 (2004).
- 61 Chastagner, P., Israel, A. & Brou, C. Itch/AIP4 mediates Deltex degradation through the formation of K29-linked polyubiquitin chains. *EMBO Rep* **7**, 1147-1153, doi:10.1038/sj.embor.7400822 (2006).
- 62 Jin, L., Williamson, A., Banerjee, S., Philipp, I. & Rape, M. Mechanism of ubiquitin-chain formation by the human anaphase-promoting complex. *Cell* **133**, 653-665, doi:10.1016/j.cell.2008.04.012 (2008).
- 63 Wertz, I. E. & Dixit, V. M. Signaling to NF-kappaB: regulation by ubiquitination. *Cold Spring Harb Perspect. Biol.* **2**, a003350, doi:10.1101/cshperspect.a003350 (2010).
- 64 Iwai, K., Fujita, H. & Sasaki, Y. Linear ubiquitin chains: NF-kappaB signalling, cell death and beyond. *Nat. Rev. Mol. Cell Biol.* **15**, 503-508, doi:10.1038/nrm3836 (2014).
- 65 Rahighi, S., Ikeda, F., Kawasaki, M., Akutsu, M., Suzuki, N., Kato, R., Kensche, T., Uejima, T., Bloor, S., Komander, D., Randow, F., Wakatsuki, S. & Dikic, I. Specific recognition of linear ubiquitin chains by NEMO is important for NF-kappaB activation. *Cell* **136**, 1098-1109, doi:10.1016/j.cell.2009.03.007 (2009).
- 66 Kristariyanto, Y. A., Choi, S. Y., Rehman, S. A., Ritorto, M. S., Campbell, D. G., Morrice, N. A., Toth, R. & Kulathu, Y. Assembly and structure of Lys33-linked polyubiquitin reveals distinct conformations. *Biochem. J.* **467**, 345-352, doi:10.1042/BJ20141502 (2015).
- 67 Michel, M. A., Elliott, P. R., Swatek, K. N., Simicek, M., Pruneda, J. N., Wagstaff, J. L., Freund, S. M. & Komander, D. Assembly and specific recognition of k29- and k33-linked polyubiquitin. *Mol. Cell* **58**, 95-109, doi:10.1016/j.molcel.2015.01.042 (2015).
- 68 McKenna, S., Moraes, T., Pastushok, L., Ptak, C., Xiao, W., Spyropoulos, L. & Ellison, M. J. An NMR-based model of the ubiquitin-bound human ubiquitin conjugation complex Mms2.Ubc13. The structural basis for lysine 63 chain catalysis. *J. Biol. Chem.* **278**, 13151-13158, doi:10.1074/jbc.M212353200 (2003).
- 69 McKenna, S., Spyropoulos, L., Moraes, T., Pastushok, L., Ptak, C., Xiao, W. & Ellison, M. J. Noncovalent interaction between ubiquitin and the human DNA repair protein Mms2 is required for Ubc13-mediated

- polyubiquitination. *J. Biol. Chem.* **276**, 40120-40126, doi:10.1074/jbc.M102858200 (2001).
- 70 Lewis, M. J., Saltibus, L. F., Hau, D. D., Xiao, W. & Spyrapopoulos, L. Structural basis for non-covalent interaction between ubiquitin and the ubiquitin conjugating enzyme variant human MMS2. *J. Biomol. NMR* **34**, 89-100, doi:10.1007/s10858-005-5583-6 (2006).
- 71 Markin, C. J., Saltibus, L. F., Kean, M. J., McKay, R. T., Xiao, W. & Spyrapopoulos, L. Catalytic proficiency of ubiquitin conjugation enzymes: balancing pK(a) suppression, entropy, and electrostatics. *J. Am. Chem. Soc.* **132**, 17775-17786, doi:10.1021/ja105267w (2010).
- 72 Wu, P. Y., Hanlon, M., Eddins, M., Tsui, C., Rogers, R. S., Jensen, J. P., Matunis, M. J., Weissman, A. M., Wolberger, C. & Pickart, C. M. A conserved catalytic residue in the ubiquitin-conjugating enzyme family. *EMBO J.* **22**, 5241-5250, doi:10.1093/emboj/cdg501 (2003).
- 73 Metzger, M. B., Pruneda, J. N., Klevit, R. E. & Weissman, A. M. RING-type E3 ligases: master manipulators of E2 ubiquitin-conjugating enzymes and ubiquitination. *Biochim. Biophys. Acta* **1843**, 47-60, doi:10.1016/j.bbamcr.2013.05.026 (2014).
- 74 Plechanovova, A., Jaffray, E. G., Tatham, M. H., Naismith, J. H. & Hay, R. T. Structure of a RING E3 ligase and ubiquitin-loaded E2 primed for catalysis. *Nature* **489**, 115-120, doi:10.1038/nature11376 (2012).
- 75 Pruneda, J. N., Littlefield, P. J., Soss, S. E., Nordquist, K. A., Chazin, W. J., Brzovic, P. S. & Klevit, R. E. Structure of an E3:E2~Ub complex reveals an allosteric mechanism shared among RING/U-box ligases. *Mol. Cell* **47**, 933-942, doi:10.1016/j.molcel.2012.07.001 (2012).
- 76 Berndsen, C. E. & Wolberger, C. New insights into ubiquitin E3 ligase mechanism. *Nat. Struct. Mol. Biol.* **21**, 301-307, doi:10.1038/nsmb.2780 (2014).
- 77 Juang, Y. C., Landry, M. C., Sanches, M., Vittal, V., Leung, C. C., Ceccarelli, D. F., Mateo, A. R., Pruneda, J. N., Mao, D. Y., Szilard, R. K., Orlicky, S., Munro, M., Brzovic, P. S., Klevit, R. E., Sicheri, F. & Durocher, D. OTUB1 co-opts Lys48-linked ubiquitin recognition to suppress E2 enzyme function. *Mol. Cell* **45**, 384-397, doi:10.1016/j.molcel.2012.01.011 (2012).
- 78 Nakada, S., Tai, I., Panier, S., Al-Hakim, A., Iemura, S., Juang, Y. C., O'Donnell, L., Kumakubo, A., Munro, M., Sicheri, F., Gingras, A. C., Natsume, T., Suda, T. & Durocher, D. Non-canonical inhibition of DNA damage-dependent ubiquitination by OTUB1. *Nature* **466**, 941-946, doi:10.1038/nature09297 (2010).
- 79 Fujimuro, M. & Yokosawa, H. Production of antipolyubiquitin monoclonal antibodies and their use for characterization and isolation of polyubiquitinated proteins. *Methods Enzymol.* **399**, 75-86, doi:10.1016/S0076-6879(05)99006-X (2005).
- 80 Pierce, A. J., Johnson, R. D., Thompson, L. H. & Jasin, M. XRCC3 promotes homology-directed repair of DNA damage in mammalian cells. *Genes Dev.* **13**, 2633-2638 (1999).
- 81 Pierce, A. J., Hu, P., Han, M., Ellis, N. & Jasin, M. Ku DNA end-binding protein modulates homologous repair of double-strand breaks in mammalian cells. *Genes Dev.* **15**, 3237-3242, doi:10.1101/gad.946401 (2001).

- 82 Sowa, M. E., Bennett, E. J., Gygi, S. P. & Harper, J. W. Defining the human deubiquitinating enzyme interaction landscape. *Cell* **138**, 389-403, doi:10.1016/j.cell.2009.04.042 (2009).
- 83 Wiener, R., Zhang, X., Wang, T. & Wolberger, C. The mechanism of OTUB1-mediated inhibition of ubiquitination. *Nature* **483**, 618-622, doi:10.1038/nature10911 (2012).
- 84 Markin, C. J., Xiao, W. & Spyrapoulos, L. Mechanism for recognition of polyubiquitin chains: balancing affinity through interplay between multivalent binding and dynamics. *J. Am. Chem. Soc.* **132**, 11247-11258, doi:10.1021/ja103869x (2010).
- 85 Hurley, J. H., Lee, S. & Prag, G. Ubiquitin-binding domains. *Biochem. J.* **399**, 361-372, doi:10.1042/BJ20061138 (2006).
- 86 Sims, J. J., Scavone, F., Cooper, E. M., Kane, L. A., Youle, R. J., Boeke, J. D. & Cohen, R. E. Polyubiquitin-sensor proteins reveal localization and linkage-type dependence of cellular ubiquitin signaling. *Nat. Methods* **9**, 303-309, doi:10.1038/nmeth.1888 (2012).
- 87 Ismail, I. H., Andrin, C., McDonald, D. & Hendzel, M. J. BMI1-mediated histone ubiquitylation promotes DNA double-strand break repair. *J. Cell Biol.* **191**, 45-60, doi:10.1083/jcb.201003034 (2010).
- 88 Bergink, S., Salomons, F. A., Hoogstraten, D., Groothuis, T. A., de Waard, H., Wu, J., Yuan, L., Citterio, E., Houtsmuller, A. B., Neefjes, J., Hoeijmakers, J. H., Vermeulen, W. & Dantuma, N. P. DNA damage triggers nucleotide excision repair-dependent monoubiquitylation of histone H2A. *Genes Dev.* **20**, 1343-1352, doi:10.1101/gad.373706 (2006).
- 89 Chagraoui, J., Hebert, J., Girard, S. & Sauvageau, G. An anticlastogenic function for the Polycomb Group gene Bmi1. *Proc. Natl. Acad. Sci. U. S. A.* **108**, 5284-5289, doi:10.1073/pnas.1014263108 (2011).
- 90 Facchino, S., Abdouh, M., Chatoo, W. & Bernier, G. BMI1 confers radioresistance to normal and cancerous neural stem cells through recruitment of the DNA damage response machinery. *J. Neurosci.* **30**, 10096-10111, doi:10.1523/JNEUROSCI.1634-10.2010 (2010).
- 91 Ginjala, V., Nacerddine, K., Kulkarni, A., Oza, J., Hill, S. J., Yao, M., Citterio, E., van Lohuizen, M. & Ganesan, S. BMI1 is recruited to DNA breaks and contributes to DNA damage-induced H2A ubiquitination and repair. *Mol. Cell. Biol.* **31**, 1972-1982, doi:10.1128/MCB.00981-10 (2011).
- 92 Pan, M. R., Peng, G., Hung, W. C. & Lin, S. Y. Monoubiquitination of H2AX protein regulates DNA damage response signaling. *J. Biol. Chem.* **286**, 28599-28607, doi:10.1074/jbc.M111.256297 (2011).
- 93 Wu, C. Y., Kang, H. Y., Yang, W. L., Wu, J., Jeong, Y. S., Wang, J., Chan, C. H., Lee, S. W., Zhang, X., Lamothe, B., Campos, A. D., Darnay, B. G. & Lin, H. K. Critical role of monoubiquitination of histone H2AX protein in histone H2AX phosphorylation and DNA damage response. *J. Biol. Chem.* **286**, 30806-30815, doi:10.1074/jbc.M111.257469 (2011).
- 94 Ikura, T., Tashiro, S., Kakino, A., Shima, H., Jacob, N., Amunugama, R., Yoder, K., Izumi, S., Kuraoka, I., Tanaka, K., Kimura, H., Ikura, M., Nishikubo, S., Ito, T., Muto, A., Miyagawa, K., Takeda, S., Fishel, R., Igarashi, K. & Kamiya, K. DNA damage-dependent acetylation and ubiquitination of H2AX enhances chromatin dynamics. *Mol. Cell. Biol.* **27**, 7028-7040, doi:10.1128/MCB.00579-07 (2007).

- 95 Acs, K., Luijsterburg, M. S., Ackermann, L., Salomons, F. A., Hoppe, T. & Dantuma, N. P. The AAA-ATPase VCP/p97 promotes 53BP1 recruitment by removing L3MBTL1 from DNA double-strand breaks. *Nat. Struct. Mol. Biol.* **18**, 1345-1350, doi:10.1038/nsmb.2188 (2011).
- 96 Mallette, F. A., Mattioli, F., Cui, G., Young, L. C., Hendzel, M. J., Mer, G., Sixma, T. K. & Richard, S. RNF8- and RNF168-dependent degradation of KDM4A/JMJD2A triggers 53BP1 recruitment to DNA damage sites. *EMBO J.* **31**, 1865-1878, doi:10.1038/emboj.2012.47 (2012).
- 97 Botuyan, M. V., Lee, J., Ward, I. M., Kim, J. E., Thompson, J. R., Chen, J. & Mer, G. Structural basis for the methylation state-specific recognition of histone H4-K20 by 53BP1 and Crb2 in DNA repair. *Cell* **127**, 1361-1373, doi:10.1016/j.cell.2006.10.043 (2006).
- 98 Sanders, S. L., Portoso, M., Mata, J., Bahler, J., Allshire, R. C. & Kouzarides, T. Methylation of histone H4 lysine 20 controls recruitment of Crb2 to sites of DNA damage. *Cell* **119**, 603-614, doi:10.1016/j.cell.2004.11.009 (2004).
- 99 Kato, K., Nakajima, K., Ui, A., Muto-Terao, Y., Ogiwara, H. & Nakada, S. Fine-tuning of DNA damage-dependent ubiquitination by OTUB2 supports the DNA repair pathway choice. *Mol. Cell* **53**, 617-630, doi:10.1016/j.molcel.2014.01.030 (2014).
- 100 Watanabe, S., Watanabe, K., Akimov, V., Bartkova, J., Blagoev, B., Lukas, J. & Bartek, J. JMJD1C demethylates MDC1 to regulate the RNF8 and BRCA1-mediated chromatin response to DNA breaks. *Nat. Struct. Mol. Biol.* **20**, 1425-1433, doi:10.1038/nsmb.2702 (2013).
- 101 Orthwein, A., Fradet-Turcotte, A., Noordermeer, S. M., Canny, M. D., Brun, C. M., Strecker, J., Escribano-Diaz, C. & Durocher, D. Mitosis inhibits DNA double-strand break repair to guard against telomere fusions. *Science* **344**, 189-193, doi:10.1126/science.1248024 (2014).
- 102 Belotserkovskaya, R. & Jackson, S. P. Keeping 53BP1 out of focus in mitosis. *Cell Res.* **24**, 781-782, doi:10.1038/cr.2014.62 (2014).
- 103 Giunta, S., Belotserkovskaya, R. & Jackson, S. P. DNA damage signaling in response to double-strand breaks during mitosis. *J. Cell Biol.* **190**, 197-207, doi:10.1083/jcb.200911156 (2010).
- 104 Zhao, H., Zhu, M., Dou, G., Zhao, H., Zhu, B., Li, J., Liao, J. & Xu, X. BCL10 regulates RNF8/RNF168-mediated ubiquitination in the DNA damage response. *Cell cycle* **13**, 1777-1787, doi:10.4161/cc.28707 (2014).
- 105 Laine, A., Topisirovic, I., Zhai, D., Reed, J. C., Borden, K. L. & Ronai, Z. Regulation of p53 localization and activity by Ubc13. *Mol. Cell. Biol.* **26**, 8901-8913, doi:10.1128/MCB.01156-06 (2006).
- 106 Topisirovic, I., Gutierrez, G. J., Chen, M., Appella, E., Borden, K. L. & Ronai, Z. A. Control of p53 multimerization by Ubc13 is JNK-regulated. *Proc. Natl. Acad. Sci. U. S. A.* **106**, 12676-12681, doi:10.1073/pnas.0900596106 (2009).
- 107 Cohen, J. I. Epstein-barr virus vaccines. *Clin Transl Immunology* **4**, e32, doi:10.1038/cti.2014.27 (2015).
- 108 Yang, J., Deng, W., Hau, P. M., Liu, J., Lau, V. M., Cheung, A. L., Huen, M. S. & Tsao, S. W. Epstein-Barr virus BZLF1 protein impairs accumulation of host DNA damage proteins at damage sites in response to DNA damage. *Lab. Invest.*, doi:10.1038/labinvest.2015.69 (2015).

- 109 Tsurumi, T., Fujita, M. & Kudoh, A. Latent and lytic Epstein-Barr virus replication strategies. *Rev. Med. Virol.* **15**, 3-15, doi:10.1002/rmv.441 (2005).
- 110 Chaurushiya, M. S., Lilley, C. E., Aslanian, A., Meisenhelder, J., Scott, D. C., Landry, S., Ticau, S., Boutell, C., Yates, J. R., 3rd, Schulman, B. A., Hunter, T. & Weitzman, M. D. Viral E3 ubiquitin ligase-mediated degradation of a cellular E3: viral mimicry of a cellular phosphorylation mark targets the RNF8 FHA domain. *Mol. Cell* **46**, 79-90, doi:10.1016/j.molcel.2012.02.004 (2012).
- 111 Drozdetskiy, A., Cole, C., Procter, J. & Barton, G. J. JPred4: a protein secondary structure prediction server. *Nucleic Acids Res.* **43**, W389-394, doi:10.1093/nar/gkv332 (2015).
- 112 Drenth, J. *Principles of Protein X-ray Crystallography*. 3 edn, 1-332 (Springer-Verlag New York, 2007).
- 113 Putnam, C. D., Hammel, M., Hura, G. L. & Tainer, J. A. X-ray solution scattering (SAXS) combined with crystallography and computation: defining accurate macromolecular structures, conformations and assemblies in solution. *Q. Rev. Biophys.* **40**, 191-285, doi:10.1017/S0033583507004635 (2007).
- 114 Pelikan, M., Hura, G. & Hammel, M. Structure and flexibility within proteins as identified through small angle X-ray scattering. *Gen Physiol Biophys* **28**, 174-189, doi:10.4149/gpb_2009_02_174 (2009).
- 115 Nguyen, H. H., Park, J., Kang, S. & Kim, M. Surface plasmon resonance: a versatile technique for biosensor applications. *Sensors (Basel)* **15**, 10481-10510, doi:10.3390/s150510481 (2015).
- 116 Adams, P. D., Afonine, P. V., Bunkoczi, G., Chen, V. B., Davis, I. W., Echols, N., Headd, J. J., Hung, L. W., Kapral, G. J., Grosse-Kunstleve, R. W., McCoy, A. J., Moriarty, N. W., Oeffner, R., Read, R. J., Richardson, D. C., Richardson, J. S., Terwilliger, T. C. & Zwart, P. H. PHENIX: a comprehensive Python-based system for macromolecular structure solution. *Acta crystallographica. Section D, Biological crystallography* **66**, 213-221, doi:10.1107/S0907444909052925 (2010).
- 117 Grigoryan, G. & Degrado, W. F. Probing designability via a generalized model of helical bundle geometry. *J. Mol. Biol.* **405**, 1079-1100, doi:10.1016/j.jmb.2010.08.058 (2011).
- 118 Berger, B., Wilson, D. B., Wolf, E., Tonchev, T., Milla, M. & Kim, P. S. Predicting coiled coils by use of pairwise residue correlations. *Proc. Natl. Acad. Sci. U. S. A.* **92**, 8259-8263 (1995).
- 119 McDonnell, A. V., Jiang, T., Keating, A. E. & Berger, B. Paircoil2: improved prediction of coiled coils from sequence. *Bioinformatics* **22**, 356-358, doi:10.1093/bioinformatics/bti797 (2006).
- 120 Lupas, A. N. & Gruber, M. The structure of alpha-helical coiled coils. *Adv Protein Chem* **70**, 37-78, doi:10.1016/S0065-3233(05)70003-6 (2005).
- 121 Michelle, C., Vourc'h, P., Mignon, L. & Andres, C. R. What was the set of ubiquitin and ubiquitin-like conjugating enzymes in the eukaryote common ancestor? *J. Mol. Evol.* **68**, 616-628, doi:10.1007/s00239-009-9225-6 (2009).
- 122 van Wijk, S. J. & Timmers, H. T. The family of ubiquitin-conjugating enzymes (E2s): deciding between life and death of proteins. *FASEB J.* **24**, 981-993, doi:10.1096/fj.09-136259 (2010).

- 123 Lu, C. S., Truong, L. N., Aslanian, A., Shi, L. Z., Li, Y., Hwang, P. Y., Koh, K. H., Hunter, T., Yates, J. R., 3rd, Berns, M. W. & Wu, X. The RING finger protein RNF8 ubiquitinates Nbs1 to promote DNA double-strand break repair by homologous recombination. *J. Biol. Chem.* **287**, 43984-43994, doi:10.1074/jbc.M112.421545 (2012).
- 124 Iwai, K. Diverse ubiquitin signaling in NF-kappaB activation. *Trends Cell Biol.* **22**, 355-364, doi:10.1016/j.tcb.2012.04.001 (2012).
- 125 Strickson, S., Campbell, D. G., Emmerich, C. H., Knebel, A., Plater, L., Ritorto, M. S., Shpiro, N. & Cohen, P. The anti-inflammatory drug BAY 11-7082 suppresses the MyD88-dependent signalling network by targeting the ubiquitin system. *Biochem. J.* **451**, 427-437, doi:10.1042/BJ20121651 (2013).
- 126 Pulvino, M., Liang, Y., Oleksyn, D., DeRan, M., Van Pelt, E., Shapiro, J., Sanz, I., Chen, L. & Zhao, J. Inhibition of proliferation and survival of diffuse large B-cell lymphoma cells by a small-molecule inhibitor of the ubiquitin-conjugating enzyme Ubc13-Uev1A. *Blood* **120**, 1668-1677, doi:10.1182/blood-2012-02-406074 (2012).
- 127 Berndsen, C. E., Wiener, R., Yu, I. W., Ringel, A. E. & Wolberger, C. A conserved asparagine has a structural role in ubiquitin-conjugating enzymes. *Nat. Chem. Biol.* **9**, 154-156, doi:10.1038/nchembio.1159 (2013).
- 128 Yunus, A. A. & Lima, C. D. Lysine activation and functional analysis of E2-mediated conjugation in the SUMO pathway. *Nat. Struct. Mol. Biol.* **13**, 491-499, doi:10.1038/nsmb1104 (2006).
- 129 Pierce, J. W., Schoenleber, R., Jesmok, G., Best, J., Moore, S. A., Collins, T. & Gerritsen, M. E. Novel Inhibitors of Cytokine-induced I B Phosphorylation and Endothelial Cell Adhesion Molecule Expression Show Anti-inflammatory Effects in Vivo. *J. Biol. Chem.* **272**, 21096-21103, doi:10.1074/jbc.272.34.21096 (1997).
- 130 Andersen, P. L., Zhou, H., Pastushok, L., Moraes, T., McKenna, S., Ziola, B., Ellison, M. J., Dixit, V. M. & Xiao, W. Distinct regulation of Ubc13 functions by the two ubiquitin-conjugating enzyme variants Mms2 and Uev1A. *J. Cell Biol.* **170**, 745-755, doi:10.1083/jcb.200502113 (2005).
- 131 Arango Duque, G. & Descoteaux, A. Macrophage cytokines: involvement in immunity and infectious diseases. *Front. Immunol.* **5**, 491, doi:10.3389/fimmu.2014.00491 (2014).
- 132 Huleihel, M., Douvdevani, A., Segal, S. & Apte, R. N. Different regulatory levels are involved in the generation of hemopoietic cytokines (CSFs and IL-6) in fibroblasts stimulated by inflammatory products. *Cytokine* **5**, 47-56 (1993).
- 133 Takatsu, K. Revisiting the identification and cDNA cloning of T cell-replacing factor/interleukin-5. *Front. Immunol.* **5**, 639, doi:10.3389/fimmu.2014.00639 (2014).
- 134 Teferedegne, B., Green, M. R., Guo, Z. & Boss, J. M. Mechanism of action of a distal NF-kappaB-dependent enhancer. *Mol. Cell. Biol.* **26**, 5759-5770, doi:10.1128/MCB.00271-06 (2006).
- 135 Huen, M. S., Huang, J., Yuan, J., Yamamoto, M., Akira, S., Ashley, C., Xiao, W. & Chen, J. Noncanonical E2 variant-independent function of UBC13 in promoting checkpoint protein assembly. *Mol. Cell. Biol.* **28**, 6104-6112, doi:10.1128/MCB.00987-08 (2008).

- 136 Rout, M. K., Hodge, C. D., Markin, C. J., Xu, X., Glover, J. N., Xiao, W. & Spyropoulos, L. Stochastic gate dynamics regulate the catalytic activity of ubiquitination enzymes. *J. Am. Chem. Soc.* **136**, 17446-17458, doi:10.1021/ja505440b (2014).
- 137 Soss, S. E., Klevit, R. E. & Chazin, W. J. Activation of UbcH5c~Ub is the result of a shift in interdomain motions of the conjugate bound to U-box E3 ligase E4B. *Biochemistry* **52**, 2991-2999, doi:10.1021/bi3015949 (2013).
- 138 Singh, J., Petter, R. C., Baillie, T. A. & Whitty, A. The resurgence of covalent drugs. *Nat. Rev. Drug Discov.* **10**, 307-317, doi:10.1038/nrd3410 (2011).
- 139 Vass, M., Hruska, K. & Franek, M. Nitrofurantoin antibiotics: a review on the application, prohibition and residual analysis. *Vet Med-Czech* **53**, 469-500 (2008).
- 140 Krishnan, N., Bencze, G., Cohen, P. & Tonks, N. K. The anti-inflammatory compound BAY-11-7082 is a potent inhibitor of protein tyrosine phosphatases. *FEBS J.* **280**, 2830-2841, doi:10.1111/febs.12283 (2013).
- 141 Rauert-Wunderlich, H., Siegmund, D., Maier, E., Giner, T., Bargou, R. C., Wajant, H. & Stuhmer, T. The IKK inhibitor Bay 11-7082 induces cell death independent from inhibition of activation of NFkappaB transcription factors. *PLoS one* **8**, e59292, doi:10.1371/journal.pone.0059292 (2013).
- 142 Ceccarelli, D. F., Tang, X., Pelletier, B., Orlicky, S., Xie, W., Plantevin, V., Neculai, D., Chou, Y. C., Ogunjimi, A., Al-Hakim, A., Varelas, X., Koszela, J., Wasney, G. A., Vedadi, M., Dhe-Paganon, S., Cox, S., Xu, S., Lopez-Girona, A., Mercurio, F., Wrana, J., Durocher, D., Meloche, S., Webb, D. R., Tyers, M. & Sicheri, F. An allosteric inhibitor of the human Cdc34 ubiquitin-conjugating enzyme. *Cell* **145**, 1075-1087, doi:10.1016/j.cell.2011.05.039 (2011).
- 143 Su, W. P., Hsu, S. H., Wu, C. K., Chang, S. B., Lin, Y. J., Yang, W. B., Hung, J. J., Chiu, W. T., Tzeng, S. F., Tseng, Y. L., Chang, J. Y., Su, W. C. & Liaw, H. Chronic treatment with cisplatin induces replication-dependent sister chromatid recombination to confer cisplatin-resistant phenotype in nasopharyngeal carcinoma. *Oncotarget* **5**, 6323-6337 (2014).
- 144 Wu, Z., Shen, S., Zhang, Z., Zhang, W. & Xiao, W. Ubiquitin-conjugating enzyme complex Uev1A-Ubc13 promotes breast cancer metastasis through nuclear factor- κ B mediated matrix metalloproteinase-1 gene regulation. *Breast Cancer Res.* **16**, R75, doi:10.1186/bcr3692 (2014).
- 145 Wu, X., Zhang, W., Font-Burgada, J., Palmer, T., Hamil, A. S., Biswas, S. K., Poidinger, M., Borcherdig, N., Xie, Q., Ellies, L. G., Lytle, N. K., Wu, L. W., Fox, R. G., Yang, J., Dowdy, S. F., Reya, T. & Karin, M. Ubiquitin-conjugating enzyme Ubc13 controls breast cancer metastasis through a TAK1-p38 MAP kinase cascade. *Proc. Natl. Acad. Sci. U. S. A.* **111**, 13870-13875, doi:10.1073/pnas.1414358111 (2014).
- 146 Crawford, S. Is it time for a new paradigm for systemic cancer treatment? Lessons from a century of cancer chemotherapy. *Front. Pharmacol.* **4**, 68, doi:10.3389/fphar.2013.00068 (2013).
- 147 Moraes, T. F., Edwards, R. A., McKenna, S., Pastushok, L., Xiao, W., Glover, J. N. & Ellison, M. J. Crystal structure of the human ubiquitin

- conjugating enzyme complex, hMms2-hUbc13. *Nat. Struct. Biol.* **8**, 669-673, doi:10.1038/90373 (2001).
- 148 Carvalho, A. F., Pinto, M. P., Grou, C. P., Vitorino, R., Domingues, P., Yamao, F., Sa-Miranda, C. & Azevedo, J. E. High-yield expression in *Escherichia coli* and purification of mouse ubiquitin-activating enzyme E1. *Mol. Biotechnol.* **51**, 254-261, doi:10.1007/s12033-011-9463-x (2012).
- 149 Marley, J., Lu, M. & Bracken, C. A method for efficient isotopic labeling of recombinant proteins. *J. Biomol. NMR* **20**, 71-75 (2001).
- 150 Hau, D. D., Lewis, M. J., Saltibus, L. F., Pastushok, L., Xiao, W. & Spyropoulos, L. Structure and interactions of the ubiquitin-conjugating enzyme variant human Uev1a: implications for enzymatic synthesis of polyubiquitin chains. *Biochemistry* **45**, 9866-9877, doi:10.1021/bi060631r (2006).
- 151 Kay, L., Keifer, P. & Saarinen, T. Pure absorption gradient enhanced heteronuclear single quantum correlation spectroscopy with improved sensitivity. *J. Am. Chem. Soc.* **114**, 10663-10665, doi:10.1021/ja00052a088 (1992).
- 152 Delaglio, F., Grzesiek, S., Vuister, G. W., Zhu, G., Pfeifer, J. & Bax, A. NMRPipe: a multidimensional spectral processing system based on UNIX pipes. *J. Biomol. NMR* **6**, 277-293 (1995).
- 153 Goddard, T. D. & Kneller, D. G. SPARKY 3. *University of California, San Francisco* (2008).
- 154 Carpenter, A. E., Jones, T. R., Lamprecht, M. R., Clarke, C., Kang, I. H., Friman, O., Guertin, D. A., Chang, J. H., Lindquist, R. A., Moffat, J., Golland, P. & Sabatini, D. M. CellProfiler: image analysis software for identifying and quantifying cell phenotypes. *Genome Biol.* **7**, R100, doi:10.1186/gb-2006-7-10-r100 (2006).
- 155 Kamentsky, L., Jones, T. R., Fraser, A., Bray, M. A., Logan, D. J., Madden, K. L., Ljosa, V., Rueden, C., Eliceiri, K. W. & Carpenter, A. E. Improved structure, function and compatibility for CellProfiler: modular high-throughput image analysis software. *Bioinformatics* **27**, 1179-1180, doi:10.1093/bioinformatics/btr095 (2011).
- 156 Sezgin, M. & Sankur, B. Survey over image thresholding techniques and quantitative performance evaluation. *J. Electron Imaging* **13**, 146-168, doi:10.1117/1.16313161 (2004).
- 157 Wang, B., Matsuoka, S., Ballif, B. A., Zhang, D., Smogorzewska, A., Gygi, S. P. & Elledge, S. J. Abraxas and RAP80 form a BRCA1 protein complex required for the DNA damage response. *Science* **316**, 1194-1198, doi:10.1126/science.1139476 (2007).
- 158 Penengo, L., Mapelli, M., Murachelli, A. G., Confalonieri, S., Magri, L., Musacchio, A., Di Fiore, P. P., Polo, S. & Schneider, T. R. Crystal structure of the ubiquitin binding domains of rabex-5 reveals two modes of interaction with ubiquitin. *Cell* **124**, 1183-1195, doi:10.1016/j.cell.2006.02.020 (2006).
- 159 Dou, H., Buetow, L., Sibbet, G. J., Cameron, K. & Huang, D. T. BIRC7-E2 ubiquitin conjugate structure reveals the mechanism of ubiquitin transfer by a RING dimer. *Nat. Struct. Mol. Biol.* **19**, 876-883, doi:10.1038/nsmb.2379 (2012).
- 160 Plechanovova, A., Jaffray, E. G., McMahon, S. A., Johnson, K. A., Navratilova, I., Naismith, J. H. & Hay, R. T. Mechanism of ubiquitylation

- by dimeric RING ligase RNF4. *Nat. Struct. Mol. Biol.* **18**, 1052-1059, doi:10.1038/nsmb.2108 (2011).
- 161 Das, R., Liang, Y. H., Mariano, J., Li, J., Huang, T., King, A., Tarasov, S. G., Weissman, A. M., Ji, X. & Byrd, R. A. Allosteric regulation of E2:E3 interactions promote a processive ubiquitination machine. *EMBO J.* **32**, 2504-2516, doi:10.1038/emboj.2013.174 (2013).
- 162 Pollard, T. D. A guide to simple and informative binding assays. *Mol Biol Cell* **21**, 4061-4067, doi:10.1091/mbc.E10-08-0683 (2010).
- 163 Rambo, R. P. & Tainer, J. A. Characterizing flexible and intrinsically unstructured biological macromolecules by SAS using the Porod-Debye law. *Biopolymers* **95**, 559-571, doi:10.1002/bip.21638 (2011).
- 164 Schneidman-Duhovny, D., Hammel, M. & Sali, A. FoXS: a web server for rapid computation and fitting of SAXS profiles. *Nucleic Acids Res.* **38**, W540-544, doi:10.1093/nar/gkq461 (2010).
- 165 Schneidman-Duhovny, D., Hammel, M., Tainer, J. A. & Sali, A. Accurate SAXS profile computation and its assessment by contrast variation experiments. *Biophys. J.* **105**, 962-974, doi:10.1016/j.bpj.2013.07.020 (2013).
- 166 Pruneda, J. N., Stoll, K. E., Bolton, L. J., Brzovic, P. S. & Klevit, R. E. Ubiquitin in motion: structural studies of the ubiquitin-conjugating enzyme approximately ubiquitin conjugate. *Biochemistry* **50**, 1624-1633, doi:10.1021/bi101913m (2011).
- 167 Capp, J. A., Hagarman, A., Richardson, D. C. & Oas, T. G. The statistical conformation of a highly flexible protein: small-angle X-ray scattering of *S. aureus* protein A. *Structure* **22**, 1184-1195, doi:10.1016/j.str.2014.06.011 (2014).
- 168 Hodge, C. D., Edwards, R. A., Markin, C. J., McDonald, D., Pulvino, M., Huen, M. S., Zhao, J., Spyropoulos, L., Hendzel, M. J. & Glover, J. N. Covalent Inhibition of Ubc13 Affects Ubiquitin Signaling and Reveals Active Site Elements Important for Targeting. *ACS Chem Biol* **10**, 1718-1728, doi:10.1021/acscchembio.5b00222 (2015).
- 169 Deshpande, R. A., Williams, G. J., Limbo, O., Williams, R. S., Kuhnlein, J., Lee, J. H., Classen, S., Guenther, G., Russell, P., Tainer, J. A. & Paull, T. T. ATP-driven Rad50 conformations regulate DNA tethering, end resection, and ATM checkpoint signaling. *EMBO J.* **33**, 482-500, doi:10.1002/emboj.201386100 (2014).
- 170 Hashizume, R., Fukuda, M., Maeda, I., Nishikawa, H., Oyake, D., Yabuki, Y., Ogata, H. & Ohta, T. The RING heterodimer BRCA1-BARD1 is a ubiquitin ligase inactivated by a breast cancer-derived mutation. *J. Biol. Chem.* **276**, 14537-14540, doi:10.1074/jbc.C000881200 (2001).
- 171 Yin, Q., Lin, S. C., Lamothe, B., Lu, M., Lo, Y. C., Hura, G., Zheng, L., Rich, R. L., Campos, A. D., Myszkowski, D. G., Lenardo, M. J., Darnay, B. G. & Wu, H. E2 interaction and dimerization in the crystal structure of TRAF6. *Nat. Struct. Mol. Biol.* **16**, 658-666, doi:10.1038/nsmb.1605 (2009).
- 172 Zhang, M., Windheim, M., Roe, S. M., Pegg, M., Cohen, P., Prodromou, C. & Pearl, L. H. Chaperoned ubiquitylation--crystal structures of the CHIP U box E3 ubiquitin ligase and a CHIP-Ubc13-Uev1a complex. *Mol. Cell* **20**, 525-538, doi:10.1016/j.molcel.2005.09.023 (2005).
- 173 Soss, S. E., Yue, Y., Dhe-Paganon, S. & Chazin, W. J. E2 conjugating enzyme selectivity and requirements for function of the E3 ubiquitin ligase

- CHIP. *J. Biol. Chem.* **286**, 21277-21286, doi:10.1074/jbc.M111.224006 (2011).
- 174 Bentley, M. L., Corn, J. E., Dong, K. C., Phung, Q., Cheung, T. K. & Cochran, A. G. Recognition of UbcH5c and the nucleosome by the Bmi1/Ring1b ubiquitin ligase complex. *EMBO J.* **30**, 3285-3297, doi:10.1038/emboj.2011.243 (2011).
- 175 Zheng, N., Wang, P., Jeffrey, P. D. & Pavletich, N. P. Structure of a c-Cbl-UbcH7 complex: RING domain function in ubiquitin-protein ligases. *Cell* **102**, 533-539, doi:S0092-8674(00)00057-X [pii] (2000).
- 176 Hibbert, R. G., Huang, A., Boelens, R. & Sixma, T. K. E3 ligase Rad18 promotes monoubiquitination rather than ubiquitin chain formation by E2 enzyme Rad6. *Proc. Natl. Acad. Sci. U. S. A.* **108**, 5590-5595, doi:10.1073/pnas.1017516108 (2011).
- 177 Mace, P. D., Linke, K., Feltham, R., Schumacher, F. R., Smith, C. A., Vaux, D. L., Silke, J. & Day, C. L. Structures of the cIAP2 RING domain reveal conformational changes associated with ubiquitin-conjugating enzyme (E2) recruitment. *J. Biol. Chem.* **283**, 31633-31640, doi:10.1074/jbc.M804753200 (2008).
- 178 Lorick, K. L., Jensen, J. P., Fang, S., Ong, A. M., Hatakeyama, S. & Weissman, A. M. RING fingers mediate ubiquitin-conjugating enzyme (E2)-dependent ubiquitination. *Proc. Natl. Acad. Sci. U. S. A.* **96**, 11364-11369 (1999).
- 179 Liew, C. W., Sun, H., Hunter, T. & Day, C. L. RING domain dimerization is essential for RNF4 function. *Biochem. J.* **431**, 23-29, doi:10.1042/BJ20100957 (2010).
- 180 Landre, V., Rotblat, B., Melino, S., Bernassola, F. & Melino, G. Screening for E3-ubiquitin ligase inhibitors: challenges and opportunities. *Oncotarget* **5**, 7988-8013 (2014).
- 181 Classen, S., Hura, G. L., Holton, J. M., Rambo, R. P., Rodic, I., McGuire, P. J., Dyer, K., Hammel, M., Meigs, G., Frankel, K. A. & Tainer, J. A. Implementation and performance of SIBYLS: a dual endstation small-angle X-ray scattering and macromolecular crystallography beamline at the Advanced Light Source. *J Appl Crystallogr* **46**, 1-13, doi:10.1107/S0021889812048698 (2013).
- 182 McCoy, A. J. Solving structures of protein complexes by molecular replacement with Phaser. *Acta crystallographica. Section D, Biological crystallography* **63**, 32-41, doi:10.1107/S0907444906045975 (2007).
- 183 McCoy, A. J., Grosse-Kunstleve, R. W., Adams, P. D., Winn, M. D., Storoni, L. C. & Read, R. J. Phaser crystallographic software. *J Appl Crystallogr* **40**, 658-674, doi:10.1107/S0021889807021206 (2007).
- 184 Hura, G. L., Menon, A. L., Hammel, M., Rambo, R. P., Poole, F. L., 2nd, Tsutakawa, S. E., Jenney, F. E., Jr., Classen, S., Frankel, K. A., Hopkins, R. C., Yang, S. J., Scott, J. W., Dillard, B. D., Adams, M. W. & Tainer, J. A. Robust, high-throughput solution structural analyses by small angle X-ray scattering (SAXS). *Nat. Methods* **6**, 606-612, doi:10.1038/nmeth.1353 (2009).
- 185 Dyer, K. N., Hammel, M., Rambo, R. P., Tsutakawa, S. E., Rodic, I., Classen, S., Tainer, J. A. & Hura, G. L. High-throughput SAXS for the characterization of biomolecules in solution: a practical approach. *Methods in molecular biology* **1091**, 245-258, doi:10.1007/978-1-62703-691-7_18 (2014).

- 186 Minter-Dykhouse, K., Ward, I., Huen, M. S., Chen, J. & Lou, Z. Distinct versus overlapping functions of MDC1 and 53BP1 in DNA damage response and tumorigenesis. *J. Cell Biol.* **181**, 727-735, doi:10.1083/jcb.200801083 (2008).
- 187 Harbury, P. B., Zhang, T., Kim, P. S. & Alber, T. A switch between two-, three-, and four-stranded coiled coils in GCN4 leucine zipper mutants. *Science* **262**, 1401-1407 (1993).
- 188 Berman, H. M. The Protein Data Bank: a historical perspective. *Acta Crystallogr A* **64**, 88-95, doi:10.1107/S0108767307035623 (2008).
- 189 Farmer, H., McCabe, N., Lord, C. J., Tutt, A. N., Johnson, D. A., Richardson, T. B., Santarosa, M., Dillon, K. J., Hickson, I., Knights, C., Martin, N. M., Jackson, S. P., Smith, G. C. & Ashworth, A. Targeting the DNA repair defect in BRCA mutant cells as a therapeutic strategy. *Nature* **434**, 917-921, doi:10.1038/nature03445 (2005).
- 190 Thompson, J. M., Nguyen, Q. H., Singh, M. & Razorenova, O. V. Approaches to Identifying Synthetic Lethal Interactions in Cancer. *Yale J Biol Med* **88**, 145-155 (2015).
- 191 Yun, C. H., Mengwasser, K. E., Toms, A. V., Woo, M. S., Greulich, H., Wong, K. K., Meyerson, M. & Eck, M. J. The T790M mutation in EGFR kinase causes drug resistance by increasing the affinity for ATP. *Proc. Natl. Acad. Sci. U. S. A.* **105**, 2070-2075, doi:10.1073/pnas.0709662105 (2008).
- 192 Lok, G. T., Sy, S. M., Dong, S. S., Ching, Y. P., Tsao, S. W., Thomson, T. M. & Huen, M. S. Differential regulation of RNF8-mediated Lys48- and Lys63-based poly-ubiquitylation. *Nucleic Acids Res.* **40**, 196-205, doi:10.1093/nar/gkr655 (2012).
- 193 Scheper, J., Oliva, B., Villa-Freixa, J. & Thomson, T. M. Analysis of electrostatic contributions to the selectivity of interactions between RING-finger domains and ubiquitin-conjugating enzymes. *Proteins* **74**, 92-103, doi:10.1002/prot.22120 (2009).
- 194 Hornbeck, P. V., Kornhauser, J. M., Tkachev, S., Zhang, B., Skrzypek, E., Murray, B., Latham, V. & Sullivan, M. PhosphoSitePlus: a comprehensive resource for investigating the structure and function of experimentally determined post-translational modifications in man and mouse. *Nucleic Acids Res.* **40**, D261-270, doi:10.1093/nar/gkr1122 (2012).
- 195 Cerami, E., Gao, J., Dogrusoz, U., Gross, B. E., Sumer, S. O., Aksoy, B. A., Jacobsen, A., Byrne, C. J., Heuer, M. L., Larsson, E., Antipin, Y., Reva, B., Goldberg, A. P., Sander, C. & Schultz, N. The cBio cancer genomics portal: an open platform for exploring multidimensional cancer genomics data. *Cancer Discov* **2**, 401-404, doi:10.1158/2159-8290.CD-12-0095 (2012).
- 196 Reva, B., Antipin, Y. & Sander, C. Predicting the functional impact of protein mutations: application to cancer genomics. *Nucleic Acids Res* **39**, e118, doi:10.1093/nar/gkr407 (2011).